NASA-CR-195119

A STUDY OF THE FORMATION AND DYNAMICS OF THE EARTH'S PLASMA SHEET USING ION COMPOSITION DATA

O.W. Lennartsson
Lockheed Missiles & Space Company, Inc.
Research and Development Division
3251 Hanover Street
Palo Alto, CA 94304

April 1994
Final Report
Contract NAS5-31209

Prepared for:
Goddard Space Flight Center
Greenbelt, MD 20771

TECHNICAL REPORT STANDARD TITLE PAGE

1. Report No.	2. Government Accession No.	3. Recipient's Catalog No.

4. Title and Subtitle	5. Report Date
A STUDY OF THE FORMATION AND DYNAMICS OF THE EARTH's PLASMA SHEET USING ION COMPOSITION DATA	4/20/94
	6. Performing Organization Code
7. Author(s)	8. Performing Organization Report No.
O.W. Lennartsson	F254278
9. Performing Organization Name and Address Lockheed Missiles & Space Company, Inc. Research and Development 3251 Hanover Street Palo Alto, CA 94304	10. Work Unit No.
	11. Contract or Grant No. NAS5-31209
	13. Type of Report and Period Covered 10 Apr 91 - 9 May 94 Draft Final Report
12. Sponsoring Agency Name and Address NASA/Goddard Space Flight Center Greenbelt, Maryland 20771 Technical Officer: G.D. Bullock, Code 602	14. Sponsoring Agency Code

15. Supplementary Notes

16. Abstract

Over two years of data from the Lockheed Plasma Composition Experiment on the ISEE 1 spacecraft, covering ion energies beween 100 eV/e and about 16 keV/e, have been analyzed in an attempt to extract new information about three geophysical issues: (1) solar wind penetration of Earth's magnetic tail, (2) relationship between plasma sheet and tail lobe ion composition, and (3) possible effects of heavy terrestrial ions on plasma sheet stability.

The results suggest: (1) The solar wind enters the magnetic tail at all times along slots between the plasma sheet and tail lobes, convected inward by the electric fringe field of the low-latitude magnetopause boundary layer. (2) The density gradient between the plasma sheet and the tail lobes is the steepest for protons, and becomes gradually smoother with increasing ionic mass, possibly associated with the different characteristic gyroradii. (3) The energetic singly charged oxygen ions of terrestrial origin do not have a significant effect on the stability of the plasma sheet, in spite of the fact that they often contribute most of the ion mass density inside of the ISEE 1 apogee near 23 earth radii downtail.

17. Key Words (Selected by Author(s))	18. Distribution Statement
Ion Composition, Magnetotail, Plasma Sheet, Tail Lobes, Solar Wind Entry, Energetic Ions, Ion Flows, Current Sheet	

19. Security Classif. (of this report)	20. Security Classif. (of this page)	21. No. of Pages	22. Price*
Unclassified	Unclassified	76 *	

*For sale by the Clearinghouse for Federal Scientific and Technical Information, Springfield, Virginia 22151.

* including attachments

PREFACE

This report is an overview of the scientific results of a 3-year study under the NASA Space Physics Guest Investigator Program, using data from the Lockheed Plasma Composition Experiment on the International Sun-Earth Explorer One (ISEE 1) spacecraft. This study has aimed specifically at the formation and dynamics of the plasma sheet region in Earth's magnetic tail, a region believed to play a central role in a wide range of geomagnetic phenomena long observed from the ground. The experiment measures the differential flux of positive ions in the energy range from near 0 eV to approximately 17 keV per unit charge. In contrast to the more conventional electrostatic particle analyzers flown on many spacecraft, this experiment has the capability to select the ions to be measured by selecting their mass per unit charge. Relatively few experiments of this type have been flown to date, and no other such experiment has provided the same extensive sampling of the plasma sheet at energies representing the bulk of the plasma sheet ion population.

The primary objective of this study has been to shed new light on the issue of solar wind penetration of Earth's magnetic field, by observing the differences and similarities between ions that are believed to be of either solar or terrestrial origin, such as He^{++} and O^{+} ions, respectively. The secondary objective has been to investigate the dynamics of the plasma sheet against theoretical predictions of various ion-mass dependent effects.

TABLE OF CONTENTS

LIST OF ILLUSTRATIONS

1. INTRODUCTION

This is the final report by Lockheed Missiles & Space Company, Inc., Research and Development Division, to the National Aeronautics & Space Administration, Goddard Space Flight Center, under a contract to carry out an experimental study of the formation and dynamics of Earth's plasma sheet within the Space Physics Guest Investigator Program, using data from the Lockheed Plasma Composition Experiment on the International Sun-Earth Explorer One (ISEE 1) spacecraft. The purpose of this report is to review the principal discoveries in three areas: (1) solar wind penetration of Earth's magnetic tail, (2) relationship between plasma sheet and tail lobe ion composition, and (3) possible effects of heavy terrestrial ions on plasma sheet stability. In addition to the publications resulting from this study, the report refers to other especially relevant papers from the scientific literature, listing those near the end in the order of appearance in the text. References [1], [2], and [3] are the principal publications under this contract, copies of which are attached.

1.1 Scientific Rationale

The Lockheed Plasma Composition Experiment on ISEE 1 has provided the only extensive in situ measurements to this day of the bulk ion composition well beyond 10 R_E in Earth's magnetic tail. This makes these data uniquely well suited for the study of a number of fundamental aspects of solar-terrestrial physics, including in particular the entry of solar wind plasma into the geomagnetic field [1]. This entry process is expected to have distinct signatures in the transition region between the tail lobes and the plasma sheet. Since the plasma density in the lobes can be extremely low, it is crucial to have access to data with the highest possible sensitivity, especially at energies covering freshly injected ions from both the solar wind and Earth's atmosphere, that is about 1 keV/e or lower. The Lockheed ISEE 1 data meet this requirement well [2]. In order to understand the formation and dynamics of the plasma sheet it is necessary to understand the interaction between and relative importance of ions from both the solar and terrestrial sources. Again, the Lockheed ISEE 1 data offer the best material for such inquiry [3].

2. BRIEF DESCRIPTION OF THE EXPERIMENT

The ISEE 1 spacecraft (along with the ISEE 2) was launched on October 22, 1977, into an orbit with apogee at almost 23 R_E (geocentric), perigee at about 300 km altitude, an inclination of 29°, and an orbital period of 57 hours. It was placed in a spinning mode with the axis nearly perpendicular to the solar ecliptic plane and with a period of approximately 3 seconds. The Lockheed Plasma Composition Experiment on the ISEE 1 is one of a family of instruments using the same type of ion optics and covering nearly the same range of energies (0 eV/e to about 17 keV/e) which have also been flown on GEOS 1 and 2, DE 1 and AMPTE/CCE [4]. The ISEE 1 instrument consists of two nearly identical mass spectrometers with the respective fields of view centered 5° above and 5° below the spin plane, that is about 5°above and below the solar ecliptic plane. Data used in this study are from one of these, the one looking below the spin plane (seeing ions moving upward). Each field of view is about 10° wide along the spin plane, and some 10° to 50° wide transverse to this plane, being the widest at the low energy end (due to preacceleration) and gradually decreasing toward 10° with increasing energy. Information on the instantaneous pitch angles (at center of field of view) is provided by the ISEE 1 Fluxgate Magnetometer [5].

Each spectrometer consists of an electrostatic analyzer to select energy per charge, followed by a combined electrostatic and magnetic analyzer to select mass per charge. Both analyzer sections have particle detectors, so at each energy setting the experiment provides both

the total ion flux and the partial flux at a selected mass per charge. On ISEE 1 each combination of energy and mass is maintained for at least 1/16 sec in high telemetry bit rate and 1/4 sec in low (normal) bit rate. Different combinations are stepped through in a cyclic fashion according to patterns controlled by a random access memory which is programmable from the ground. The various ISEE 1 patterns, or "modes", used inside the magnetosphere require anywhere from 2 to 20 minutes to complete. The mass selections usually include one that blocks all ions from reaching the second detector, allowing intermittent measurements during each cycle of the noise associated with penetrating radiation. These measurements are later used to correct the count rates of mass analyzed ions. The total count rate in the first detector is not corrected this way, but this detector is much less susceptible to penetrating radiation because of its small size (spiraltron).

The maximum energy range of the ISEE 1 instrument is 0 eV/e (or spacecraft potential) to 17.9 keV/e, divided into 32 contiguous channels, although only a subset of these may be used in a given mode. The lowest channel, from 0 eV/e to about 100 eV/e, is normally limited to energies above 10 eV/e by an RPA (retarding potential analyzer) in the entrance. That same RPA is used to provide "cold plasma" data from 0 to 100 eV/e (retarding within the lowest channel) during parts of some scan cycles. Because of measurement uncertainties associated with spacecraft charging and plasma convection, the lowest energy channel is treated separately when calculating velocity moments. Data from the highest energy channel (above 16 keV/e) are excluded altogether here, because of a slight variation over time of the mass response of the ISEE 1 instrument in that channel. The numerical procedures used for weighting and summing counts from the various energy channels are such that the velocity moments correspond to an energy range of either 100 eV/e to 16 keV/e (in all figures) or 10 eV/e to 100 eV/e (discussed separately), the latter assuming no spacecraft charging.

The data used here have been obtained in several different energy-mass scan modes, but usually only in modes spanning at least the 0.1- to 16-keV/e energy range, whether that range is covered in a contiguous fashion (normally true) or not (see below), and only in modes which provide H^+ data from the mass analyzer, as opposed to modes which rely on "total ion" counts for approximate H^+ measurements. Any sampling that has not been corrected for background noise, because of gaps in the telemetry, for example, has been discarded.

3. DATA FORMATS

This study has made use of two archival data sets produced at Lockheed in, respectively, 1986 and 1991, for NASA's Explorer Project and placed in the NSSDC under index numbers 77-102A-12F and 77-102A-12I. The first set consists of detector count rates for H^+, He^{++}, He^+, and O^+ ions, sorted by 32 energy channels and 16 look-angle bins, including both spacecraft spin phase and ion pitch angle, averaged over time for 1/2 to 3 hours, depending on distance from Earth. This set requires that ion velocity moments be calculated by the user, although a complete computer program for that purpose is provided with the data. This set, containing data from 1978 and 1979, formed the sole basis for several previous statistical studies (e.g. [6]).

The second set is designed to be a more compact representation of the data with roughly the same time resolution as that provided by the instrument energy-mass scan cycle. Although this set also includes various spectral information, this study has used mainly the files which contain velocity moments. A detailed explanation (user guide) may be obtained from the NSSDC. The time coverage of these data spans the so called "prime period" of ISEE operations, from the time of launch of ISEE 1 and 2 through the end of February, 1980.

The main type of file used here contains separate velocity moments for the four principal ion species, H^+, He^{++}, He^+, and O^+, or in some cases a subset of these ions, depending on the instrument operating mode. The moments have been calculated once each energy-mass scan cycle, using two different methods to be explained below. In cases where the energy scans have left some channels unsampled, sometimes every other channel, an interpolation procedure has

been employed, essentially assuming a linear variation of the differential flux. Each moment has a statistical uncertainty (standard deviation) assigned to it, calculated with standard formulas for error propagation assuming Poisson counting statistics and including the uncertainty in background subtraction [7].

A second type of file has velocity moments for "total ions", based on the total ion count rate in the electrostatic analyzer and assuming that this rate is due entirely to H^+ ions. These moments have been calculated once per energy scan, providing a time resolution of a couple of minutes or better, and usually have nearly continuous time coverage. The reason for using "total" moments here is to help interpret the mass-resolved moments at times when ion fluxes may be changing significantly during the course of a full energy-mass scan cycle.

To calculate full three-dimensional velocity moments from the raw ISEE 1 data, the ion fluxes measured within the near-ecliptic field of view have been extrapolated to other angles using either of two sets of approximating assumptions:

1. The principal ion flow is parallel to the solar ecliptic plane and the ion fluxes have rotational symmetry around the flow vector, regardless of the magnetic field orientation. The direction of the flow vector within this plane is determined by the measured flow within the instrument field of view. The single angular variable in this case is divided among twelve 30° spin-angle bins, roughly approximating the inherent angular resolution of the ISEE 1 instrument in normal low-bit-rate operation.

2. Fluxes are gyrotropic (independent of gyration angle) over the sampled range of pitch angles, and isotropic outside of this range, maintaining the values measured at the smallest and largest pitch angles, respectively. The pitch angles are divided among nine 20° bins. This assumption is only applied to number densities, mean energies, parallel and perpendicular to the magnetic field, and energy densities. It ignores any net bulk flow perpendicular to the magnetic field.

The moments reported here are those obtained with 1, except when they refer specifically to components parallel and perpendicular to the magnetic field, thus necessitating the use of 2. The two sets of assumptions usually provide about the same densities and total mean energies, within statistical uncertainties, but the numbers obtained with 1 are believed to be at least marginally more accurate in most cases. Although the drift direction in 1 is determined from average fluxes in 30° wide bins, the weighting involved in the integrations usually provides an accuracy much better than 30°.

The moment data have been supplemented with a third type of file,
containing a form of energy-angle spectra for the same four ion species (and for O^{++} ions). These spectra consist of spin-averaged count rates in each energy channel (typically all 32 channels), averaged over a single energy-mass scan cycle, combined with information about the maximum count rate at each energy during that cycle. This information includes the time and spin angle of the maximum, the maximum rate, and the angular range of counts greater than 1/3 of the maximum rate. These have been used to verify that the moments still have reasonable values when count rates are narrowly focused in angle or energy and are otherwise low, as often happens in the tail lobes [8].

4. PRINCIPAL SCIENTIFIC RESULTS

This study has also made use of archived solar wind data, both particle data and magnetic field (IMF) data. The ones used here are from the NSSDC OMNI file, and consist of hourly averages of the proton density and flow vector (in GSE coordinates) and of the IMF vector components (in GSE and GSM coordinates) and magnitude. These are a combination of data from several instruments and spacecraft. Descriptions of the various instruments are referenced in the data handbook by *Couzens and King* [9]. These solar wind data were either obtained in the

close vicinity of the magnetosphere (within a few tens of R_E) or were time shifted to the magnetosphere according to the observed solar wind flow (in the case of ISEE 3; cf. [9]).

4.1 Solar Wind Penetration of Earth's Magnetic Tail

Data from the Plasma Composition Experiment on the ISEE 1 spacecraft [4] show that Earth's plasma sheet, inside of the ISEE 1 apogee near 23 R_E, always has a large population of H^+ and He^{++} ions, the principal positive components of the solar wind [1] and [6]. This population is the largest during periods of extremely weak geomagnetic activity, and is then also the most "solar-wind like" in the sense that the He^{++}/H^+ density ratio is at its peak (about 3% on average in 1978 and 1979) and the H^+ and He^{++} ions have mean (thermal) energies that are proportional to ionic mass and barely exceed the typical bulk flow energies in the solar wind [1] and [6]. These quiet-time conditions occur when the IMF is persistently northward and not excessively strong [1].

One aspect of these results is shown in Figure 1, which is based on the first of the two sets of Lockheed/ISEE 1 archival data sets described in Section 3 above. In this case the data have been further averaged over space within the nightside central plasma sheet between 10 and 23 R_E from Earth. The data represented by the dashed lines have been obtained while the concurrent hourly IMF B_Z remained positive (for up to 3 hours at a time), but they are not the most extremely quiet data. If the IMF is further restricted to being more nearly northward and to stay that way for extended periods of time, allowing the auroral AE index to approach very small values (a few tens of nT), the plasma sheet H^+ and He^{++} densities become a larger fraction of the solar wind density, and the mean energies approach a mere 1 keV/nucleon [1] and [10].

The reduction in the plasma sheet H^+ and He^{++} densities during times of southward IMF is somewhat exaggerated in Figure 1, due to the heating which removes ions from the measured energy range, but the trend is clearly real, and the resulting ion pressure in the 0.1 to 16 keV/e range, including terrestrial O^+ and He^+ ions, is roughly comparable for northward and southward IMF, and is a function of the solar wind ram pressure [1].

As illustrated in [1], the plasma sheet densities do increase somewhat with increasing strength of the IMF, when the IMF has a northward component, but the increase is no stronger, within statistical uncertainties, than can be expected given the typical corresponding increase in the solar wind density [9]. Hence, although a northward IMF allows quieter conditions, favoring a higher solar ion density in the plasma sheet, these data show no evidence that the solar wind must be magnetized in order to enter. Actually, for IMF stronger than 15 nT the plasma sheet H^+ and He^{++} densities level off or decline, despite a further increase in the solar wind density [1].

As discussed more fully in [1], these data are consistent with persistent entry of solar wind plasma into the geotail, even when the IMF is extremely weak and probably of little consequence. The effects of the IMF on the solar ions in the tail may instead be related to the decrease in density and increase in energy observed in conjunction with substorms, when the IMF is stronger and preferentially southward. The decrease in density, in particular, which amounts to a reduction of the total number of solar ions between 10 and 23 R_E [1] and [10], may be caused by increased earthward flow, supplying new particles to the ring current, perhaps in combination with tailward ejection of "plasmoids" (cf. [11]).

In order to explain the ample abundance of solar ions in the plasma sheet during northward IMF, and especially the "solar-wind like" appearance of these ions during extended quiet periods, it is argued in [1] that the entry is a consequence of the low latitude magnetopause boundary layer (LLBL), which is always present and is at least partially located on closed geomagnetic field lines (e.g. [12] and [13]). A possible theoretical argument for this is illustrated in Figure 2, which assumes that the equipotential surfaces associated with the LLBL electric field [12] and [13], or at least some of these, close through the tail. For simple geometrical reasons, the associated electric field (perpendicular to each equipotential) will combine with the tail

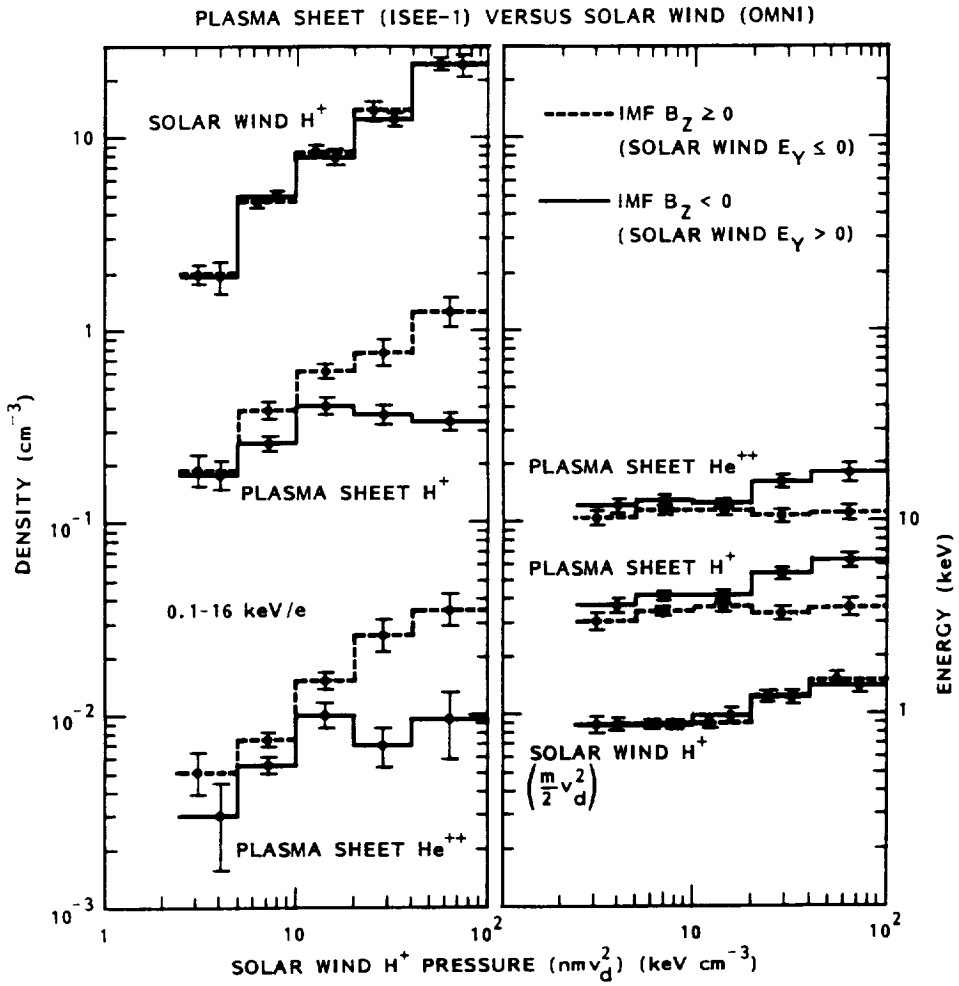

Fig. 1. Densities (left) and mean energies (right) in the central plasma sheet and solar wind, ordered by the solar wind ram pressure and the IMF BZ (Z being northward in GSM coordinates; from [1]).

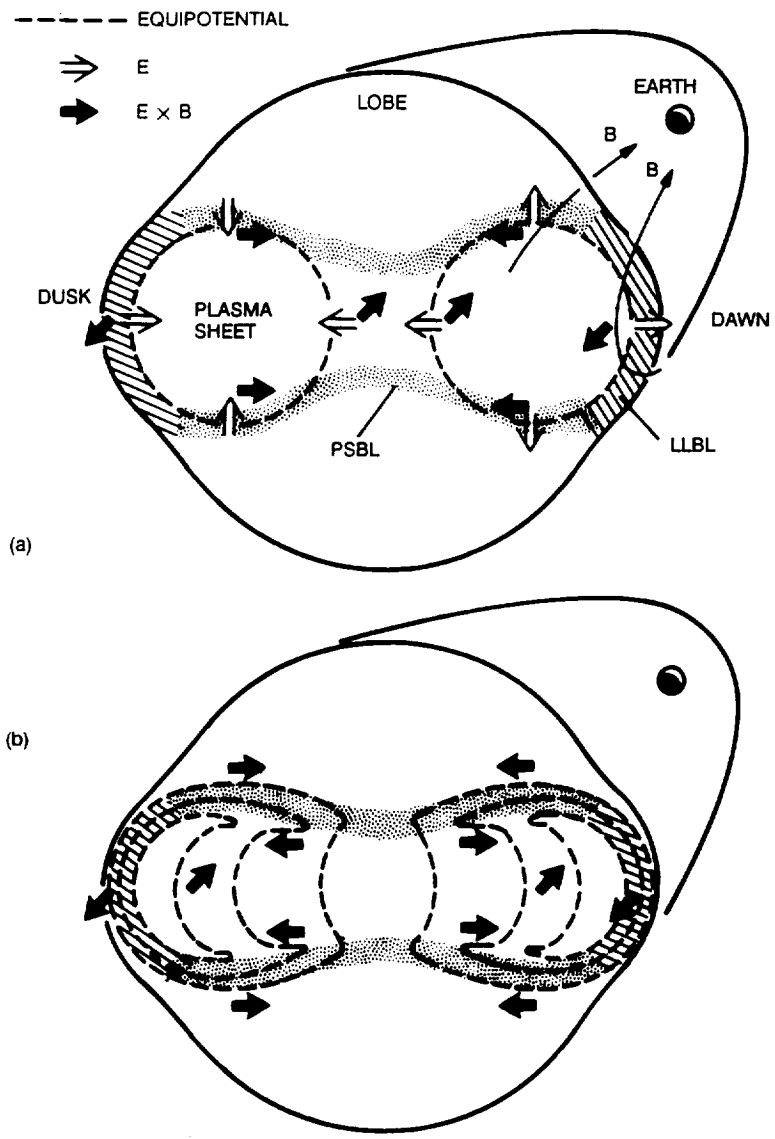

Fig. 2. Cross sections of a geomagnetic tail with internal closure of equipotentials (tubular) associated with electric field in the low latitude magnetopause boundary layer (LLBL). (a) Conceptual geometry showing associated electric field (open arrows) and $\mathbf{E} \times \mathbf{B}$ drift (solid arrows). (b) Equipotentials adjusted to fit observed cross-B drifts in central plasma sheet (see text; from [1]).

magnetic field vectors to project the $\mathbf{E} \times \mathbf{B}$ drift inward and earthward, as illustrated.

Figure 2 may also help explain a special class of ion flows reported in [1], namely antisunward flows of "solar-wind like" H^+ and He^{++} ions close to the tail lobes, presumably located in the plasma sheet boundary layer (PSBL), or immediately adjacent to it. About two dozen events with such flows have been studied in detail, most of which are associated with plasma sheet thinning, or boundary motion, preceding the onset of a weak to moderate substorm (C. Y. Huang, private communication, 1988). These flows, observed from the ISEE 1 and 2 spacecraft, occur in both the dawn and dusk halves of the tail, at varying distance from the tail flanks, and are in some cases seen near local midnight when the spacecraft are near apogee. An example of such flows from near the dawn flank is illustrated in Figure 3, where the ion velocity moments have been calculated under Assumption 1 in Section 3 above. It may be noted that the H^+ and He^{++} drift in the fourth panel down, after 9:50 UT, is directed tailward, not along the magnetic field, but duskward of the field direction, towards the interior of the tail. This is in the direction of the local $\mathbf{E} \times \mathbf{B}$ drift prescribed by Figure 2a.

The event shown in Figure 3 is not from the main set of data used in this study, but was chosen to coincide with an event previously described in the literature on the basis of other kinds of ISEE data [14]. However, in all of these events the H^+ and He^{++} ions have approximately equal flow velocity, ranging from a few tens to a few hundred km s^{-1}, and nearly equal thermal energy per nucleon. The total energy, flow and thermal energies combined, is at most a few keV/nucleon, and in some cases less than 1 keV/nucleon. The antisunward, or tailward, sense of motion persists for many minutes and in some cases for an hour or longer. These ions are observed mixed with terrestrial O^+ ions, which are also flowing tailward, but the H^+ and He^{++} energies show no correlation with the energy of the O^+ ions. As pointed out in [1], these flows, which are dominated by H^+ ions with about 1 keV energy, would probably be mistaken for purely terrestrial outflows, if seen by an instrument with no mass discrimination.

It is suggested in [1] that these antisunward-flowing H^+ and He^{++} ions owe their magnetic field-aligned velocity component to their initial sense of motion in the magnetosheath, by way of inertia, and that they have been diverted into the tail by the $\mathbf{E} \times \mathbf{B}$ drifts of Figure 2a. The local cross-B drift in the GSE X-Y plane, at the time of observation, is in several cases measured to be directed toward the tail flanks, however. To account for that, it is argued that the potential surfaces be modified as shown in Figure 2b, as though the plasma sheet boundary were a layer of net electric charge of the same polarity as the inside of the adjacent magnetopause LLBL. Additionally, this modification brings Figure 2 into general agreement with independent ISEE 1 and 2 observations of tailward ion flows inside and adjacent to the PSBL by *Orsini et al.* [15]. The latter authors have studied a number of events of strongly collimated low-energy (mostly hundreds of eV) ion flows occurring during disturbed conditions and identified as O^+ flows, and have concluded that the local $\mathbf{E} \times \mathbf{B}$ drift is toward the center of the tail on the lobe sides of the PSBL, and toward the tail flanks inside the plasma sheet, adjacent to the PSBL.

4.2 Relationship Between Plasma Sheet and Tail Lobe Ion Composition

As far as plasma measurements are concerned, the tail lobe regions of Earth's magnetosphere are unique in that they are usually not identified by characteristic particle signatures, but rather by the disappearance of instrument response, or "plasma dropout" (e.g. [16]). What has been known for some time is that the particle density is extremely low, probably about 10^{-2} cm^{-3} or lower (e.g. [17]) and that ion energies are significantly lower there than in the plasma sheet [17] and [18]. It has also been known that the lobes contain narrowly collimated tailward streams of ions, at least part of the time, and that these streams consist not only of H^+ ions but to an even greater extent of O^+ ions, presumably of terrestrial origin [8]. The data on these streams have been the only information available on the ionic composition of the tail lobe

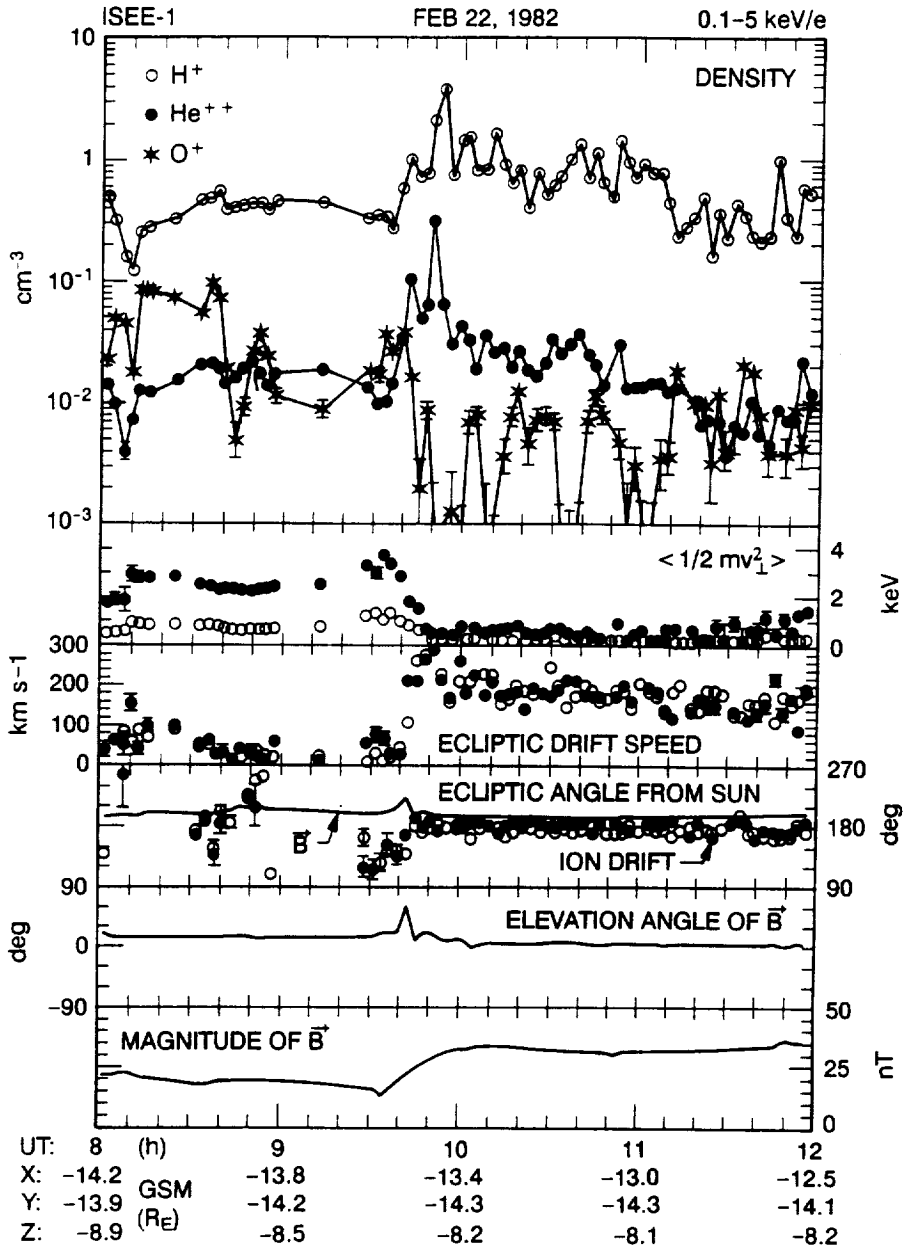

Fig. 3. From top to bottom: number densities; thermal energies associated with motion perpendicular to bulk flow vector (in solar ecliptic plane); bulk flow speeds; longitude angles of bulk flows and of local magnetic field (solid line) counted positive eastward from sun direction; elevation angle of local magnetic field (above and below ecliptic plane); magnitude of same. Error bars show standard deviations (± one sigma) carried over from counting statistics (mostly smaller than data symbol; from [1]).

plasma prior to this study [2].

This study is an extension of the work by *Sharp et al.* [8], using a much larger data set from the same experiment (the Lockheed experiment on ISEE 1) and taking a different approach. The approach differs from that of Sharp et al. in that all detector counts are included here (corrected for background noise), not merely isolated counts exceeding three standard deviations of a Poisson distribution (at least 10 counts per unit sampling). The deficiency in individual counts has been compensated for by summing them (weighted) into ion velocity moments, while keeping score of the resulting total standard deviations. The objective with this approach has been to extract the maximum possible information from the only available data.

This study was motivated in large part by a recent theory of tail pressure equilibria by *Kiessling and Ziegler* [19], who used statistical mechanics rather than the more conventional magnetohydrodynamic equations. Their theory is the first one to consider two ion components in the plasma sheet, namely H^+ and O^+ ions. Under fairly general assumptions about the relative bulk velocities of the two ion components and the electrons (affecting the cross-tail current) this theory requires that the O^+ ions form a spatially thicker sheet, in the south-north direction (GSM Z-direction), than do the H^+ ions (Figures 4 through 7 in that paper). As a consequence, the O^+/H^+ density ratio becomes larger than one in the tail lobes, even if it is much less than one in the central plasma sheet.

This theoretical result may seem to be in agreement with the experimental result of *Sharp et al.* [8], even though the theoretical velocity distributions are essentially isotropic, not narrow streams. Since the theory assumes that each ion component has identical thermal velocity distributions in the plasma sheet and the lobes, except for the overall amplitudes, it suggests that a variation of the O^+/H^+ ratio with Z can be due to local conditions in the tail rather than to a latitudinal variation of the ionospheric particle sources, as originally assumed in [8]. The implication is, as stated by Kiessling and Ziegler, that the effect is produced by the different ionic mass of the two components.

In order to test the theoretical predictions, data from the second Lockheed/ISEE 1 archival set discussed in Section 3 above were sorted according to the measured ion beta value, that is according to the measured ratio between the total ion pressure perpendicular to the tail magnetic field, including H^+, He^{++}, He^+, and O^+ ions, and the magnetic field pressure (derived from the ISEE 1 magnetometer data [5]). One result of this sorting is shown in Figure 4, where data have been limited to a central tail region within 10 R_E of local midnight (and beyond 10 R_E from Earth).

The O^+/H^+ density ratio in the bottom panels of Figure 4 does indeed vary with beta in a fashion that would be expected from [19], at least qualitatively, and the He^+/H^+ and He^{++}/H^+ ratios vary as might be extrapolated from the theory, considering that He^+ and He^{++} ions are also heavier than the H^+ ions. However, the measured ion energies do vary with beta, in contrast to the theoretical assumptions, so it is not clear how to make a quantitative comparison. As an alternative, a much simpler theory is considered in [2], one in which these measured effects might be explained in terms of finite and mass-dependent gyroradii. Some quantitative agreement is achieved this way, but the agreement is incomplete [2].

Considering that the result in Figure 4 may be a finite gyroradii effect [2], and considering that it is in qualitative agreement with a theory [19] which explicitly assumes that the particle drift motion is along surfaces of constant beta, it is again argued in [2] that the tail lobe $\mathbf{E} \times \mathbf{B}$ drift may be directed mainly inward from both the dawn and dusk flanks of the tail, as illustrated in Figure 5. This same configuration is also inferred from other aspects of the data [2]. Figure 5 differs from Figure 2 only in that equipotential surfaces are shown here to originate in either the low latitude magnetopause boundary layer or in the solar wind.

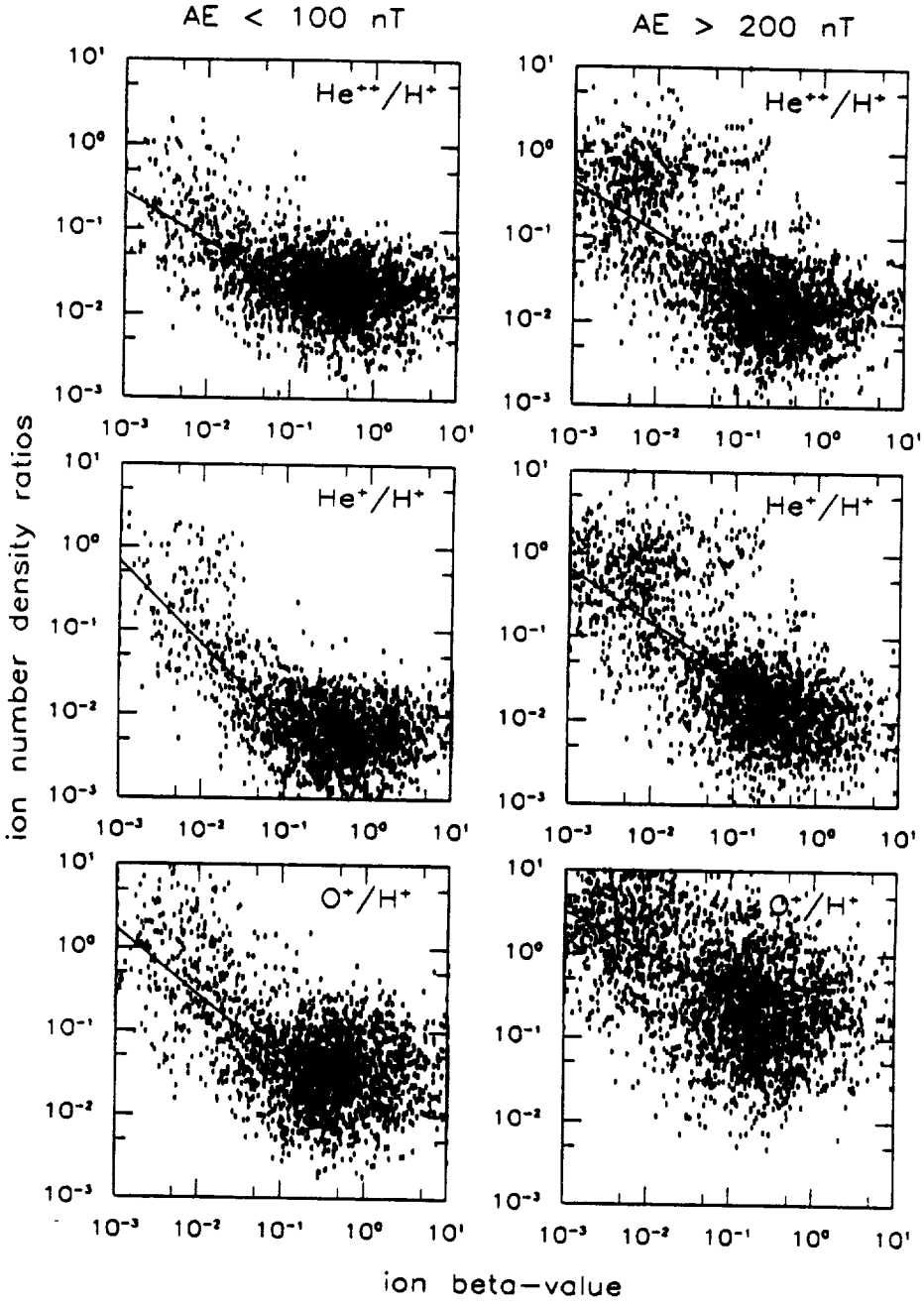

Fig. 4. Densities of He^{++} (top), He^{+} (middle), and O^{+} (bottom), normalized by the H^{+} density measured during same energy-mass scan cycle and ordered by total ion beta and by the hourly AE index during current hour and immediately preceding hour. The sloping straight lines in each panel represent least-squares fits to the points (unweighted) at beta < 0.1 on a log-log scale (from [2]).

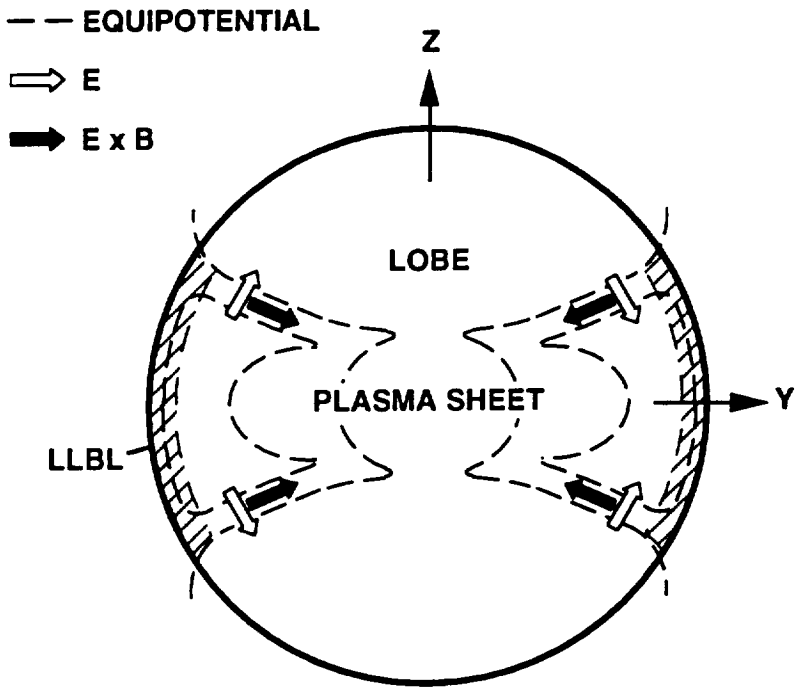

Fig. 5. Hypothetical electric equipotentials (dashed lines)allowing inward tail convection from dawn and dusk flanks. These may originate in the low latitude boundary layer (LLBL), as indicated by closed contours [1], or in the solar wind, as indicated by open contours (assuming dawn-dusk directed E-field in solar wind; from [2]).

4.3 Possible Effects of Heavy Terrestrial Ions on Plasma Sheet Stability

Singly charged oxygen is a variable but usually substantial component of the magnetospheric plasmas at most energies (e.g. [6], [7], [8], [20], [21], and [22]). It is, besides H^+ and He^{++} ions, the probably most important ion component from a scientific point of view, for at least two reasons. One is its principal source, the earth's atmosphere (e.g. [20] and [21]), which makes it a unique measure of electrical solar-terrestrial interactions. Another reason, however, is the large mass or mass per charge of the O^+ ions compared to that of the H^+ ions. A mere 10% admixture of O^+ ions in an otherwise pure H^+ population will more than double the mass density of the plasma, even though the number density (and charge density) remains almost the same. And a fifty-fifty mixture of O^+ and H^+ ions, often reached in the inner magnetosphere [7] and sometimes in the central plasma sheet (locally) as far out as 20 R_E [22], will have almost an order of magnitude greater mass density than the corresponding number of only H^+ ions.

This property of the O^+ component might conceivably have significant consequences for the plasma dynamics, including the dynamics of the plasma sheet. Several authors have indeed argued convincingly that the presence of large numbers of O^+ ions in the tail current sheet (midplane of plasma sheet), where the geomagnetic field is weak, must have a destabilizing effect by decreasing the net magnetization of the ion population as a whole and inducing tearing mode perturbations (e.g. [23] and [24]). That way the O^+ ions might be a twofold element of geomagnetic activity, both a product, emitted in association with ionospheric electric currents, and a driving or modulating agent, once they reach the equatorial plasma sheet.

One observational fact that may seem to suggest active feedback from substorm-produced O^+ ions is the tendency of very strong substorms, those with a peak AE index of 1000 nT or greater, to occur in clusters during extended periods (often a day or longer) of elevated AE (see for instance [25]). On the other hand, more long-term records of geomagnetic and solar activity, covering several years, may not seem to fit the same trend, because the energetic O^+ population has been found to vary substantially in density over the course of a solar cycle without causing a parallel long-term variation of geomagnetic activity [20] and [26].

This study [3] has been an attempt to clarify whether there really is a geomagnetic feedback specific to the O^+ ions, because of their large mass, by comparing extensive sets of near-equatorial ion composition data with common geomagnetic and solar activity indices. In order to utilize the long-term observations now available from similar experiments, data obtained during the rising and maximum phases of solar cycle 21 by the Lockheed Plasma Composition Experiment on the ISEE 1 have been intercompared with data obtained near the end of the same cycle, at the minimum phase, by the same kind of Lockheed experiment on the Charge Composition Explorer (CCE) spacecraft of the Active Magnetosphere Particle Tracer Explorer (AMPTE) mission (with additional support from a NASA/Lockheed AMPTE contract).

Statistical intercomparisons of the ion data and the activity indices have been made both on short-term (hours and days) and long-term (years) bases in [3], but this brief review will be focused on the long-term solar-cycle related aspects. The end result of these intercomparisons, whether short- or long-term, is that no evidence of O^+ feedback can be found.

While the ISEE 1 data, from the second archival set described in Section 3 above, cover both the plasma sheet, beyond 10 R_E, and the inner magnetosphere, the CCE data only cover the inner magnetosphere, inside of 9 R_E. This poses no real problem, however, since earlier studies of the ISEE 1 data have shown that the concentration of O^+ ions, although different in different regions, vary in essentially the same fashion with solar activity in all regions [26].

The time coverage of the ISEE 1 and AMPTE/CCE data sets through solar cycle 21 is illustrated in Figure 6, along with the daily index of 10.7-cm wavelength solar radio flux. This index is commonly used as a proxy for the solar extreme ultraviolet (EUV) radiation (which is not observable from the ground), and is therefore an indirect measure of the solar radiant effects on the terrestrial (upper atmosphere) O^+ source (e.g. [20]). This figure shows the reason for intercomparing the two data sets; the ISEE 1 set was aquired during strongly varying solar

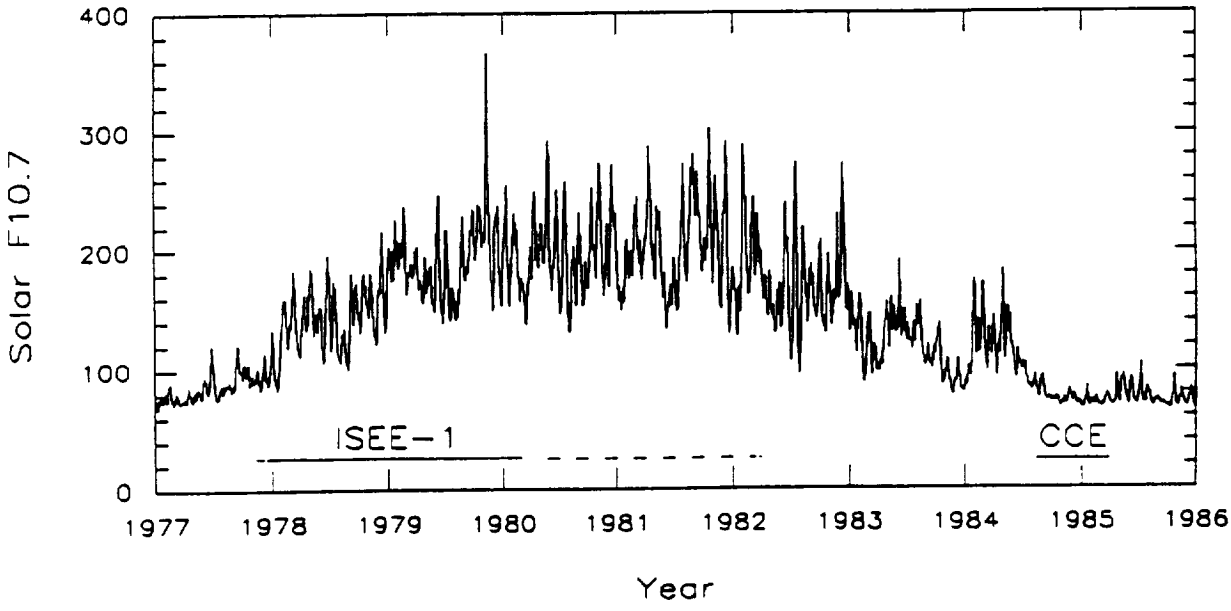

Fig. 6. Time ranges of ion composition data in relation to solar activity. Only the solid-line (archived) portion of theISEE 1 data has been used here (years labeled at beginning;from [3]).

activity, including the peak, the CCE set during weak and extremely steady solar activity.

Figure 7 relates the average ion mass (average of H^+, He^{++}, He^+, and O^+ ions) in the central plasma sheet (ISEE 1 data) to solar surface activity, as measured by the F10.7, as well as geomagnetic activity. The ion mass samplings in the left panel are from geomagnetically "quiet" times, defined by requiring that the hourly AE index be consistently less than 100 nT over a 3-hour period, where the middle hour contains the mass sampling. The right panel has samplings from "disturbed" times, similarly defined by hourly AE indices being consistently greater than 200 nT over that same 3-hour period. By considering AE indices taken both before and after the mass sampling it is ensured that no bias is placed on the causal relationship between the AE and the ion mass. The average ion mass is found to increase with increasing solar activity, regardless of substorm activity level, and this is mainly a consequence of an increasing O^+ density.

Figure 8 shows one kind of comparison between ISEE 1 and CCE data within the bounds of available AE indices. In this case each ion sampling has been associated with the average of 6 successive hourly AE indices, the last of which is concurrent. There is no special reason for choosing a 6-hour period per se, but the statistical correlation is somewhat better when an average of several hourly AE values is used rather than some single preceding value. Using preceding rather than succeeding AE values here in the inner magnetosphere seems intuitively right [3], regardless of the role of O^+ ions in the plasma sheet, and that choice is also justified by improved correlation.

Figure 8 confirms that the O^+/H^+ ratio has declined quite substantially in late 1984, near solar minimum, as compared to typical values during the rising phase of 1978 to early 1980. This decline can be inferred to apply to the plasma sheet as well, beyond 10 R_E, because of the global nature of the solar influence [26]. In spite of this long-term reduction in the O^+/H^+ ratio, there is no corresponding reduction in substorm activity. Instead, there is a modest but statistically significant increase over the same time period, as measured by for instance daily averages of the AE index [25]. This trend is reflected in Figure 8 by the different grand average AE values during the two intervals of ion sampling (203 nT in the ISEE 1 interval, 280 nT in the CCE interval, the two mean values differing by more than ten times the standard deviation of either mean; see figure caption).

The long-term variation of geomagnetic activity is perhaps better illustrated in the last figure, Figure 9. It can be seen from this figure that, during solar cycle 21, the geomagnetic activity actually reaches a minimum at a time (early 1980) when solar activity, according to Figure 6, is near maximum and the O^+ concentration in the plasma sheet, as is known from in situ ISEE 1 observations and illustrated in Figure 7, has extremely large values more often than it had in the preceding two years, when solar activity was increasing and still lower on average. This trend clearly contradicts the notion that enhanced O^+ concentration would trigger, enhance, or prolong geomagnetic substorms. This, together with the fact that the geomagnetic activity begins to increase again in mid 1980, seemingly without any relationship to the long-term variation of solar activity in Figure 6, is interpreted in [3] as strong evidence against a geomagnetic feedback mechanism specific to O^+ ions. This result will have to be accounted for in any future theory of plasma sheet dynamics [3].

5. NEW TECHNOLOGY

The analysis of data from the Lockheed Plasma Composition Experiment on the ISEE 1 spacecraft has been carried out with conventional tools and methods and has not led to the development of new technology. The data from the instrument, although refined in the archival formats used here, have the same basic form that has been utilized with spaceborne electrostatic particle analyzers for decades. The only fundamental difference between these and most earlier data lies in the selection of ions by mass per charge. Our knowledge about the ion mass has so far been utilized for scientific purposes only, and no technological application has yet been discovered.

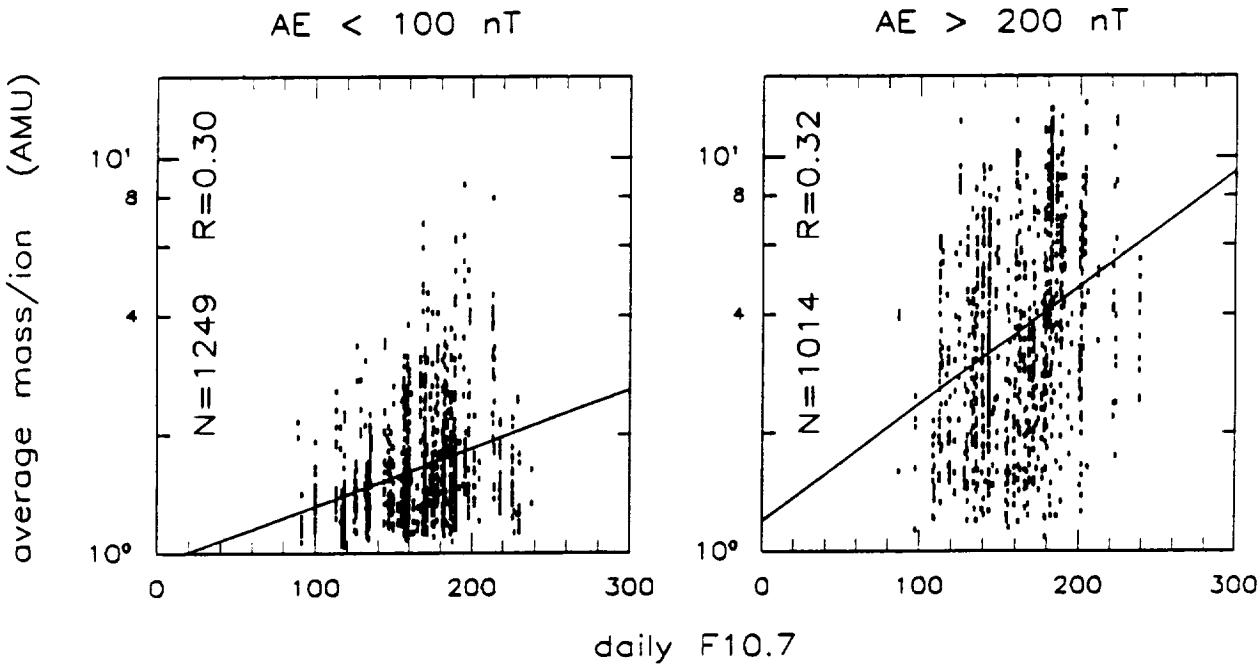

Fig. 7. Comparison of average ion mass in plasma sheet with the Ottawa daily F10.7 index (solar radio flux) during geomagnetically quiet (left) and disturbed (right) conditions (see text for selection of AE). The ion samplings have been ordered by Ottawa local time here, rather than by the usual UT. Sloping straight lines represent least-squares fits to the points (unweighted) on a log-lin scale, with the number of points and the correlation coefficient shown by N and R, respectively (from [3]).

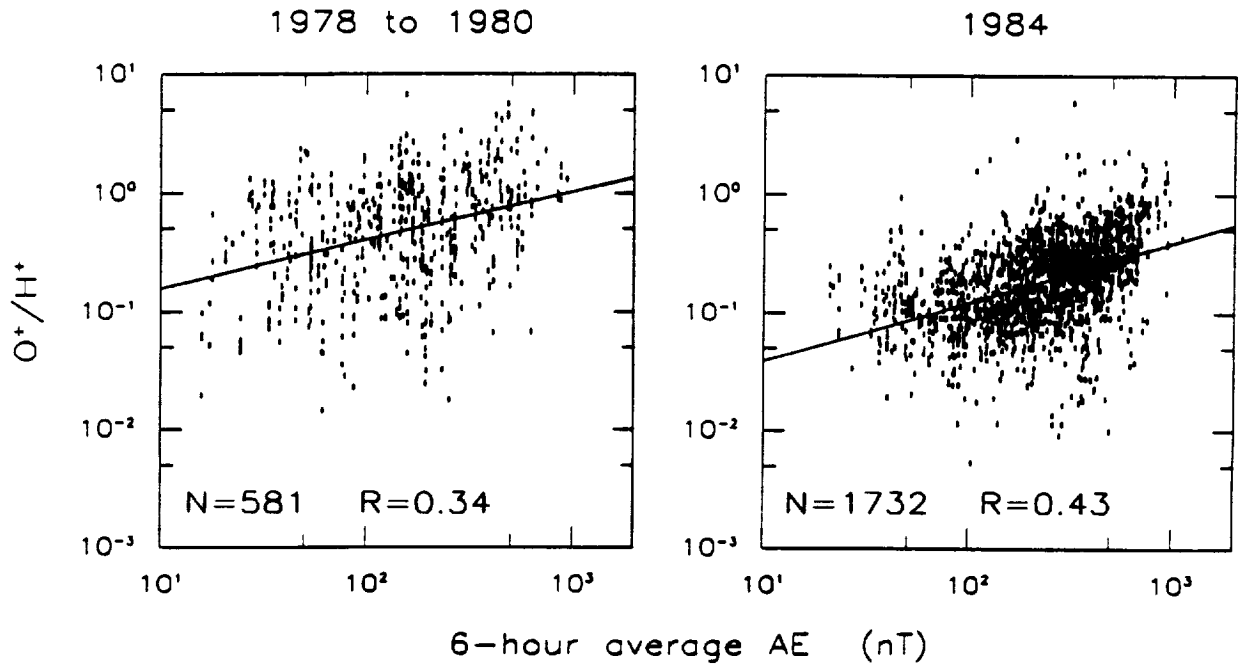

Fig. 8. Comparison of O^+/H^+ density ratio in the equatorial magnetosphere (dawn to noon) with the preceding 6-hour average AE index during rising-to-maximum (left) and minimum (right) solar activity. The grand average AE during the two data sampling intervals was 203 ±7 nT (left) and 280 ±5 nT (right; from [3]).

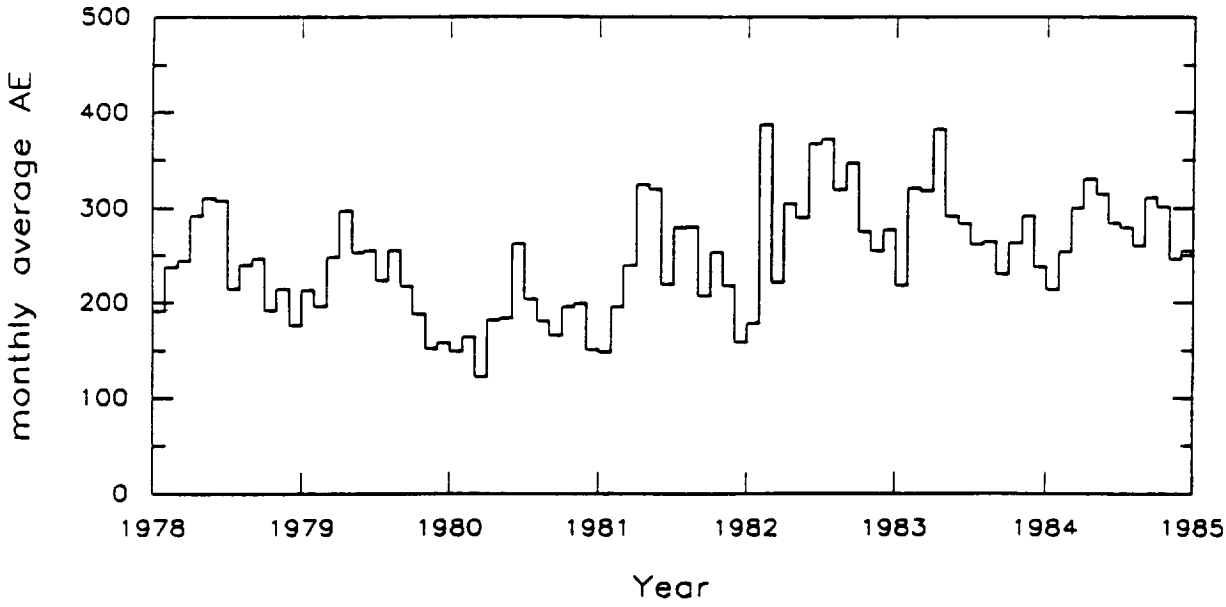

Fig. 9. Long-term variation of monthly averaged AE index (in units of nanotesla; from [3]).

6. CONCLUSIONS

Whether or not this study has provided definitive answers in its three areas of inquiry, it has at least added substantial new material to the list of reasons why ion mass spectrometers are indispensable components of any spacecraft dedicated to solar-terrestral plasma physics. Beginning with the original discovery more than 20 years ago that Earth's atmosphere is a significant source of energetic ions [27], especially O^+ ions, results obtained with this kind of instrument have gradually undermined many of the once popular assumptions in this field, a trend that may have culminated about 15 years later with a widespread perception that almost all plasma in the magnetosphere may be of terrestrial origin (e.g. [28]). The results from this study may in some sense have partially re-established the once preeminent role of the solar wind, and, at the same time, they suggest new ways to look at it. Three specific points may be worth reiterating:

1. Tailward flows of ions in regions that appear to be well inside of the magnetopause, especially in the plasma sheet boundary layer, are not necessarily of terrestrial origin; some of the strongest such flows have the signatures of solar wind particles [1].

2. When the vast volume of the plasma sheet is taken into account, it is probably true to say that the larger portion of magnetospheric plasmas, outside of the plasmasphere, is of solar rather than terrestrial origin most, if not all, of the time [2] and [3]. Although only the ionic component can be ascribed to a solar origin with some degree of certainty, it does appear reasonable that solar electrons enter along with the ions [1].

3. Although the terrestrial O^+ ions are often numerous enough to substantially increase the mass density of the plasma sheet, at least inside of the ISEE 1 apogee near 23 R_E, they do not appear to have a decisive influence on the plasma sheet dynamics [3].

7. RECOMMENDATIONS

During its approximately 4 1/2 years of operation (until March 20, 1982) the Lockheed Plasma Composition Experiment on ISEE 1 gathered a very large and in many respects entirely unique set of data on the ion populations with energies in the 0-17 keV/e range. Due to the orbital characteristics of the ISEE 1 spacecraft, data have been obtained in regions of space where no ion mass spectrometer had been flown before, and the few such instruments that have since been flown in the same general regions, especially the geomagnetic tail beyond 10 R_E, have either been designed for much more energetic ions or have failed to provide useful data.

Barely more than half (2 1/3 years) of these Lockheed data were archived at the NSSDC by the end of the three-spacecraft ISEE mission, both because of the emphasis on the first two years of data by the ISEE Project and because of rapidly dwindling funding towards the end of the mission. In light of the very uncertain future of new missions, including the GGS/Polar, it would seem to be prudent on the part of NASA to make some additional funding available to Lockheed to complete this archiving, funding that would have to be very modest by the standards that apply to new missions. It is therefore recommended by this author that such funding be made available, and that NASA acts on this matter very soon, before the Lockheed magnetic tape records of the raw ISEE 1 data risk disposal as obsolete in these times of cost savings in the aerospace industry, or otherwise become illegible.

8. REFERENCES

1. Lennartsson, W., A scenario for solar wind penetration of Earth's magnetic tail based on ion composition data from the ISEE 1 spacecraft, *J. Geophys. Res., 97,* 19221, 1992.

2. Lennartsson, O.W., Tail lobe ion composition at energies of 0.1 to 16 keV/e: evidence for mass-dependent density gradients, *J. Geophys. Res., 99,* 2387, 1994.

3. Lennartsson, O.W., D.M. Klumpar, E.G. Shelley, and J.M. Quinn, Experimental investigation of possible geomagnetic feedback from energetic (0.1 to 16 keV) terrestrial O^+ ions in the magnetotail current sheet, *J. Geophys. Res., 98,* 19443, 1993.

4. Shelley, E.G., R.D. Sharp, R.G. Johnson, J. Geiss, P. Eberhardt, H. Balsiger, G. Haerendel, and H. Rosenbauer, Plasma composition experiment on ISEE-A, *IEEE Trans. Geosci. Electron., GE-16,* 266, 1978.

5. Russell, C.T., The ISEE 1 and 2 fluxgate magnetometers, *IEEE Trans. Geosci. Electron., GE-16,* 239, 1978.

6. Lennartsson, W., and E.G. Shelley, Survey of 0.1- to 16-keV/e plasma sheet ion composition, *J. Geophys. Res., 91,* 3061, 1986.

7. Lennartsson, W., and R.D. Sharp, A comparison of the 0.1-17 keV/e ion composition in the near equatorial magnetosphere between quiet and disturbed conditions, *J. Geophys. Res., 87,* 6109, 1982.

8. Sharp, R.D., D.L. Carr, W.K. Peterson, and E.G. Shelley, Ion streams in the magnetotail, *J. Geophys. Res., 86,* 4639, 1981.

9. Couzens, D.A., and J.H. King, Interplanetary medium data book, supplement 3, 1977-1985, Rep. *NSSDC/WDC-A-R&S 86-04,* NASA Goddard Space Flight Cent., Greenbelt, Md., 1986.

10. Lennartsson, W., Plasma sheet ion composition at various levels of geomagnetic and solar activity, *Phys. Scripta, 36,* 367, 1987.

11. Hones, E.W., Jr., in *Dynamics of the Magnetosphere* (Edited by S.I. Akasofu), p. 545, D. Reidel, Hingham, Mass., 1979.

12. Eastman, T.E., E.W. Hones, Jr., S.J. Bame, and J.R. Asbridge, The magnetospheric boundary layer: Site of plasma, momentum, and energy transfer from the magnetosheath into the magnetosphere, *Geophys. Res. Lett., 3,* 685, 1976.

13. Mitchell, D.G., F. Kutchko, D.J. Williams, T.E. Eastman, L.A. Frank, and C.T. Russell, An extended study of the low-latitude boundary layer on the dawn and dusk flanks of the magnetosphere, *J. Geophys. Res., 92,* 7394, 1987.

14. Etcheto, J., and A. Saint-Marc, Anomalously high plasma densities in the plasma sheet boundary layer, *J. Geophys. Res., 90,* 5338, 1985.

15. Orsini, S., M. Candidi, M. Stokholm, and H. Balsiger, Injection of ionospheric ions into the plasma sheet boundary layer, *J. Geophys. Res., 95,* 7915, 1990.

16. Hones, E.W., Jr., T. A. Fritz, J. Birn, J. Cooney, and S.J. Bame, Detailed observations of the

plasma sheet during a substorm on April 24, 1979, *J. Geophys. Res., 91,* 6845, 1986.

17. Akasofu, S.-I., E.W. Hones, Jr., S.J. Bame, J.R. Asbridge, and A.T.Y. Lui, Magnetotail and boundary layer plasmas at a geocentric distance of ~18 RE: VELA 5 and 6 observations, *J. Geophys. Res., 78,* 7257, 1973.

18. Hardy, D.A., H.K. Hills, and J.W. Freeman, Occurrence of lobe plasma at lunar distance, *J. Geophys. Res., 84,* 72, 1979.

19. Kiessling, M., and H.J. Ziegler, A theory of self-consistent two-dimensional tail equilibria for quasi-neutral e-H+O+ mixtures, *J. Geophys. Res., 94,* 261, 1989.

20. Young, D.T., H. Balsiger, and J. Geiss, Correlations of magnetospheric ion composition with geomagnetic and solar activity, *J. Geophys. Res., 87,* 9077, 1982.

21. Gloeckler, G., and D.C. Hamilton, AMPTE ion composition results, *Phys. Scr., T18,* 73, 1987.

22. Peterson, W.K., R.D. Sharp, E.G. Shelley, and R.G. Johnson, Energetic ion composition of the plasma sheet, *J. Geophys. Res., 86,* 761, 1981.

23. Baker, D.N., E.W. Hones, Jr., D.T. Young, and J. Birn, The possible role of ionospheric oxygen in the initiation and development of plasma sheet instabilities, *Geophys. Res. Lett., 9,* 1337, 1982.

24. Delcourt, D.C., C.R. Chappell, T.E. Moore, and J.H. Waite, Jr., A three-dimensional numerical model of ionospheric plasma in the magnetosphere, *J. Geophys. Res., 94,* 11893, 1989.

25. Kamei, T., and H. Maeda, Auroral electrojet indices (AE) for January-June 1978, *Data Book 3,* World Data Center C2 for Geomagn., Kyoto, Japan, April 1981.

26. Lennartsson, W., Energetic (0.1-16 keV/e) magnetospheric ion composition at different levels of solar F10.7, *J. Geophys. Res., 94,* 3600, 1989.

27. Shelley, E.G., R.G. Johnson, and R.D. Sharp, Satellite observations of energetic heavy ions during a geomagnetic storm, *J. Geophys. Res., 77,* 6104, 1972.

28. Chappell, C.R., T.E. Moore, and J.H. Waite, Jr., The ionosphere as a fully adequate source of plasma for the Earth's magnetosphere, *J. Geophys. Res., 92,* 5896, 1987.

ACKNOWLEDGMENTS

The author of this report wishes to acknowledge all the people responsible for the design and development of the Lockheed Plasma Composition Experiment on ISEE 1, especially E.G. Shelley, R.D. Sharp, R.G. Johnson, A. Ghielmetti, T.C. Sanders, E. Hertzberg, D.L. Carr, and W.K. Peterson of the Lockheed Palo Alto Research Laboratory; H. Balsiger, J. Geiss, and P. Eberhardt of the University of Bern; H. Rosenbauer and W.K.H. Schmidt of the Max-Planck Institut in Lindau; G. Haerendel and G. Paschmann of the Max-Planck Institut in Garching; and C.R. Chappell and C.R. Baugher of the NASA Marshall Space Flight Center.

He also wishes to thank C.T. Russell for the use of ISEE 1 magnetometer data, the National Space Science Data Center for the use of computer files of the IMF and solar wind data, the National Oceanic and Atmospheric Administration for the use of magnetic tape records of the geophysical and solar indices, and H.L. Collin for helpful discussions and for his assistance in preparing computer plotting routines and computer records of geophysical and solar indices.

Finally he wishes to express his sincere gratitude towards the personnel of the ISEE Project Office at NASA Goddard Space Flight Center, especially G.D. Bullock, for their technical and administrative support.

JOURNAL OF GEOPHYSICAL RESEARCH, VOL. 97, NO. A12, PAGES 19,221-19,238, DECEMBER 1, 1992

A Scenario for Solar Wind Penetration of Earth's Magnetic Tail Based on Ion Composition Data From the ISEE 1 Spacecraft

W. LENNARTSSON

Lockheed Missiles and Space Company, Inc., Research and Development, Palo Alto, California

Energetic (0.1–16 keV/*e*) ion data from the Plasma Composition Experiment on the ISEE 1 spacecraft show that Earth's plasma sheet (inside of 23 R_E) always has a large population of H^+ and He^{++} ions. This population is the largest, both in absolute numbers and relative to the terrestrial ions, during periods of extremely weak geomagnetic activity and is then also the most "solar wind like", in the sense that the He^{++}/H^+ density ratio is at its peak (about 3% on average in 1978 and 79), and the H^+ and He^{++} ions have mean (thermal) energies that are proportional to ionic mass and barely exceed the typical bulk flow energies in the solar wind. These quiet time conditions occur when the IMF is persistently northward and not excessively strong. At more active times the H^+ and He^{++} ions are heated in the central plasma sheet, but they can still be found with lower solar wind like energies closer to the tail lobes, at least during plasma sheet thinning. In a number of cases examined here, such low-energy H^+ and He^{++} ions are found flowing antisunward close to the lobes, flowing roughly parallel (or antiparallel) to the tail magnetic field at speeds ranging from a few tens to a few hundred kilometers per second, as though they have recently entered the tail earthward of the ISEE 1. In some cases the flow vector appears to contain a significant $\mathbf{E} \times \mathbf{B}$ component directed away from the nearest tail flank. In order to explain these flows, as well as the solar wind like appearance of the plasma sheet as a whole during northward interplanetary magnetic field, it is argued that the solar plasma enters along slots between the tail lobes and the plasma sheet, even quite close to Earth, convected inward along the plasma sheet boundary layer, or adjacent to it, by the electric fringe field of the ever present low-latitude magnetopause boundary layer (LLBL). The main point of the argument is that the required $\mathbf{E} \times \mathbf{B}$ drifts are produced by closing LLBL equipotential surfaces through the plasma sheet.

1. INTRODUCTION

Although it is one of the oldest topics of magnetospheric physics, the entry of solar wind plasma into Earth's magnetic field is still a complex and elusive issue. It has been further complicated by the observations that energetic (hundreds of eV to tends of keV) plasmas inside the magnetosphere can have a terrestrial rather than solar origin [e.g., *Shelley et al.*, 1972; *Ghielmetti et al.*, 1978; *Balsiger et al.*, 1980; *Sharp et al.*, 1981; *Lundin et al.*, 1982; *Hamilton et al.*, 1988]. Based on gross estimates of the total number of charged particles in various parts of the magnetosphere, it can even be argued that the known outflow of terrestrial ions from Earth's polar regions, as measured in a range of energies from less than 1 eV/*e* to about 20 keV/*e*, is sufficiently strong to supply the entire positive plasma component, given the proper mechanisms for final adjustment of energies [*Chappell et al.*, 1987].

The traditional view has been that the solar wind plasma does indeed enter, provided it is magnetized and that the embedded magnetic field, the interplanetary magnetic field (IMF), has a proper direction. The conditions for entry have been assumed to be the most favorable when the IMF is pointing southward, opposite the equatorial direction of Earth's magnetic field [e.g., *Cowley*, 1980]. According to this view, the IMF and the geomagnetic field merge on the front of the magnetopause, causing the electric field in the solar wind, that is the field associated with solar wind motion across the IMF ($\mathbf{E} = -\mathbf{v} \times \mathbf{B}$), to be conducted into the high-latitude magnetosphere and into the geomagnetic tail, where it will have a general dawn-to-dusk direction, at least as long as the IMF has a southward component. Under the influence of this internal electric field, part of the solar wind plasma is thought to convect ($\mathbf{E} \times \mathbf{B}$ drift) into the geotail, across the northern and southern tail lobes, and to converge at the tail midplane beyond some distant location downtail [e.g., *Speiser*, 1965; *Pilipp and Morfill*, 1978; *Cowley*, 1980]. Part of this converging plasma, it is thought, finds itself on closed (newly reconnected) geomagnetic field lines and is subsequently transported earthward (sunward) by a combination of $\mathbf{E} \times \mathbf{B}$ drift and field-aligned jetting [e.g., *Speiser*, 1965] to form the body of the plasma sheet, as well as the near-Earth ring current. The eventual fate of this same plasma is to be partially precipitated into Earth's atmosphere and otherwise ejected through the equatorial magnetopause.

The plasma circulation described by this theory was originally postulated on the basis of observed $\mathbf{E} \times \mathbf{B}$ drifts in the high-latitude regions of Earth's ionosphere [*Axford and Hines*, 1961], and has been corroborated by numerous electric field and plasma drift and plasma dispersion measurements by polar orbiting spacecraft [e.g., *Heppner*, 1972; *Reiff et al.*, 1977; *Heelis et al.*, 1982; *Heppner and Maynard*, 1987], but it has not yet been unambiguously verified by in situ observations in the distant tail. Observations made from the ISEE 3 spacecraft, for instance, show well-defined tail lobes separated by a plasma sheet as far as 225 R_E downtail [*Tsurutani et al.*, 1984; *Zwickl et al.*, 1984]. Judging from measured electron flows, the $\mathbf{E} \times \mathbf{B}$ drift in the plasma sheet appears to be almost exclusively antisunward beyond about 180 R_E [*Zwickl et al.*, 1984], which would be expected where southward pointing IMF field lines have reconnected, but the antisunward motion persists even though the local tail magnetic field between 180 and 225 R_E is northward, and hence the electric field is dawnward, at least half the time [*Tsurutani et al.*, 1984]. Under such conditions it even seems

Paper number 92JA01604.
0148-0227/92/92JA-01604$05.00

improbable that the plasma sheet particles have converged through the lobes. On the other hand, the plasma measurements that have been made closer to Earth show that earthward jetting of particles is commonplace [e.g., *DeCoster and Frank*, 1979; *Lyons and Speiser*, 1982; *Eastman et al.*, 1985], whether those particles previously traversed the tail lobes or not.

The purpose of this study is to explore an alternative scenario, one which may not necessarily require that the solar wind plasma be magnetized. This study does not take issue with the notion that Earth's magnetic field merges with the solar wind magnetic field on a regular basis, but it tries to focus on certain other aspects of the interaction between the solar wind particles and Earth's field. It is inspired in part by the simple fact that the geomagnetic tail, as far as we know, always has a plasma sheet, even during times when the physical signs of magnetic merging are weak or absent. In fact, ion composition measurements in the tail have shown that the plasma sheet contains the greatest number of H^+ and He^{++} ions, the principal positive components of the solar wind plasma, during extended periods of extremely weak geomagnetic activity [*Lennartsson and Shelley*, 1986; *Lennartsson*, 1987].

This study is also inspired by other recent plasma observations in the tail, observations that may seem, at least on the surface, to require some modifications of the traditional view of solar plasma circulation. One set of observations in this category consists of the many ISEE measurements of the boundaries between the plasma sheet and the northern and southern tail lobes, boundaries now commonly referred to as the "plasma sheet boundary layer" (PSBL) [e.g., *Parks et al.*, 1984; *Eastman et al.*, 1985]. Among the reported features of the PSBL is its frequently very sharp definition (hundreds of kilometers), as well as its layered structure, which includes layers of low-energy (hundreds of eV) ions and electrons streaming along the magnetic field, both earthward and tailward [*Parks et al.*, 1984]. Such features may suggest that the net plasma motion, including $\mathbf{E} \times \mathbf{B}$ drifts, is often parallel to the boundary, rather than directed from the lobes into the plasma sheet [cf. *Eastman et al.*, 1985].

Another set of relevant observations pertains to the so called "low-latitude magnetopause boundary layer" (LLBL) [e.g., *Eastman et al.*, 1976; *Mitchell et al.*, 1987], especially to its tailward extension along the dawn and dusk flanks of the magnetopause. The LLBL is known to be at least partially located on closed geomagnetic field lines, and it is believed to always contain solar wind plasma streaming tailward (antisunward) under the influence of a local electric field which is directed from dusk to dawn (tailward $\mathbf{E} \times \mathbf{B}$ drift). Of particular interest here is the fact that the LLBL appears to exist at all times, even when the IMF is northward [cf. *Mitchell et al.*, 1987], that is when the IMF points in the same direction as the equatorial portion of Earth's magnetic field lines, and is therefore not expected to be merged with Earth's field at the LLBL. The objective of this study is specifically to examine the possible roles of the LLBL and the PSBL in the transport of solar wind plasma from the magnetosheath to the central plasma sheet. In doing so, it will rely heavily on ion composition data from the Lockheed Plasma Composition Experiment on the ISEE 1 spacecraft.

2. INSTRUMENTATION

The ISEE 1 spacecraft (along with the ISEE 2) was launched on October 22, 1977, into an orbit with apogee at almost 23 R_E (geocentric), perigee at about 300 km altitude, an inclination of 29°, and an orbital period of 57 hours. The spacecraft was placed in a spinning mode with the axis nearly perpendicular to the solar ecliptic plane and with a period of approximately 3 s. It reentered almost 10 years later, on September 26, 1987.

The Lockheed Plasma Composition Experiment flown on ISEE 1 is one of a family of instruments using the same type of ion optics and covering nearly the same range of energies (0 eV/e to about 17 keV/e) which have also been flown on GEOS 1 and 2, Dynamics Explorer 1, and Active Magnetospheric Particle Tracer Explorers (AMPTE) CCE [*Shelley et al.*, 1978]. The ISEE 1 instrument consists of two nearly identical mass spectrometers with the respective fields of view centered 5° above and 5° below the spin plane, that is about 5° above and below the solar ecliptic plane. Each field of view is 10° wide along the spin plane and 10°–50° wide transverse to this plane, being the widest at the low-energy end and gradually decreasing to 10° with increasing energy. All data used in this study were obtained with one spectrometer, the one looking below the spin plane. The lowest-energy channel used here, one that extends from about 100 to 300 eV/e, has a field of view that extends from about 10° above the ecliptic plane to 20° below. Information on the instantaneous pitch angles (at center of field of view) is provided by the ISEE 1 fluxgate magnetometer [*Russell*, 1978].

Each spectrometer consists of an electrostatic analyzer to select energy per charge, followed by a combined electrostatic and magnetic analyzer to select mass per charge. Both analyzer sections have particle detectors, so at each energy setting the experiment provides both the total ion flux and the partial flux at a selected mass per charge. Each combination of energy and mass is maintained for at least 1/16 s in high telemetry bit rate and 1/4 in low (normal) bit rate. Different combinations are stepped through in a cyclic fashion according to various patterns controlled by a random access memory which is programmable from the ground. Some patterns, or "modes", may require only a couple of minutes per cycle, others may take 15 to 20 min. The mass selections usually include one that blocks all ions from reaching the second detector, which is a modified Johnston electron multiplier, allowing intermittent measurements of the noise associated with penetrating radiation. These measurements are later used to correct the count rates of mass analyzed ions. The background count rate in the first detector, which is a so-called "spiraltron", is generally negligible and is not corrected for.

The maximum energy range is 0 eV/e (or spacecraft potential) to 17.9 keV/e, divided into 32 contiguous channels, but the lowest channel, from 0 eV/e to about 100 eV/e, is normally limited to energies above 10 eV/e by a retarding potential analyzer (RPA) in the entrance. That same RPA is used to provide "cold plasma" data from 0 to 100 eV/e (retarding within the lowest channel) during part of some measurement cycles. Because of measurement uncertainties associated with spacecraft charging and plasma convection, the lowest-energy channel has not been used in this study. Neither has the highest-energy channel (above 16 keV/e)

been used, because of a slight variation over time of the mass peak locations in that channel. The energy range of these data is therefore generally 100 eV/e to 16 keV/e, unless further limited by a particular instrument mode (see below).

The mass range is from below 1 amu/e to about 150 amu/e, divided into 64 channels, but the most common measurement cycles only sample four to five channels, corresponding to the principal ions, plus a background channel (below 1 amu/e).

This study also makes use of archived solar wind data, both particle data and magnetic field (IMF) data. The ones used here are from the National Space Science Data Center (NSSDC) OMNI files and consist of hourly averages of the proton density and flow vector (in GSE coordinates) and of the IMF vector components (in GSE and GSM coordinates) and magnitude. These are a combination of data from several instruments and spacecraft. Descriptions of the various instruments are referenced in the data handbook by *Couzens and King* [1986]. These solar wind data were either obtained in the close vicinity of the magnetosphere (within a few tens of R_E) or time shifted to the magnetosphere according to the observed solar wind flow (in the case of ISEE 3 [cf. *Couzens and King*, 1986]).

3. Data Format

The ion data used here are mainly in the form of velocity moments, calculated as sums over discrete energy-angle matrix elements. To calculate full three-dimensional moments from the ISEE 1 data, the ion fluxes measured within the near-ecliptic field of view have been extrapolated to other angles using either of two sets of assumptions:

1. In the central plasma sheet, where most of the statistical material was obtained, the fluxes are assumed to be gyrotropic (independent of gyration angle) over the sampled range of pitch angles and isotropic outside of this range, maintaining the values measured at the smallest and largest pitch angles, respectively. The pitch angles are measured in terms of five bins, covering 0°–15°, 16°–44°, 45°–135°, 136°–164°, and 165°–180°, respectively. This assumption applies to number densities, mean energies, and energy densities. The two-dimensional bulk flow within the field of view, which is generally small compared to the thermal velocities in the central plasma sheet [cf. *Eastman et al.*, 1985], is derived from the partial flow density and partial number density actually measured, using twelve 30° spin angle bins, without extrapolating the ion fluxes into the third dimension. This set of assumptions is expected to be inaccurate at very low ion energies and is the main reason for not including data from the lowest energy channel (below 100 eV/e).

2. In the outer fringes of the plasma sheet, including the plasma sheet boundary layer, and in the lobes, it is assumed that the principal ion flow is parallel to the solar ecliptic plane and that the ion fluxes have rotational symmetry around the flow vector, rather than around the magnetic field. The direction of the flow vector within this plane is determined by the measured flow within the instrument field of view. The only angular variable in this case is measured in terms of the twelve 30° spin angle bins (the width of these bins equals the inherent angular resolution of the instrument in normal low-bit-rate operation). Since the magnetic field is often parallel to the ecliptic plane in these regions of space and since the ion flow is often parallel to the magnetic field, this second set of assumptions commonly produces about the same numbers as the first set. However, in cases of substantial ion drift across the magnetic field (substantial when compared to thermal velocities) the second set appears to provide more accurate moments, especially number densities. This has been verified by comparing the ion densities with electron densities derived from ISEE 1 and 2 wave experiments on several occasions (one such comparison is made below).

4. Statistical Results From Central Plasma Sheet

This section revisits a large set of survey data previously described by *Lennartsson and Shelley* [1986]. Those data were selected from a still larger set of magnetotail data using criteria designed to represent the central plasma sheet. One of those criteria, requiring that the mean energy of the ion population as a whole be at least 1 keV, averaged over H^+, He^{++}, He^+, and O^+ ions, has been dropped here, since it proved essentially redundant. The data were acquired over a 2-year period, 1978–1979 and include about 900 samplings of the plasma sheet, where each sampling consists of a 1- to 3-hour averaging of the ion fluxes, sorted by mass and by energy channel into the various spin and pitch angle bins. The duration of each sampling corresponds to about 1 R_E of spacecraft travel along the orbit. The spatial coverage is fairly uniform and extends from a geocentric distance of 10 R_E to the ISEE 1 apogee near 23 R_E, only including points tailward of the dawn-dusk meridian (GSM $X < 0$). These time-averaged flux samplings have been converted to velocity moments using the first set of assumptions described above (gyrotropy). About 630 of these samplings (70%) are covered by concurrent solar wind and IMF data in the NSSDC OMNI files.

4.1. *Evidence of a Solar Plasma Component in the Plasma Sheet*

Figure 1 illustrates several features of the principal plasma sheet ions that are relevant to the following discussion. Consider first the He^{++} and the O^+ densities in the left panel. These two species clearly behave differently in response to varying geomagnetic substorm activity, as measured by the auroral AE index in Figure 1 (see *Kamei and Maeda* [1981] and subsequent data books): the He^{++} ions are most numerous during extended periods of low activity, whereas the O^+ ions are by far the most abundant during active times. Since O^+ ions are known to be a major component of the auroral and polar outflow of energetic terrestrial ions [e.g., *Yau et al.*, 1985], but He^{++} ions are not, this comparison alone suggests an extraterrestrial, or solar, source for the He^{++}. If the helium were largely of terrestrial origin, it would probably be mostly singly charged, since He^+ ions are a well-known and often significant component of the ion outflow [*Collin et al.*, 1988]. This is not the case in the plasma sheet, however, since the He^{++} density in Figure 1 is substantially higher than the He^+ density at all but the most strongly disturbed times.

Since the solar wind consists mainly of H^+ ions one would thus expect the plasma sheet to have a large component of such ions behaving in much the same manner as the He^{++} component. That is indeed the case, as Figure 1 shows. The H^+ ions are also the most numerous during extended periods of low substorm activity, and the H^+ ions, like the

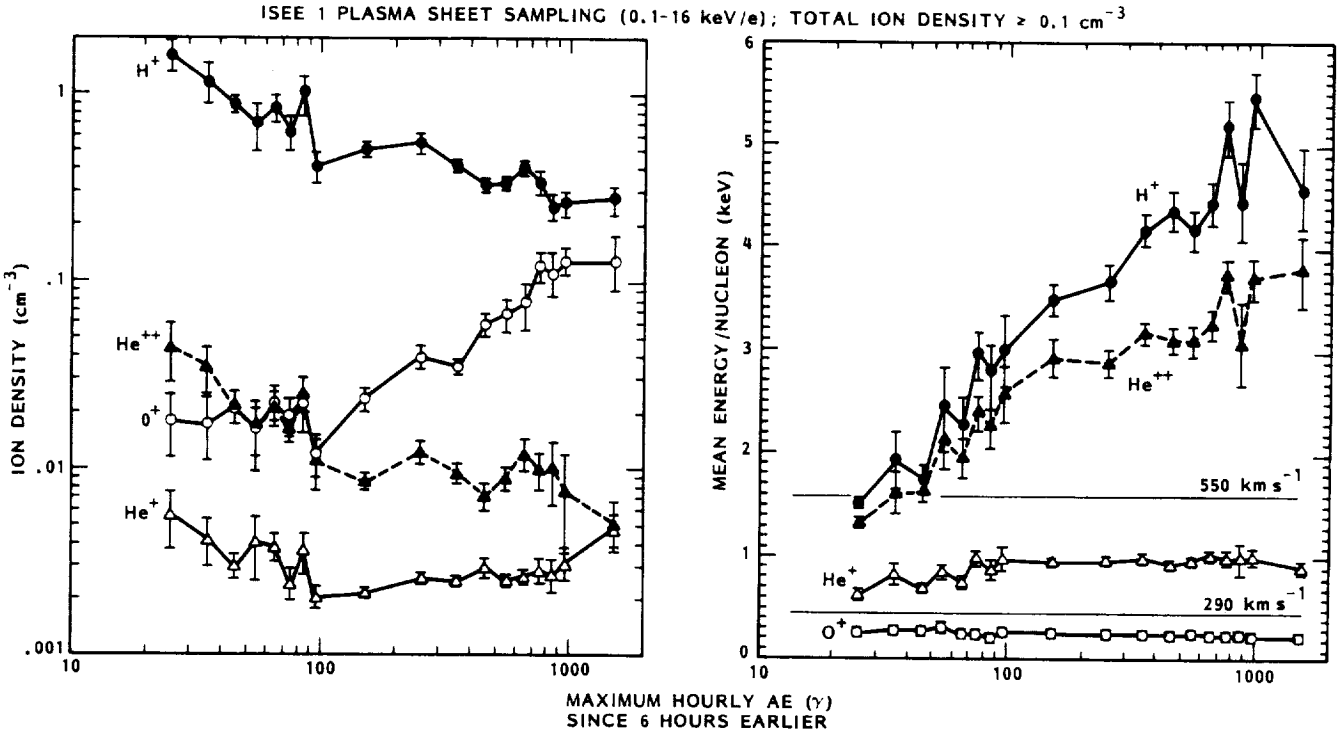

Fig. 1. Central plasma sheet densities (left) and mean energies (right) of the four major ions, averaged over all samples and sorted according to the maximum level of auroral elecrojet (AE) activity during the sampling and the preceding 6 hours. The thin horizontal lines in the right panel indicate the range of energy per nucleon that corresponds to the most common range of solar wind bulk speeds. Error bars in this figure, and in Figures 3–7 and Figure 14 below, show standard deviations of the averages (± one sigma [from *Lennartsson*, 1987]).

He^{++} ions but unlike the O^+ and He^+ ions, increase in energy, on average, with increasing activity, as shown in the right panel. If the mean energies are normalized by the number of nucleons specific to each ion species, as done here, then the H^+ and He^{++} ions clearly show more resemblence to each other than to either of the He^+ or O^+ ions.

The similarlity between the normalized energies of H^+ and He^{++} ions would probably seem greater still if the energy range of the data were extended upward, since the cutoff is measured in energy per charge, not energy per nucleon. For an illustration of that point, see Figure 2. The measured mean energies of the He^{++} and H^+ ions in this example are about 3.1 and 4.0, respectively, when expressed in units of keV/nucleon. However, if a complete Maxwell-Boltzmann distribution is fitted to the measured portion of each distribution function, as described by *Lennartsson and Shelley* [1986], the resulting thermal energies (kT) are 10.2 and 2.7 keV, respectively, which correspond to mean energies (3 kT/2) that are significantly closer in keV/nucleon (3.8 and 4.1). The distributions in Figure 2 are "typical" in the sense that they are fairly well approximated by Maxwell-Boltzmann distributions within the 0.1 to 16 keV/*e* energy range, but that same approximation probably does not hold for the high energy tails [cf. *Christon et al.*, 1991]. On the other hand, the high energy tails, above a few tens of keV/*e*, probably do not follow the same heating trend with increasing activity as the bulk of the distributions [*Christon et al.*, 1991].

As far as the H^+ population is concerned, there is some inherent ambiguity in the relative importance of the solar and terrestrial sources. The He^{++}/H^+ density ratio in the central plasma sheet is on average lower than it is in the solar wind, as can be seen from the left panel in Figure 1. The ratio here peaks at about 3% during quiet times and is an average over

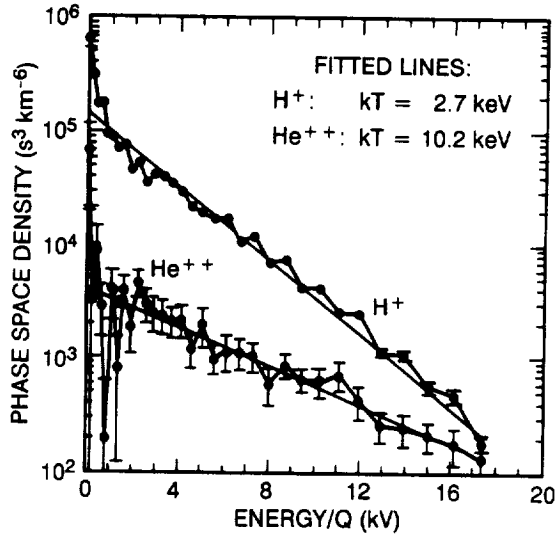

Fig. 2. Typical examples of H^+ and He^{++} energy distributions (spin averaged) in the central plasma sheet. The error bars here show the Poisson standard deviation of the count rates (±one sigma). The thin straight lines represent Maxwell-Boltzmann distributions fitted as described in *Lennartsson and Shelley* [1986]. (The "zigzag" of the data points is partly due to the sampling procedure, which included separate scans of odd and even energy channels.)

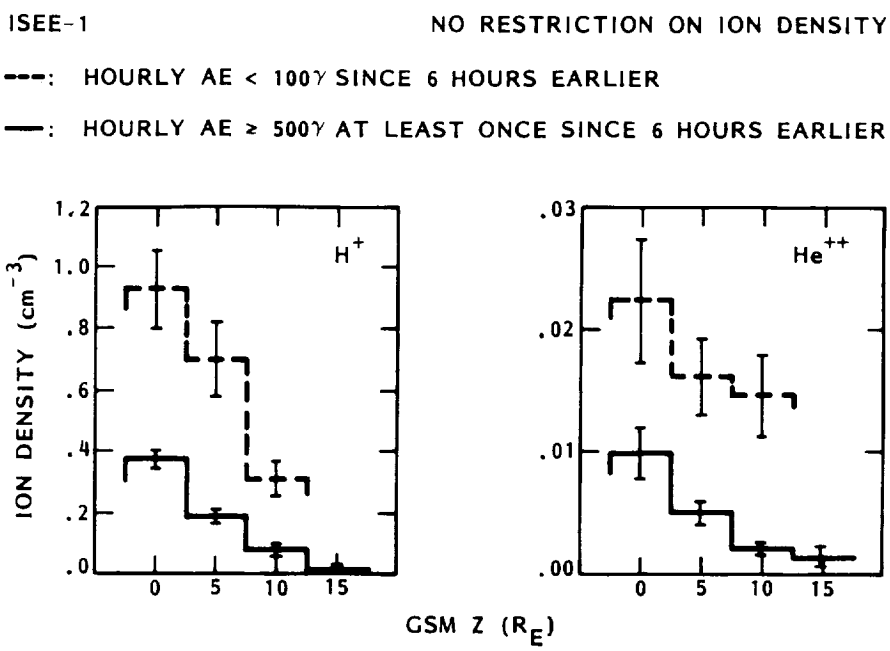

Fig. 3. Densities of the H^+ (left) and the He^{++} (right) during quiet (dashed lines) and active conditions (solid lines), sorted according to the GSM Z coordinate. The averages include samples from the lobe here [from *Lennartsson*, 1987].

the rising phase of solar cycle 21. The average ratio in the solar wind during the corresponding phase of solar cycle 20 has been reported to rise from about 3.3% to about 4.5% [*Feldman et al.*, 1978], suggesting a value around 4% for the solar component in Figure 1. A value of 3%, however, is sufficiently close to suggest a predominant role of the solar source. Whether the balance can be fully accounted for by a terrestrial H^+ population, even during quiet times, or requires some kind of discrimination against He^{++} ions during their transport to the central plasma sheet, is a question that will be addressed in a future study.

4.2. *Some Conditions on a Mechanism for Solar Plasma Entry*

According to the right hand panel of Figure 1, those solar wind ions that find their way to the central plasma sheet are heated to energies substantially above their initial bulk flow energy, except during extended periods of low substorm activity, and this heating becomes stronger with increasing activity. Since this process affects the H^+ ions, which are generally the most numerous, the result is a heating of the plasma sheet ion population as a whole when substorm activity is enhanced. This effect is well documented in the literature [e.g., *Hones et al.*, 1971; *Huang and Frank*, 1986; *Baumjohann et al.*, 1989]. When the H^+ and He^{++} ions are heated, their density is reduced, according to the left panel of Figure 1. This seems to imply that the heating process is associated with an increasing rate of ion loss, perhaps through a combination of injection into the ring current and ejection downtail [e.g., *Hones*, 1979], and that this loss rate temporarily exceeds the rate of solar ion entry.

Because the H^+ ions are so abundant during quiet times, the reduction in their density during active times translates to a reduction of the plasma sheet ion density as a whole [cf. *Lennartsson and Shelley*, 1986]. This reduction takes place all across the GSM Z extent ("thickness") of the plasma sheet, as illustrated in Figure 3, and amounts to a reduction in the total number of particles. This effect is not as well documented in the literature as is the heating [cf. *Huang and Frank*, 1986; *Baumjohann et al.*, 1989], but it is consistent with the substorm-related effect of "plasma sheet thinning", since that thinning occurs without compression of the pre-existing plasma [*Hones et al.*, 1971]. Furthermore, the two panels of Figure 1 can be seen to complement each other in a physical sense, when these data are compared with available solar wind data (about 70% coverage). In particular, by combining the densities and energies of the four ion species in Figure 1 to form a total ion pressure, this pressure is seen to be related to the proton ram pressure of the solar wind, as shown in Figure 4.

The energies used in Figure 4 are those associated with motion perpendicular to the local magnetic field, but because the ion distributions are fairly isotropic, especially the H^+ and the He^{++} distributions, those energies are approximately equal to 2/3 of the energies in Figure 1 (only 2 degrees of freedom). The solar wind pressures in each bin include both single hourly values, and averages of two or three hourly values, depending on the length of the concurrent plasma sheet samplings. Of the 2- and 3-hour plasma sheet samplings available, only those that were obtained while the GSM Z component of the hourly IMF remained either positive or negative for the duration have been used in Figure 4.

Given the relationship in Figure 4, it seems natural that an increase in the average ion energy of the plasma sheet would be accompanied by a decrease in its ion density, or vice versa, in order that the "right" pressure be maintained. This is not to say that the energy and density variations in the plasma sheet always take place while the solar wind pressure remains constant, but for any given solar wind pressure there is probably a wide range of possible combinations of plasma sheet energy and density, depending on other condi-

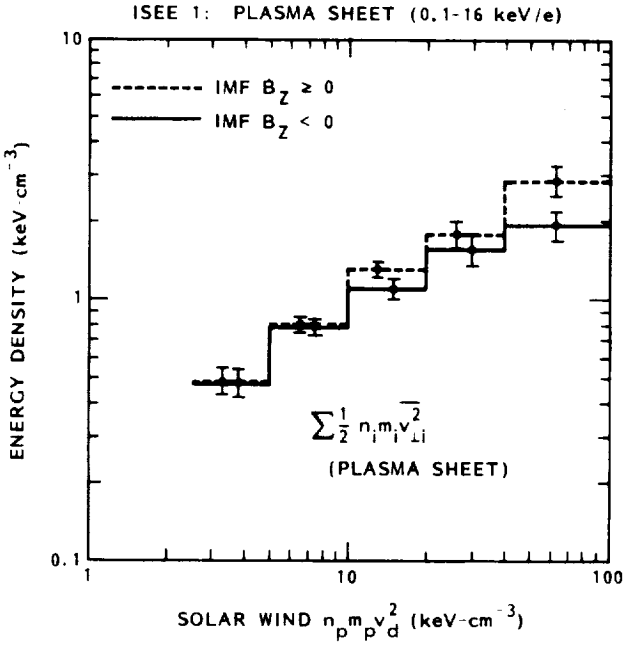

Fig. 4. Average relationship between solar wind (proton) ram pressure and central plasma sheet total ion pressure perpendicular to the tail magnetic field during northward (dashed line) and southward IMF (solid line). The plasma sheet pressure includes the four major ions from Figure 1.

tions. In fact, the heating of the plasma sheet is usually associated with a negative (southward) GSM Z component of the IMF, whereas the solar wind ram pressure is independent of the sign of this IMF component [cf. *Cowzens and King*, 1986]. This situation is illustrated in Figure 5.

As Figure 5 shows, the variations of the solar wind ram pressure are mainly due to the large variations of the solar wind density, and the relationship between pressure and density is the same whether the IMF has a positive or a negative B_Z. By contrast, the solar wind ion component in the plasma sheet displays a pronounced asymmetry with respect to the sign of the IMF Z component. The average density is substantially reduced from solar wind values for both polarities, but it stays at the lowest levels for a negative, or southward, B_Z (solid lines). Hence it does not appear that a southward B_Z "opens" the magnetopause to let solar wind plasma enter; it may rather seem as though it shuts out the solar wind. However, another interpretation is that the magnetopause is always open but that a southward B_Z is associated with a higher rate of loss of solar wind plasma from the region between 10 and 23 R_E of the plasma sheet, due to increased earthward and/or tailward convection [cf. *Hones*, 1979].

The positive B_Z case in Figure 5 (dashed lines) is somewhat too coarsely defined to represent the maximum solar ion content in the plasma sheet, with a given solar wind density. By comparing with Figure 1, it is clear that the plasma sheet ion energies in Figure 5 (right panel) remain too high for this case to be limited to AE < 100 nT. One reason is that hourly averages of the IMF components, as used here, do not account for all significant variations of the B_Z; another reason may be that the plasma sheet content depends not only on the concurrent conditions in the solar wind but also on conditions during the preceding hour, or even earlier. In any case, it does appear from these data that the closer the IMF is to being northward, the weaker the geomagnetic activity is and the larger the plasma sheet H^+ and He^{++} densities are in comparison to the solar wind density. This relationship is further clarified in Figure 6, where the IMF direction within the GSM Y-Z plane is divided into four ranges, but the solar wind pressure has been averaged over. The IMF from the 1 hour preceding the plasma sheet sampling has been used here in order to also allow for some time delay between cause and effect. It is worth remembering that high average H^+ and He^{++} densities are associated with a "thick" (in GSM Z) plasma sheet (Figure 3) and thus with a large total number of particles.

Considering Figure 6, one may ask the question: Does a northward B_Z control the entry process, making it easier for the solar wind plasma to reach Earth's plasma sheet? To address that question, it is necessary to consider the magnitude of the IMF as well. Clearly, a vanishingly small IMF can be of little physical consequence, regardless of its direction, so the effect of the B_Z on the entry process, if any, must increase with increasing field strength, at least increase over some range of field strength. This is examined in Figure 7, which shows the ion densities sorted by four ranges of the IMF strength, under the condition that B_Z be positive. Two sets of IMF values have been used, namely, the hourly value obtained immediately preceding the plasma sheet sampling (solid lines) and the maximum hourly value obtained while the plasma sheet was being sampled (for up to 3 hours at a time; dashed lines).

According to Figure 7, the plasma sheet H^+ and He^{++} densities (top panels) do show some increase with increasing IMF, at least for $|\mathbf{B}| < 15$ nT, but so does the solar wind density as well (bottom left panel). The solar wind densities refer to the same hours as the IMF measurements here, and only the hours preceding the plasma sheet samplings are covered by the solid line. The dotted lines show, for comparison, the averages of all available solar wind samplings in 1978 and 1979 with positive B_Z (the corresponding averages with negative B_Z are identical). As found previously (in Figure 5), the plasma sheet densities are expected to increase with increasing solar wind density for northward B_Z, so the result in Figure 7 is probably negative: an increasing IMF, with a northward Z component, does not cause a larger fraction of the solar wind plasma to enter the plasma sheet. Actually, when $|\mathbf{B}|$ exceeds 15 nT, the plasma sheet H^+ density becomes a smaller fraction of the solar wind density, presumably due to enhanced geomagnetic activity and increasing loss rates. It appears that the plasma sheet He^{++} density increases marginally more than does the H^+ density, but that is probably to be expected, since larger values of the IMF tend to be associated with larger solar wind He^{++}/H^+ ratios, as reported by *Borrini et al.* [1983] and illustrated in the bottom right panel.

In view of Figures 5 and 7 it seems logical to conclude that the solar wind plasma would have ready access to Earth's plasma sheet even if the IMF vanished altogether. Given a typical solar wind density of about 8 cm^{-3}, the density of the solar ion component in the plasma sheet would apparently be about 0.5 cm^{-3}, when averaged over the volume sampled here and averaged over solar wind velocities. The hourly averaged IMF is not actually zero before or during any of the plasma sheet samplings, but several values about 1.5–2.5 nT are included, and those are associated with normal plasma sheet densities (as high as 0.9 cm^{-3}). When Figures 1–7 are

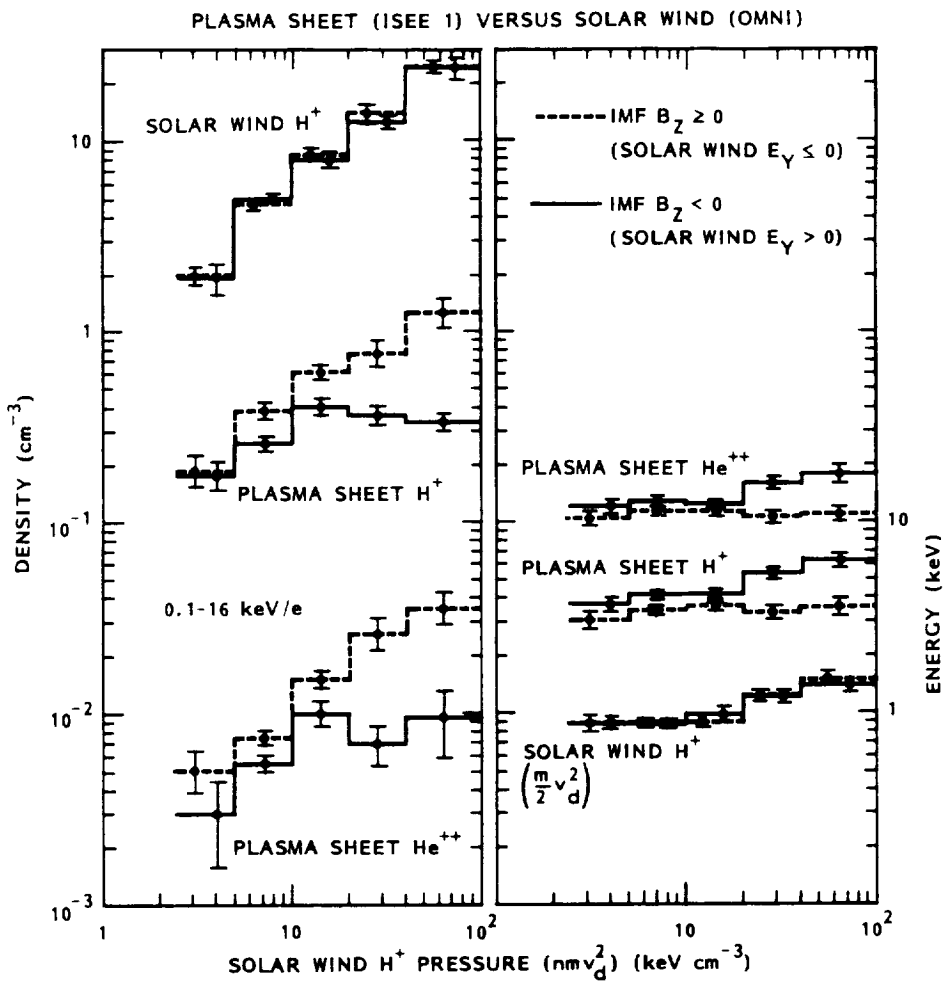

Fig. 5. Densities (left) and mean energies (right) in the central plasma sheet and solar wind, ordered by the solar wind ram pressure and the IMF B_Z.

combined, these statistical data thus seem to suggest the following conditions for solar plasma entry into the plasma sheet: (1) It takes place during a wide range of geomagnetic conditions, including times of extreme quiescence (Figures 1 and 3). (2) It can occur without a substantial increase in the mean ion energies (Figure 1; quiet conditions). (3) It occurs even when the solar wind magnetic field (IMF) is extremely weak, and it may not require any such field at all (Figure 7).

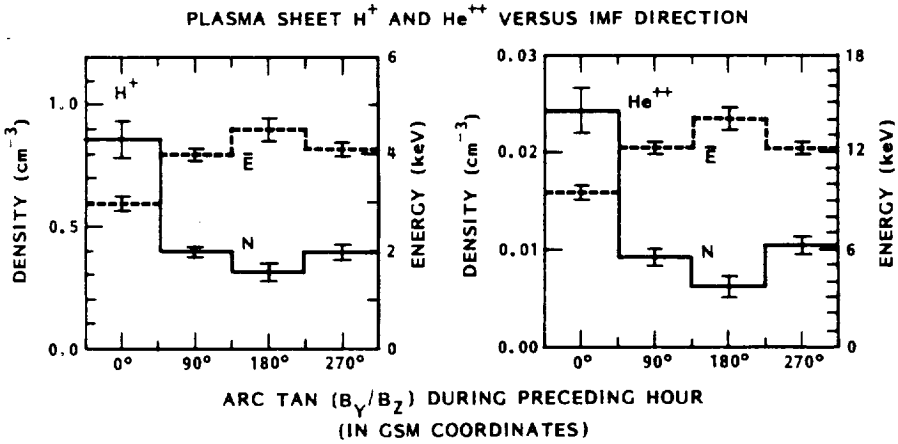

Fig. 6. Densities (solid lines) and mean energies (dashed lines of the H^+ (left) and the He^{++} (right) in the central plasma sheet, ordered by the IMF direction angle in the GSM *Y-Z* plane (during the hour preceding each plasma sheet sampling).

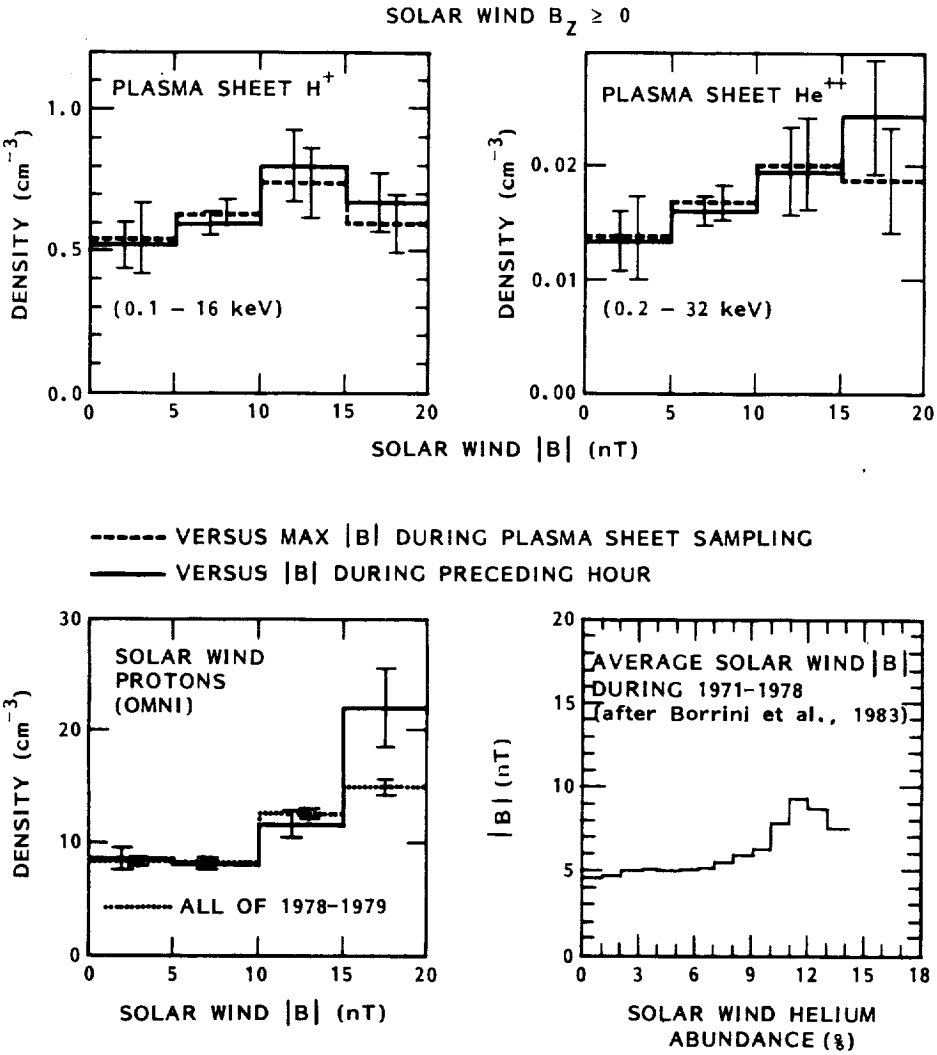

Fig. 7. Ion densities in the central plasma sheet (top) and solar wind (bottom left), ordered by the magnitude of the IMF (while $B_Z \geq 0$), and average IMF magnitude ordered by the solar wind helium abundance in percent (bottom right). The far right bin in the top two and bottom left panels includes $|B| > 20$ nT.

5. Antisunward Flow of H^+ and He^{++} Ions in the Tail

If one were to trace the solar ions backward in space, from the central plasma sheet to the magnetosheath, one approach would be to look for H^+ and He^{++} ions with increasingly "solar wind like" velocity distributions, assuming that their distributions change gradually along their path. No such tracing has been attempted with these data yet, except that it was found in the statistical studies of the central plasma sheet that the H^+ and He^{++} ions become less energetic away from the center axis of the tail, that is, their mean energies decrease both toward dawn and dusk and toward the northern and southern boundaries of the plasma sheet (e.g., Figure 12 of *Lennartsson and Shelley* [1986]).

As shown by Figure 1, the entire (spatially averaged) population of H^+ and He^{++} ions in the central plasma sheet becomes solar wind like in energy when substorm activity subsides and the AE goes to zero. The principal remaining difference from the solar wind is that the plasma sheet ions have become isotropized and dispersed in energy during the entry. If some adjacent region of the tail, inside of the magnetopause boundary layers, can be found to contain such solar wind like ions under more disturbed conditions, or better yet, if it contains H^+ and He^{++} ions that are still flowing antisunward, then it seems logical to assume that this region lies on the path of the solar plasma, and that it is closer to the source. Of particular interest here are the regions forming the boundaries between the plasma sheet and the northern and southern lobes, that is the PSBL. As a case in point, consider Figure 8.

5.1. *A Case From the Literature*

Figure 8, from about 0930 UT and onward, covers an event that has been discussed previously by *Etcheto and Saint-Marc* [1985], although the ion composition aspect of this event has not been explored in depth before. The Plasma Composition Experiment on this occasion was being operated in an abbreviated energy-mass scan mode, only scanning energies between 0.1 and 5 keV/*e* and only sampling four M/Q channels, corresponding to H^+ (open circles), He^{++} (solid circles), O^+ (stars), and background (not

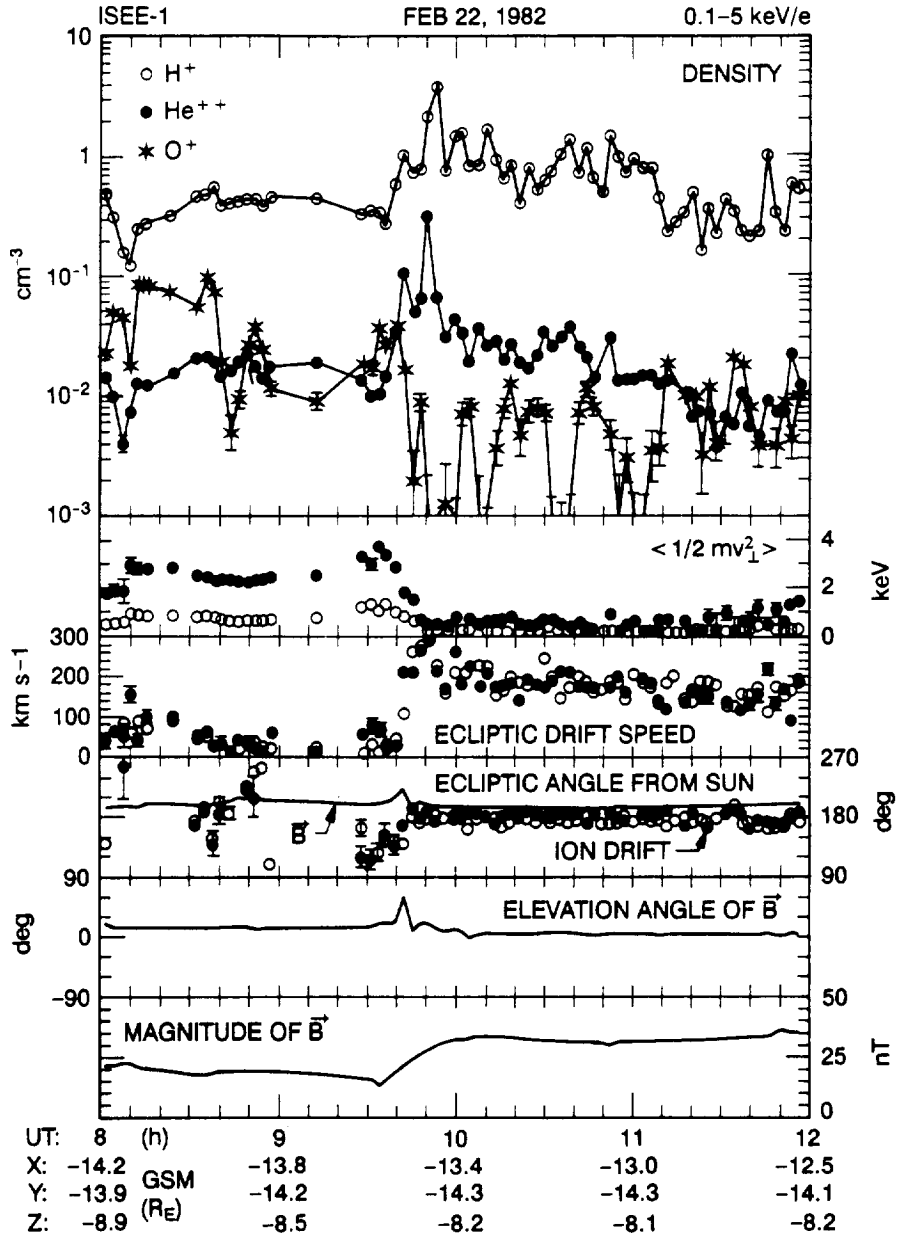

Fig. 8. From top to bottom: number densities; thermal energies associated with motion perpendicular to bulk flow vector (in solar ecliptic plane); bulk flow speeds; longitude angles of bulk flows and of local magnetic field (solid line) counted positive eastward from Sun direction; elevation angle of local magnetic field (above and below ecliptic plane); magnitude of same. Error bars show standard deviations (±one sigma) carried over from counting statistics (mostly smaller than data symbol).

shown). As a result, the time resolution is fairly high here, with each scan cycle requiring about 2.8 min. The coverage is continuous, except for a few data gaps prior to 0930 UT. The ISEE 1 magnetic field data [*Russell*, 1978] in the bottom three panels have been averaged over the 2.8-min cycle time of the mass spectrometer and are represented by points centered at the middle of each cycle and interconnected by solid lines.

The ion data in Figure 8 are in the form of velocity moments, calculated by the second method described in section 3 above (assuming rotational symmetry around the flow velocity vector). Before discussing the content of Figure 8 it may be of interest to compare the resulting ion number density with the electron density that Etcheto and Saint-Marc inferred from plasma wave data obtained by the ISEE 1 and 2 relaxation sounder. Such a comparison is shown in Figure 9.

The ion density in Figure 9 is based on the total ion count rate, assuming that it is dominated by H^+ counts. This provides for a more continuous coverage in time than summing the H^+, He^{++}, and O^+ densities. In this case it is also well justified to assume that the H^+ ions are dominant, as is clear from Figure 8 (top panel). In any case, the ion density is in fair agreement with the electron density when they both peak, while it tends to be lower afterward, forming the lower envelope of the many electron density values. One

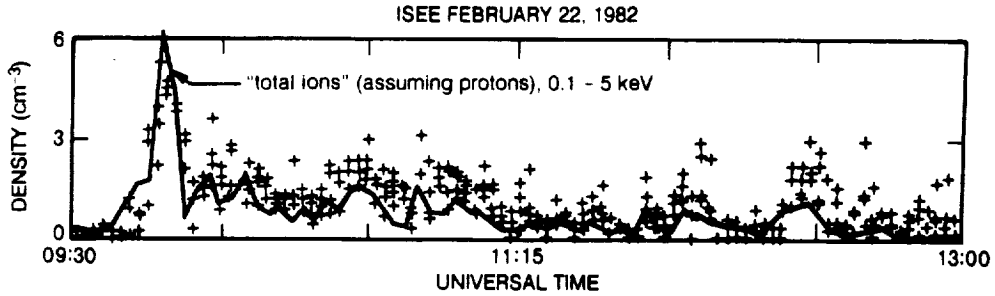

Fig. 9. Comparison between ion density calculated from total ion count rates (solid line; assuming all H^+) and the electron density inferred from wave data (pluses; the latter from *Etcheto and Saint-Marc* [1985]).

possible explanation for this trend is that the ion bulk flow is sufficiently fast to bring most ions to energies above 0.1 keV/*e* at the time of the density peak, which is indeed when the flow speeds are at their maximum (Figure 8; third panel down), while it is insufficient later on. Other explanations may involve the different temporal resolutions of the two kinds of measurements.

Returning to Figure 8, it can be seen that the population of H^+ and He^{++} ions changes character at about 0940 UT. Prior to this time the ISEE 1 spacecraft is within the central plasma sheet, although close to its southern boundary and far toward the dawn flank (fairly low thermal energies in the second panel); after this time it is within the southern PSBL, as inferred by *Etcheto and Saint-Marc* [1985]. While in the central plasma sheet, the instrument measures an essentially isotropic population of H^+ and He^{++} ions, one that is drifting only slowly (third panel) and in varying directions (fourth panel), having most of its energy in the form of thermal (random)motion (second panel). After 0940 UT, while in the PSBL, the instrument measures a strongly ansotropic population of these ions, one that is flowing rapidly and fairly steadily antisunward, or tailward, and has much lower thermal energies. The latter population appears quite solar wind like, even though the sum of the bulk flow energy and the thermal energy (including thermal motion along the flow vector), observed to vary between 0.3 and 1.2 keV/nucleon, is somewhat low compared to the solar wind energies at this time (1.3 to 1.5 keV/nucleon [cf. *Couzens and King*, 1986]).

It may be noted that this solar wind like ion population is observed on a day which is not extremely quiet but actually somewhat disturbed. The 3-hour *Kp* index during the first half of this day has the values 3+, 5−, 3−, and 4, and the hourly *AE* index ranges between 86 and 660 (being highest between 1000 and 1100 UT). Had the ISEE 1 spacecraft been well within the central plasma sheet at this time, the H^+ and He^{++} mean energies would probably have been measured to be about 3 to 4 keV/nucleon, according to Figure 1. It may also be noted that the antisunward flow of the H^+ and He^{++} ions after 0940 UT in the fourth panel of Figure 8 is not exactly along the magnetic field vector, but some 10°–40° to the right, that is toward the interior of the tail. This translates to a cross-*B* drift in the range of 30–100 km s^{-1} and is consistent with there being duskward $\mathbf{E} \times \mathbf{B}$ drift in the PSBL on the dawnside. This particular feature will be dealt with at some length in section 6.

5.2. *Some Events Observed at Substorm Onsets*

Plasma flows located in a layer of limited extent in GSM *Z*, such as the PSBL, are most readily detected when this layer moves back and forth across the path of the ISEE 1, which often happens in conjunction with substorm activity [cf. *Eastman et al.*, 1985]. Antisunward flows of the kind illustrated in Figure 8, even if they exist most of the time, may therefore tend to be observed as transient events. An example of such transient flows is illustrated in Figure 10.

Figure 10 has basically the same format as Figure 8, but the data from each accumulation period are displayed as horizontal segments or bars. The instrument energy-mass scan cycle, as indicated by the horizontal bars, is much longer in this case, about 17 min, and consists of multiple scans through every fourth energy channel at various values of M/Q, covering the full energy range for each M/Q by using alternating sets of energy channels. Each energy is maintained for 4 s (1.3 spin revolutions). This cycle time is too long to adequately resolve the substorm dynamics, but by interpolating the total ion count rates in energy and assuming that these are dominated by H^+ ions, it is possible to calculate "total ion" moments at a higher rate, as shown by the solid lines in the top three panels. The magnetic field data shown by solid lines in the bottom three panels have been averaged over the same time intervals used for the total ion data. Mass analyzed data are shown for H^+, He^{++}, and O^+, using the same symbols as in Figure 8, as well as densities only for He^+ ions (crosses; top panel). Due to the rather complex energy-mass scan, it is not practical to display the various ions with their actual sampling times within each scan cycle. It is important to remember, however, that each ion species has been measured intermittently, and that different species have been sampled minutes apart. This probably accounts for most of the differences in flow speed and direction between H^+ and He^{++} ions, for example (third and fourth panels).

The event of special note here is the density peak near noon (top panel). This peak is similar in magnitude to the peak density in Figure 8, when measured by the total ions, and like the peak in Figure 8 it contains H^+ and He^{++} ions with very low thermal energies (second panel) and rather fast antisunward flow (third and fourth panels). This particular event is one of about two dozen substorm onset events which were brought to the attention of the author by C. Y. Huang (private communication, 1988) (see also *Huang et al.* [1992]). One probable effect of this substorm [*Huang et al.*, 1992] is the sharp rise in the ion thermal energies after 1200 UT. This was a rather moderate substorm, with the hourly *AE* peaking about 300 nT. Prior to this substorm the *AE* had remained about 50–100 nT for many hours.

The antisunward flows of H^+ and He^{++} ions in Figure 10, clearly observed during five of the 14 instrument scan cycles

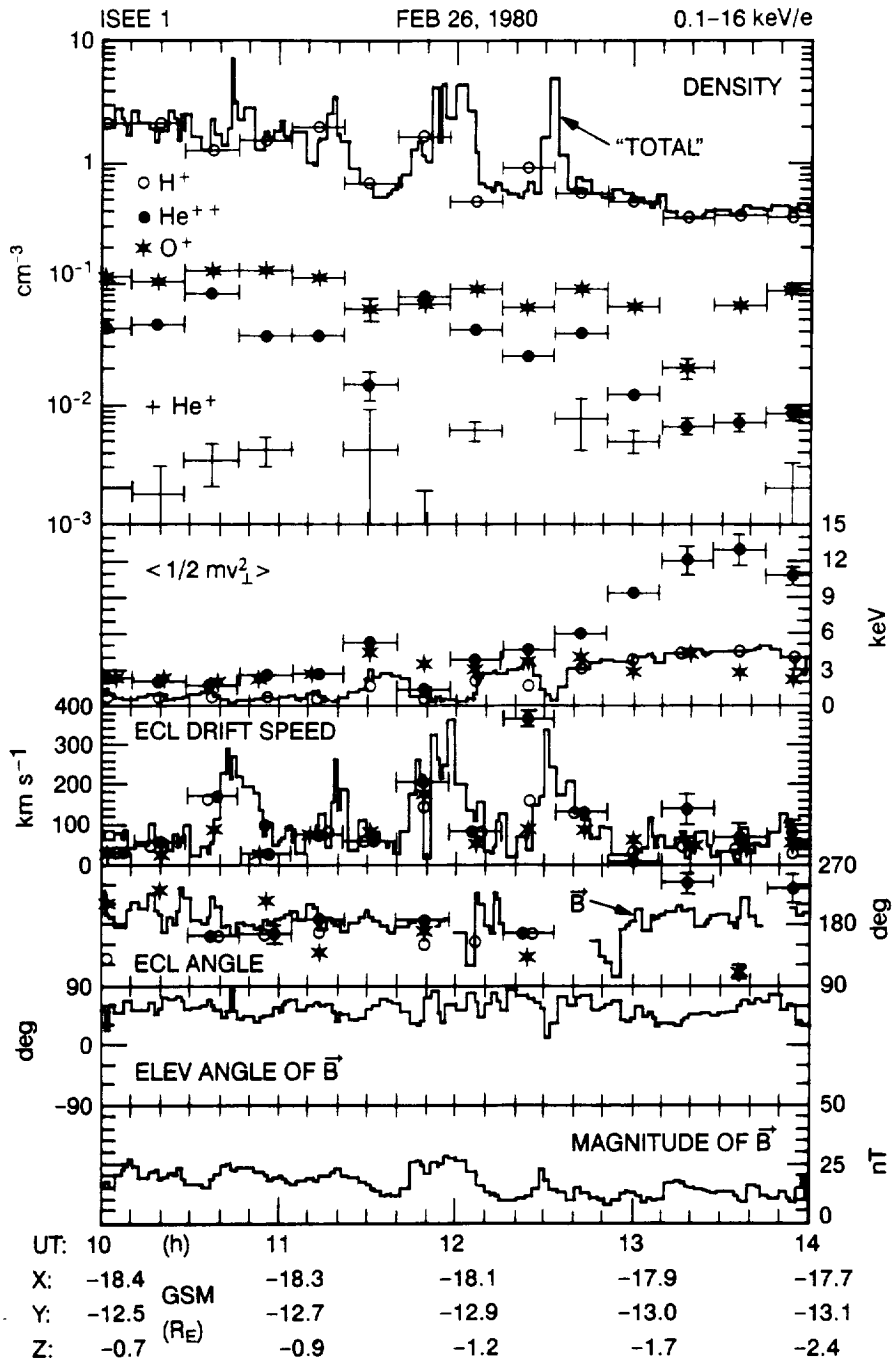

Fig. 10. Same format as Figure 8, except that the mass resolved moments have been averaged over longer intervals (horizontal bars), and the moments based on total count rates (assuming H^+ and using shorter averaging) have been included in the top three panels, shown by solid lines. Note that in the bottom three panels, solid lines refer again to the local magnetic field.

(fourth panel), are also located far toward the dawn flank, like those in Figure 8. There is, however, a significant difference in the magnetic field between the two figures. In Figure 8, after about 1000 UT, the field is nearly parallel to the ecliptic plane (second panel from bottom) and fairly constant in magnitude (bottom panel), two conditions that are common in the vicinity of the tail lobes and therefore consistent with this region being the PSBL, as inferred by *Etcheto and Saint-Marc* [1985] (compare also *Parks et al.* [1984]), although those same conditions probably apply equally well to the plasma mantle (tail lobe magnetopause boundary layer [cf. *Rosenbauer et al.*, 1975]). In Figure 10, by contrast, the magnetic field elevation angle is variable and generally greater than 30°, and the field magnitude also varies, and it is weaker than in Figure 8. These conditions are more typical of the central plasma sheet, but they are probably also consistent with the LLBL (low-latitude magnetopause boundary layer [cf. *Eastman et al.*, 1976]).

Based on the in situ data alone, it cannot be excluded that the antisunward flows in Figure 10 are located in the LLBL, rather than in the plasma sheet, although this distinction depends on one's definition of the LLBL. The data in Figure

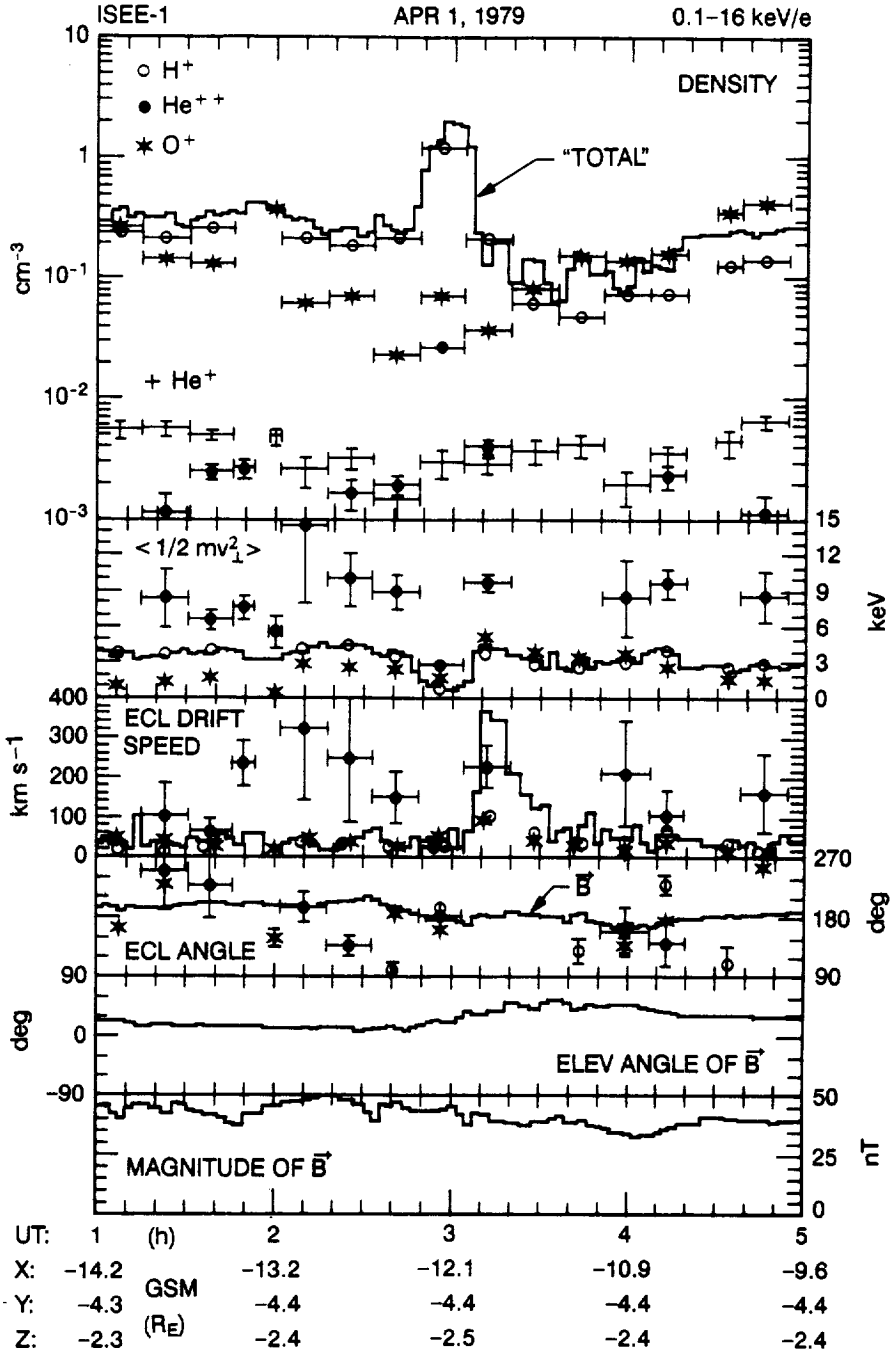

Fig. 11. Same format as Figure 10, except the energy-mass scan cycle is slightly shorter.

10 were obtained at about 13 R_E distance from the GSM X axis (from the Earth-Sun line), near GSM $X = -18$ R_E, which would seem to be well inside of a nominal magnetopause. Compared to Figure 8, the ISEE 1 is 3–4 R_E closer to the GSM X axis in Figure 10 and 4–5 R_E farther down the tail, so it ought to be several R_E farther away from the magnetopause in Figure 10 (including tail flaring). The magnetopause location does depend on solar wind conditions, but those conditions, according to *Couzens and King* [1986], do not suggest that the magnetopause is more compressed at the time of Figure 10.

Since it may be doubted that the antisunward flows of H^+ and He^{++} ions in Figures 8 and 10 are really inside the magnetotail, it is worth considering Figure 11. Figure 11 has the same identical format as Figure 10, except the energy-mass scan cycle is slightly shorter. Again of special note, the density peak is near the center of Figure 11 (top panel), around 0300 UT. As in Figures 8 and 10, this peak contains H^+ and He^{++} ions with reduced thermal energy (second panel), which are flowing antisunward (fourth panel). The most noticeable difference from before is the much lower flow speed, only a few tens of km s^{-1} (third panel). The O^+ ions are more abundant here than in either of Figures 8 and 10, but only the H^+ and He^{++} ions have a distinct peak in their densities around 0300 UT, which is consistent with the peak being dominated by ions of solar origin. Hence, in this

case a dense population of antisunward flowing solar wind like ions is located only about 5 R_E from the GSM X axis, at GSM $X = -12\ R_E$, which surely is far inside of any realistic magnetopause (solar wind conditions fairly normal at this time). Judging from the geomagnetic field magnitude and direction (bottom three panels), this event is very likely in the southern PSBL. This interpretation is further supported by the fact that the ion densities and energies are plasma sheet like both before and after (compare Figure 1).

The antisunward flow near 0300 UT in Figure 11 is yet another event from the aforementioned list of substorm onsets (C. Y. Huang, private communication, 1988). In this case there is not a marked increase in the H^+ and He^{++} thermal energies, when compared to conditions before the flow event, but there is another feature commonly associated with substorms in the ISEE data: the antisunward ion flow at substorm onset is followed by a burst of rapid sunward ion flow [cf. *Eastman et al.*, 1985]. The latter is best seen in the total ion data here by the peak drift speed between 0310 and 0320 UT (third panel). Since the flow direction is sunward at this time, also in the mass resolved H^+ and He^{++} data, it falls outside of the angular range of the fourth panel. As in the case of Figure 10, the substorm is fairly moderate, with a peak hourly *AE* of 561 nT between 0300 and 0400 UT.

Rather than showing more of these events in the format of Figures 10 and 11, the most relevant parameters of the entire set have been listed in Table 1, and the spatial location of each event has been indicated in a graphical format in Figure 12. The numbering is the same in Table 1 and Figure 12 and is ordered by dates. The events in Figures 10 and 11 have events 14 and 3, respectively. The event in Figure 8 has also been included as event 23.

The times listed in Table 1 are times of persistent antisunward flow, as defined by the total ion count rates, called "all ions" here. The flow during these intervals remains between 90° and 270° from the sunward direction in almost all cases, and it is generally between 150° and 210° when the number density peaks (assuming H^+ ions). A few of the longer intervals include one or two brief (1–3 min each) excursions into the sunward sector. The maximum flow speed during each interval either coincides with the maximum number density or occurs adjacent to it. The mass resolved data, in all but one event, refer to the single energy-mass scan cycle that contains the maximum in the "all ion" number density. The only exception is event 23 (Figure 8), where two adjacent energy-mass scan cycles at the density peak have been averaged in order to give more equal weights to the H^+ and He^{++} ions (only 2.8 min per scan cycle in that case). The mean energies listed in Table 1 are total energies, including the bulk flow energy. The percentage ratios in the rightmost column refers to number densities.

The time intervals in Table 1 generally precede the substorm onset as defined by C. Y. Huang (time of increasing energetic ion fluxes [cf. *Huang et al.*, 1992]), and some of them end as early as 10 min or more prior to onset, as the ISEE 1 moves into a tail lobe with count rates too low to provide reliable moments (plasma sheet thinning). In about half of the 23 events the antisunward flow is observed as the ISEE 1 moves from the plasma sheet and into the southern or northern tail lobe, suggesting that the flow is located in or near the PSBL in those events. In all events, except events 8 and 14, the magnetic field magnitude and direction at least make it probable that the location is adjacent to a tail lobe. This includes a consideration of the ion beta values, which

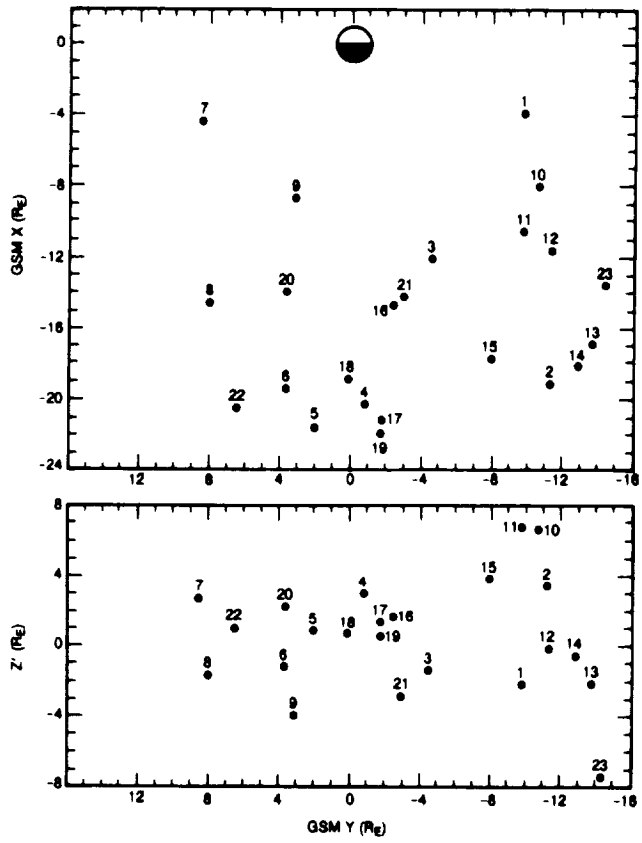

Fig. 12. Location of events of antisunward flowing H^+ and He^{++} ions (at middle of event; see Table 1). Top panel shows location in GSM X versus Y; bottom panel shows distance above and below nominal "neutral sheet", as defined by *Fairfield and Ness* [1970].

are less or much less than unity in all events but events 8 and 14. Of the latter two, event 14 has already been discussed above (Figure 10). Event 8 may be in the central plasma sheet (compare Figure 12).

In all events listed in Table 1 the H^+ ions are dominant, their density being at least 10 times higher than that of the second most abundant species, which is either the He^{++} or O^+. Considering the energies of the H^+ ions, as listed in the fourth column from the right, it would be reasonable to assume that these ions are of terrestrial origin, having been accelerated upward in the auroral regions [cf. *Yau et al.*, 1985]. This would probably seem the most logical interpretation if only the total ion flux was being measured, without the benefit of mass separation. Even with the ions separated, this interpretation comes to mind, since the H^+ ions are observed together with O^+ ions that are almost certainly of terrestrial origin. However, when the energies of those two species are compared (O^+ energies in the second column from the right), it is seen that the O^+/H^+ energy ratio ranges from a low of 0.16 to a high of 6.7, which is a 42-fold range. This contrasts with the He^{++}/H^+ energy ratio (He^{++} energies in the third column from the right), which only ranges between 2.6 and 5.1. Expressed in a statistical average and a sample standard deviation,

$$O^+\text{-energy}/H^+\text{-energy} = 2.1 \pm 2.1$$

$$He^{++}\text{-energy}/H^+\text{-energy} = 3.7 \pm 0.7$$

TABLE 1. Some Events of Antisunward Flow

Event			All Ions		Mass Resolved			
					Mean Energy, keV			
No.	Date, year/day	Time, UT	V_{max}, km/s	N_{max}, cm^{-3}	H^+	He^{++}	O^+	He^{++}/H^+, %
1	79/050	1351–1400	200	0.45	3.06	10.3	0.49	5.1
2	79/061	1104–1147	130	0.82	1.59	6.56	7.82	3.3
3	79/091	0252–0302	60	2.04	1.17	4.16	1.72	2.2
4	79/100	0441–0528	70	0.49	2.90	10.9	4.49	2.0
5	79/104	1551–1707	220	0.40	3.71	9.55	3.50	5.0
6	79/114	1445–1522	300	0.18	5.11	17.5	6.09	1.7
7	79/127	1150–1221	200	0.25	1.97	9.57	0.81	1.3
8	79/138	1749–1829	30	0.79	3.69	12.1	1.58	1.3
9	79/143	2015–2027	25	0.12	2.15	8.49	3.85	5.6
10	80/018	0754–0831	70	0.20	2.53	9.73	0.97	1.7
11	80/030	0809–0902	45	0.41	1.72	7.38	1.62	1.3
12	80/032	2000–2010	230	0.07	2.75	13.9	2.31	1.6
13	80/050	0357–0410	225	0.18	4.83	12.3	5.11	1.3
14	80/057	1145–1206	365	4.46	1.11	3.11	7.36	4.7
15	80/059	0759–0836	125	0.15	3.48	10.5	5.59	1.6
16	80/068	1509–1600	50	0.47	2.00	7.74	4.45	2.2
17	80/083	1051–1113	100	0.88	0.94	4.18	6.26	3.5
18	80/085	1406–1520	120	1.66	0.50	1.91	3.37	1.7
19	80/091	0235–0309	160	1.60	1.97	7.20	3.70	3.6
20	80/092	1228–1250	35	0.14	1.33	5.04	2.46	4.5
21	80/094	0316–0323	30	0.28	1.49	6.24	1.11	6.4
22	80/107	1026–1055	65	0.39	1.35	5.74	3.53	4.8
23	82/053	0936–1300	290	6.16	0.75	2.35	1.38	6.5

Hence there is virtually no correlation between the H^+ and O^+ ions in terms of energy (correlation coefficient = 0.1), whereas the H^+ ions are fairly well correlated with the He^{++} ions, which are presumably of solar origin (correlation coefficient = 0.9). The modest scatter in the He^{++}/H^+ energy ratio may be due in part to a small and variable terrestrial component of the H^+ but is probably also due in large part to the fact that different ion species are always sampled at slightly different times (minutes apart). This correlation between the H^+ and He^{++} energies, coupled with the fact that the He^{++}/H^+ energy ratio is close to the same as in the solar wind (about 4.0), makes it very plausible that the antisunward flows listed in Table 1 are all dominated by ions from the solar wind.

It should also be pointed out that the H^+ and He^{++} ions observed during these events resemble the ion component of a plasma region recently described by *Zwolakowska and Popielawska* [1991]. This region, named the "warm envelope of the plasma sheet" by Zwolakowska and Popielawska is located between the tail lobes and the hotter and more isotropic plasma sheet, and it is characterized by densities greater than 0.1 cm^{-3}, electron temperatures lower than 100 eV, and an ion component dominated by H^+ and He^{++} ions with a solar wind like ratio. It has the greatest thickness (in GSM Z) during periods of northward IMF and is the thickest near the flanks of the tail. It is presumably related to the PSBL, which has been defined mostly by ISEE data, but the relationship is unclear, according to the authors, perhaps due in large part to different measuring conditions. Their observations have been made from the Russian spacecraft Prognoz 8, which, like the ISEE 1 and 2 spacecraft, has a strongly elliptical orbit (apogee at 30 R_E) but an orbit of much greater inclination (65°), providing almost perpendicular traversals of the northern lobe. Zwolakowska and Popielawska suggest that this "warm envelope" consists mostly of solar wind plasma originating from the LLBL. Unfortunately, the orientation of the Prognoz 8 spin axis (sunward) precludes a direct verification of the antisunward flows described here.

6. Discussion

Given Table 1 and Figure 12, the natural question to ask is: What mechanism brings solar wind ions to these locations inside the tail, in most cases without substantially increasing their total energy (bulk flow energy plus thermal energy)?

At first glance, it might seem possible that these antisunward flowing ions actually entered much farther down the tail, where they were deflected toward Earth (sunward) by the mechanism discussed by *Speiser* [1965] and others and subsequently mirrored close to Earth before being intercepted by the ISEE 1. This interpretation does have problems in these cases, however. One is the energies; these ions do not generally have energies quite as large as one would expect from this mechanism, where the initial deflection is caused by the combined action of a dawn-to-dusk electric field, which accelerates the ions, and the Z component of the geomagnetic field [cf. *Lyons and Speiser*, 1982]. Another problem is the location; the mirrored and antisunward flowing ions would be expected to be closer to the midplane of the plasma sheet than the sunward flowing ions, due to $\mathbf{E} \times \mathbf{B}$ drift in the dawn-to-dusk electric field. In all cases where the ISEE 1 enters either of the lobes, the antisunward flowing ions are found adjacent to the lobe, and there is no evidence of sunward flows in the lobe itself (not illustrated).

Another possibility, which is the one argued here, is that

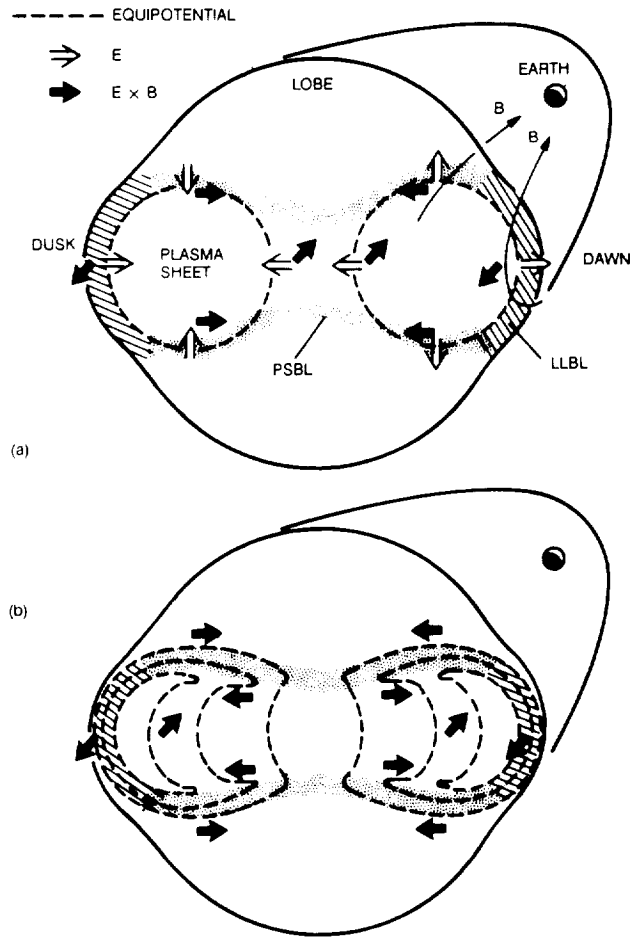

Fig. 13. Cross sections of a geomagnetic tail with internal closure of equipotentials (tubular) associated with electric field in the low latitude magnetopause boundary layer (LLBL). (*a*) Conceptual geometry showing associated electric field (open arrows) and **E** × **B** drift (solid arrows). (*b*) Equipotentials adjusted to fit observed cross-*B* drifts in central plasma sheet (see text).

these ions reach their point of observation by duskward or dawnward **E** × **B** drift parallel to the PSBL, having entered the tail on the flanks, in the LLBL (on closed field lines [cf. *Eastman et al.*, 1976]), or at the junction of the LLBL and the plasma mantle (on open field lines [cf. *Rosenbauer et al.*, 1975]). A feasible mechanism for this kind of motion is shown schematically in Figure 13.

Figure 13 is based on the fact that the LLBL on either flank is at least partially situated on closed geomagnetic field lines, and is therefore associated with a polarization electric field directed toward dawn [e.g., *Eastman et al.*, 1976; *Mitchell et al.*, 1987]. This field, having the same direction on both the dawn and dusk flanks, allows the boundary layer plasma to flow tailward (antisunward). The mechanism responsible for these boundary layers need not be an issue here; the essential aspects are empirical: the LLBL is virtually always present and appears to contain plasma of mostly solar origin at energies below 10 keV [*Mitchell et al.*, 1987].

Even though the electric field in the LLBL may vary in magnitude over the course of time, it does maintain its dawnward orientation, at least in an average sense, and therefore must have a curl-free component, as assumed in Figure 13. Another way of stating this is to integrate Faraday's law from time t_1 to time t_2, choosing these times such that the tail magnetic field has identical configurations at both t_1 and t_2:

$$\int_{t_1}^{t_2} (\text{curl } \mathbf{E})\, dt = \text{curl} \left(\int_{t_1}^{t_2} \mathbf{E}\, dt \right) = -\int_{t_1}^{t_2} \left(\frac{\partial}{\partial t} \mathbf{B} \right) dt = 0$$

In other words, the time-averaged electric field must be curl-free, at least, which means that it must be associated with closed equipotential surfaces. Whether all such surfaces close within the tail, as suggested in Figure 13, may be questionable, but the ones that do will encounter a different magnetic field orientation at different points, as indicated in Figure 13*a*. Since the electric field is perpendicular to each equipotential surface (open arrows), the associated **E** × **B** drift direction will vary as indicated by solid arrows. These arrows have the proper directions, near both dusk and dawn and near both the northern and southern lobes, to transport solar plasma (ions and electrons) from the tail flanks and into the central plasma sheet.

Is this potential configuration supported by data? The electric fields near the midplane, in both the LLBL and the central plasma sheet, have the directions usually associated with those regions in the literature, so the questionable parts are the ones ascribed to the PSBL here. Unfortunately, the spin axis of the ISEE 1 is generally parallel or antiparallel to the expected directions of the electric field in these parts, so the ISEE 1 Double Probe Experiment [*Mozer et al.*, 1978], having booms extended only within the spin plane, is not well suited to prove or disprove this picture.

Of the antisunward flows examined here, event 23 in Table 1 shows the most consistent drift across the magnetic field in a direction that agrees with Figure 13*a* (compare Figure 8, fourth panel, after 0945 UT). The other events present a more complex picture. If the total ion moments are used (assuming H^+ ions are dominant), in order to maximize time resolution (1–3 min), the drift velocity during several events shifts, once or more, from one side of the magnetic field to the other, and in some cases the drift is consistently opposite to the direction prescribed by Figure 13*a* for that quadrant of the tail. Barely more than half of the events show a clear predominance of drift in the "right" direction. On the other hand, if the equipotential surfaces are folded near the lobes, as outlined in Figure 13*b*, they can be made consistent with the observed drift directions, assuming that the events with a drift toward the flanks are observed further into the plasma sheet. This is not a mere contrivance; equipotential surfaces of this shape could be produced by a net charge in the PSBL, a charge with the same polarity as the inside of the adjacent LLBL (positive at dawn, negative at dusk).

Some indirect support for Figure 13 may be found in the works of *Orsini et al.* [1990, and references therein]. They have examined a large number of strongly collimated antisunward flows of ions in or near the PSBL, using the ISEE 2 EGD Positive Ion Experiment [*Bonifazi et al.*, 1978], covering energies between about 50 and 5 keV/*e*. The ions have been observed during geomagnetically disturbed periods, and have been identified as O^+ ions, using concurrent data from the ISEE 1 Plasma Composition Experiment. The EGD instrument, when pointing in a sunward sector, provides a higher angular resolution (5.6° or 2.8°, depending on bit rate) than the Plasma Composition Experiment and is

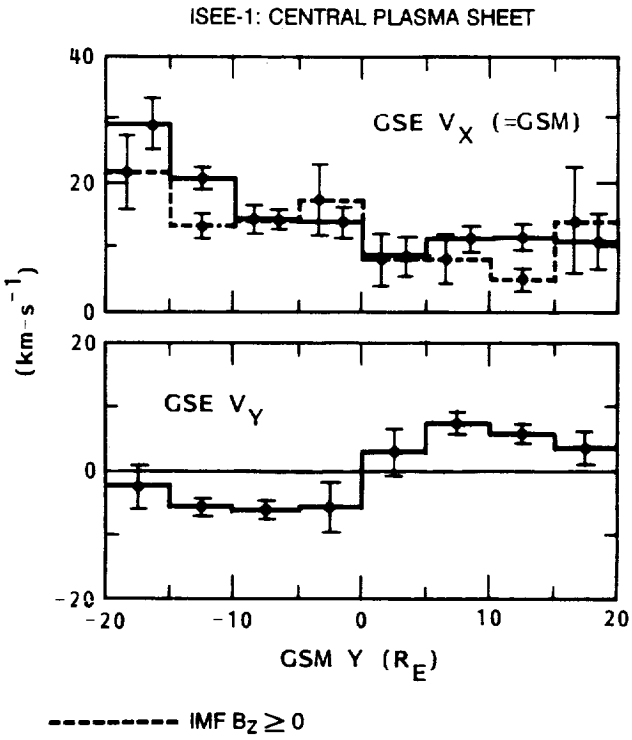

Fig. 14. Average plasma sheet H^+ drift velocity perpendicular to **B** and parallel to solar ecliptic plane (GSE X-Y plane; see text for definition). Solid lines show averages of all samplings, regardless of solar wind conditions; dashed line in upper panel only includes samplings taken while the concurrent hourly IMF B_Z remained northward (for up to 3 hours at a time). The corresponding average of the V_Y component is not significantly different from the one shown in the lower panel and has been omitted. (Error bars show standard deviation of the averages.)

more sensitive to the relative orientation between the ion flow and magnetic field directions. The statistical results of *Orsini et al.* show strong evidence of **E** × **B** drift (up to 40 km s^{-1}) from the tail flanks toward the center of the tail on the northern lobe side of the plasma sheet (e.g., Figure 10 of *Orsini et al.* [1990]), in agreement with Figure 13*a* or 13*b*. Their results suggest a similar situation on the southern lobe side of the plasma sheet, but the statistics is poor there. Their results also indicate that the **E** × **B** drift reverses direction across the PSBL and point toward the flanks immediately inside the plasma sheet. This would again suggest that the equipotential surfaces of Figure 13*a* be modified as shown in Figure 13*b*.

Further corroborating evidence for **E** × **B** drift toward the flanks inside the plasma sheet can be found among the results of the statistical study discussed in section 4 (among results not previously published). This is illustrated in Figure 14, which shows the average GSE X and Y components (spin plane components) of the H^+ bulk velocity in the central plasma sheet, derived under the restriction that only measurements at pitch angles between 45° and 135° be included in the moment calculations. These velocity components are thus rough measures of the average ion drift perpendicular to the measured magnetic field (and in the spin plane). According to this figure, the ion drift inside the plasma sheet is generally sunward, even during periods of northward IMF, and toward the dawn and dusk flanks. This is consistent with a spatial averaging of the **E** × **B** drift produced by the equipotential surfaces in Figure 13*b*, not including the drift immediately adjacent to the lobes. The lobes and the near-lobe regions of the plasma sheet were intentionally excluded from the statistical material used for Figure 14 (compare criteria used by *Lennartsson and Shelley* [1986]).

It should be mentioned that *Orsini et al.* [1990] interpreted their results in terms of a slightly different electric field model, namely the one constructed by *Rostoker and Boström* [1976]. One salient feature of that model is charge layers between the lobes and the plasma sheet, positive on the dawn side of midnight, negative on the dusk side, predicting the same kind of dawn-dusk and dusk-dawn drifts as observed by Orsini et al. around the PSBL. This is the only model feature addressed by *Orsini et al.*, so their results can also be seen as indirect support of Figure 13b. The model of Rostoker and Boström differs somewhat from Figure 13*b* in the treatment of the central plasma sheet (Figure 4 of Rostoker and Boström), and it extends through the tail lobes, which Figure 13*b* does not address. As far as the central plasma sheet is concerned, it is worth remembering that Figure 13*b* is consistent with the observed average drifts in Figure 14. Furthermore, Figure 13*b* is by its definition consistent with the known direction of the electric field in the LLBL [e.g., *Eastman et al.*, 1976]. As far as the tail lobes are concerned, the electric field structure may be largely controlled by the electromagnetic conditions in the solar wind itself. Those same conditions probably influences the electric field in the plasma sheet as well, especially during geomagnetically disturbed times, but Figure 13*b* may nevertheless represent some kind of "ground state".

7. Concluding Remarks

Closing equipotential surfaces from the LLBL in accordance with Figure 13 could, in principle, provide access of solar wind plasma along slots between the tail lobes and the plasma sheet by means of **E** × **B** drift. That kind of access would explain why solar wind like H^+ and He^{++} ions can be observed flowing antisunward, along the tail magnetic field lines, in a region between the lobes and the central plasma sheet (Table 1 and Figure 12). Figure 13 does not necessarily require that these ions maintain an antisunward flow component along the magnetic field once they have crossed the magnetopause, but such a component may remain from the initial inertia of the ions in the magnetosheath. In any case, this component must eventually be converted to thermal motion as the ions enter the central plasma sheet, since in that region the ions are well known to be nearly isotropic [e.g., *Eastman et al.*, 1985; *Orsini et al.*., 1990].

The LLBL acts as a "voltage generator" in Figure 13 [e.g., *Eastman et al.*, 1976]. Since the LLBL is present during times of northward as well as southward IMF [e.g., *Mitchell et al.*, 1987], Figure 13 may provide access of solar plasma to the plasma sheet during a wide range of geomagnetic conditions, including times of extreme quiescence. This would satisfy condition 1 of section 4.2 (end of section; compare also Figures 1 and 3). Since, according to the findings of *Mitchell et al.* [1987], the LLBL may be entirely on closed magnetic field lines for northward IMF, but only partially so for southward IMF, and since the LLBL is also thicker for northward IMF, Figure 13 may even suggest that the solar wind access is the most efficient during times of

northward IMF, that is, during quiet times. That would help explain Figures 5 and 6. However, as mentioned in section 4.2, it is also conceivable that the lower H^+ and He^{++} densities during times of southward IMF are caused by increased loss in association with substorm activity.

Figure 13 may allow solar ions to enter the central plasma sheet fairly close to the earth (inside of 23 R_E), without requiring that they first visit a thin current layer ("neutral sheet") far downtail in order to be deflected earthward [e.g., *Speiser*, 1965]. As a consequence, the ions may at times fill the plasma sheet while undergoing little or no net energization. That would satisfy condition 2 in section 4.2. Moreover, having the solar ions enter the near-Earth plasma sheet this way, rather than by earthward jetting from some distant location downtail, may be easier to reconcile with the previous finding by *Lennartsson and Shelley* [1986] that the He^{++} (and H^+) ions are significantly less energetic near the northern and southern edges of the central plasma sheet than they are near GSM $Z = 0$ (see Figure 12 of Lennartsson and Shelley). In other words, Figure 13 does not require that the northern and southern boundaries of the plasma sheet be dominated by very fast moving, earthward jetting ions, as might be the case if all solar ions were to arrive from the distant tail under the influence of a dawn-to-dusk electric field.

Finally, there are reasons to believe that the LLBL on the tail flanks would form even if the solar wind itself had no magnetic field [e.g., *Coleman*, 1971; *Eastman et al.*, 1976; *Olson and Pfitzer*, 1985]. One feasible mechanism is provided by the gradient B drifts of solar wind particles in the outer fringes of the geomagnetic field, drifts that are in opposite directions for ions and electrons and are capable of generating boundary layer electric fields with the proper polarity [*Olson and Pfitzer*, 1985]. Closing the associated equipotential surfaces in accordance with Figure 13 could therefore provide access of solar wind plasma to the earth's plasma sheet even in the absence of an interplanetary magnetic field (IMF). That would satisfy condition 3 in section 4.2.

Acknowledgments. The author is indebted to C. Y. Huang for suggesting a series of substorm onset times with evidence of antisunward ion flows at the ISEE 1 and 2 spacecraft. He is also indebted to C. T. Russell for the use of ISEE 1 magnetometer data, and to the National Space Science Data Center for the use of computer files of the IMF and solar wind data. This work was supported by NASA under contracts NAS5-33047 and NAS5-31209.

The Editor thanks H. Balsiger and G. K. Parks for their assistance in evaluating this paper.

REFERENCES

Axford, W. I., and C. O. Hines, A unifying theory of high-latitude geophysical phenomena and geomagnetic storms, *Can. J. Phys.*, *39*, 1433, 1961.

Balsiger, H., P. Eberhardt, J. Geiss, and D. T. Young, Magnetic storm injection of 0.9- to 16-keV/*e* solar and terrestrial ions into the high altitude magnetosphere, *J. Geophys. Res.*, *85*, 1645, 1980.

Baumjohann, W., G. Paschmann, and C. A. Cattell, Average plasma properties in the central plasma sheet, *J. Geophys. Res.*, *94*, 6597, 1989.

Bonifazi, C., P. Cerulli-Irelli, A. Egidi, V. Formisano, and G. Moreno, The EGD positive ion experiment on the ISEE B satellite, *IEEE Trans. Geosci. Electron.*, *GE-16*, 243, 1978.

Borrini, G., J. T. Gosling, S. J. Bame, and W. C. Feldman, Helium abundance variations in the solar wind, *Sol. Phys.*, *83*, 367, 1983.

Chappell, C. R., T. E. Moore, and J. H. Waite, Jr., The ionosphere as a fully adequate source of plasma for the Earth's magnetosphere, *J. Geophys. Res.*, *92*, 5896, 1987.

Christon, S. P., D. J. Williams, D. G. Mitchell, C. Y. Huang, and L. A. Frank, Spectral characteristics of plasma sheet ion and electron populations during disturbed geomagnetic conditions, *J. Geophys. Res.*, *96*, 1, 1991.

Coleman, P. J., Jr., A model of the geomagnetic cavity, *Radio Sci.*, *6*, 321, 1971.

Collin, H. L., W. K. Peterson, J. F. Drake, and A. W. Yau, The helium components of energetic terrestrial ion upflows: their occurrence, morphology, and intensity, *J. Geophys. Res.*, *93*, 7558, 1988.

Couzens, D. A., and J. H. King, Interplanetary medium data book, supplement 3, 1977–1985, *Rep. NSSDC/WDC-A-R&S 86-04*, NASA Goddard Space Flight Cent., Greenbelt, Md., 1986.

Cowley, S. W. H., Plasma populations in a simple open model magnetosphere, *Space Sci. Rev.*, *26*, 217, 1980.

DeCoster, R. J., and L. A. Frank, Observations pertaining to the dynamics of the plasma sheet, *J. Geophys. Res.*, *84*, 5099, 1979.

Eastman, T. E., E. W. Hones, Jr., S. J. Bame, and J. R. Asbridge, The magnetospheric boundary layer: Site of plasma, momentum and energy transfer from the magnetosheath into the magnetosphere, *Geophys. Res. Lett.*, *3*, 685, 1976.

Eastman, T. E., L. A. Frank, and C. Y. Huang, The boundary layers as the primary transport regions of the Earth's magnetotail, *J. Geophys. Res.*, *90*, 9541, 1985.

Etcheto, J., and A. Saint-Marc, Anomalously high plasma densities in the plasma sheet boundary layer, *J. Geophys. Res.*, *90*, 5338, 1985.

Fairfield, D. H., and N. F. Ness, Configuration of the geomagnetic tail during substorms, *J. Geophys. Res.*, *75*, 7032, 1970.

Feldman, W. C., J. R. Asbridge, S. J. Bame, and J. T. Gosling, Long-term variations of selected solar wind properties: IMP 6, 7, and 8 results, *J. Geophys. Res.*, *83*, 2177, 1978.

Ghielmetti, A. G., R. G. Johnson, R. D. Sharp, and E. G. Shelley, The latitudinal, diurnal, and altitudinal distributions of upward flowing energetic ions of ionospheric origin, *Geophys. Res. Lett.*, *5*, 59, 1978.

Hamilton, D. C., G. Gloeckler, F. M. Ipavich, W. Stüdemann, B. Wilken, and G. Kremser, Ring current development during the great geomagnetic storm of February 1986, *J. Geophys. Res.*, *93*, 14,343, 1988.

Heelis, R. A., J. K. Lowell, and R. W. Spiro, A model of the high-latitude ionospheric convection pattern, *J. Geophys. Res.*, *87*, 6339, 1982.

Heppner, J. P. Polar cap electric field distributions related to the interplanetary magnetic field direction, *J. Geophys. Res.*, *77*, 4877, 1972.

Heppner, J. P., and N. C. Maynard, Empirical high-latitude electric field models, *J. Geophys. Res.*, *92*, 4467, 1987.

Hones, E. W., Jr., Plasma flow in the magnetotail and its implications for substorm theories, in *Dynamics of the Magnetosphere*, edited by S. I. Akasofu, p. 545, D. Reidel, Hingham, Mass., 1979.

Hones, E. W., Jr., J. R. Asbridge, and S. J. Bame, Time variations of the magnetotail plasma sheet at 18 R_E determined from concurrent observations by a pair of Vela satellites, *J. Geophys. Res.*, *76*, 4402, 1971.

Huang, C. Y., and L. A. Frank, A statistical study of the plasma sheet: Implications for substorm models, *Geophys. Res. Lett.*, *13*, 652, 1986.

Huang, C. Y., L. A. Frank, G. Rostoker, J. Fennell, and D. G. Mitchell, Nonadiabatic heating of the central plasma sheet at substorm onset, *J. Geophys. Res.*, *97*, 1481, 1992.

Kamei, T., and H. Maeda, Auroral electrojet indices (AE) for January–June 1978, Data Book 3, World Data Cent. C2 for Geomagn., Kyoto Univ., Kyoto, Japan, April 1981.

Lennartsson, W., Plasma sheet ion composition at various levels of geomagnetic and solar activity, *Phys. Scripta*, *36*, 367, 1987.

Lennartsson, W., and E. G. Shelley, Survey of 0.1- to 16-keV/*e* plasma sheet ion composition, *J. Geophys. Res.*, *91*, 3061, 1986.

Lundin, R., B. Hultqvist, N. Pissarenko, and A. Zakharov, The plasma mantle: Composition and other characteristics as observed by means of the Prognoz-7 satellite, *Space Sci. Rev.*, *31*, 247, 1982.

Lyons, L. R., and T. W. Speiser, Evidence for current sheet

acceleration in the geomagnetic tail, *J. Geophys. Res.*, *87*, 2276, 1982.

Mitchell, D. G., F. Kutchko, D. J. Williams, T. E. Eastman, L. A. Frank, and C. T. Russell, An extended study of the low-latitude boundary layer on the dawn and dusk flanks of the magnetosphere, *J. Geophys. Res.*, *92*, 7394, 1987.

Mozer, F. S., R. B. Torbert, U. V. Fahleson, C.-G Fälthammar, A. Gonfalone, and A. Pedersen, Measurements of quasistatic and low frequency electric fields with spherical double probes on the ISEE-1 spacecraft, *IEEE Trans. Geosci. Electron.*, *GE-16*, 258, 1978.

Olson, W. P., and K. A. Pfitzer, Magnetospheric responses to the gradient drift entry of solor wind plasma, *J. Geophys. Res.*, *90*, 10,823, 1985.

Orsini, S., M. Candidi, M. Stokholm, and H. Balsiger, Injection of ionospheric ions into the plasma sheet, *J. Geophys. Res.*, *95*, 7915, 1990.

Parks, G. K., et al., Particle and field characteristics of the high-latitude plasma sheet boundary layer, *J. Geophys. Res.*, *89*, 8885, 1984.

Pilipp, W. G., and G. Morfill, The formation of the plasma sheet resulting from plasma mantle dynamics, *J. Geophys. Res.*, *83*, 5670, 1978.

Reiff, P. H., T. W. Hill, and J. L. Burch, Solar wind plasma injection at the dayside magnetospheric cusp, *J. Geophys. Res.*, *82*, 479, 1977.

Rosenbauer, H., H. Grünwaldt, M. D. Montgomery, G. Paschmann, and N. Sckopke, Heos 2 plasma observations in the distant polar magnetosphere: The plasma mantle, *J. Geophys. Res.*, *80*, 2723, 1975.

Rostoker, G., and R. Boström, A mechanism for driving the gross Birkeland current configuration in the auroral oval, *J. Geophys. Res.*, *81*, 235, 1976.

Russell, C. T., The ISEE 1 and 2 fluxgate magnetometers, *IEEE Trans. Geosci. Electron.*, *GE-16*, 239, 1978.

Sharp, R. D., D. L. Carr, W. K. Peterson, and E. G. Shelley, Ion streams in the magnetotail, *J. Geophys. Res.*, *86*, 4639, 1981.

Shelley, E. G., R. G. Johnson, and R. D. Sharp, Satellite observations of energetic heavy ions during a geomagnetic storm, *J. Geophys. Res.*, *77*, 6104, 1972.

Shelley, E. G., R. D. Sharp, R. G. Johnson, J. Geiss, P. Eberhardt, H. Balsiger, G. Haerendel, and H. Rosenbauer, Plasma composition experiment on ISEE-A, *IEEE Trans. Geosci. Electron.*, *GE-16*, 266, 1978.

Speiser, T. W., Particle trajectories in model current sheets, 1, Analytical solutions, *J. Geophys. Res.*, *70*, 4219, 1965.

Tsurutani, B. T., J. A. Slavin, E. J. Smith, R. Okida, and D. E. Jones, Magnetic structure of the distant geotail from -60 to -220 R_E: ISEE-3, *Geophys. Res. Lett.*, *11*, 1, 1984.

Yau, A. W., E. G. Shelley, W. K. Peterson, and L. Lenchyshyn, Energetic auroral and polar ion outflow at DE 1 altitudes: Magnitude, composition, magnetic activity dependence, and long-term variations, *J. Geophys. Res.*, *90*, 8417, 1985.

Zwickl, R. D., D. N. Baker, S. J. Bame, W. C. Feldman, J. T. Gosling, E. W. Hones, Jr., D. J. McComas, B. T. Tsurutani, and J. A. Slavin, Evolution of the earth's distant magnetotail: ISEE 3 electron plasma results, *J. Geophys. Res.*, *89*, 11,007, 1984.

Zwolakowska, D., and B. Popielawska, Tail plasma domains and the auroral oval-results of mapping based on the Tsyganenko 1989 magnetosphere model, *Preprint 12*, Polish Acad. of Sci., Space Res. Cent., Warsaw, Poland, Dec. 1991.

W. Lennartsson, Lockheed Missiles and Space Company, Inc., Research and Development, Dep. 91-20, Bldg. 255, 3251 Hanover Street, Palo Alto, CA 94304.

(Received March 16, 1992;
revised May 26, 1992;
accepted May 28, 1992.)

JOURNAL OF GEOPHYSICAL RESEARCH, VOL. 99, NO. A2, PAGES 2387–2401, FEBRUARY 1, 1994

Tail lobe ion composition at energies of 0.1 to 16 keV/e: Evidence for mass-dependent density gradients

O. W. Lennartsson

Lockheed Missiles and Space Company, Incorporated, Research and Development, Palo Alto, California

Abstract. A large set of energetic (0.1- to 16-keV/e) ion composition data from the central magnetotail, obtained by the ISEE 1 spacecraft between 10 and $23R_E$ from Earth, is sorted according to measured total ion beta value, in order to investigate whether bulk properties of different ions vary in different ways between plasma sheet and lobes, as suggested by a comparison of certain experimental and theoretical results in the literature. Despite inevitable difficulties with extracting statistically valid data at very low beta (10^{-2} or lower), the results seem to support a recent theoretical model suggesting that lighter ions have a steeper density gradient than heavier ions, especially when comparing H^+ ions with O^+ ions. The results also indicate that ion velocity distributions are fairly isotropic even at low beta, at least those of H^+ ions, although field-aligned flows are common. The results are evaluated in the context of plasma transport and are found to lend some support to the notion that tail lobe convection may be directed inward from the dawn and dusk flanks.

1. Introduction

As far as plasma measurements are concerned, the tail lobe regions of Earth's magnetosphere are unique in that they are typically not identified by characteristic particle signatures but rather by the disappearance of instrument response, or "plasma dropout" [e.g. *Hones et al.*, 1986]. What is known points to a very low particle density, at least inside of a few tens of Earth radii, where 10^{-2} cm^{-3} may be a typical number [*Akasofu et al.*, 1973; *Zwickl et al.*, 1984], and energies significantly lower than in the plasma sheet [*Akasofu et al.*, 1973; *Hardy et al.*, 1979]. It is also known that the lobes contain narrowly collimated tailward streams of ions, at least part of the time, and that these streams consist not only of H^+ ions but to an even greater extent of O^+ ions, presumably of terrestrial origin [*Sharp et al.*, 1981]. The data on these streams are so far the only information available on the ionic composition of the tail lobe plasma.

This study is an extension of the work by *Sharp et al.* [1981], using a much larger data set from the same experiment (on ISEE 1) and taking a different approach. It is motivated by some apparent discrepancies between different sets of tail ion composition data and between data and theory. The difference in the data refers to the studies by *Sharp et al.* [1981] and *Lennartsson and Shelley* [1986]. As already mentioned, the former study found the O^+ ions to be more abundant than H^+ ions in the tail lobes, at least when the geomagnetic 3-hour range index Kp is above 3+, whereas the latter study found the H^+ ions to be the usually most abundant in the central plasma sheet, even during geomagnetically disturbed conditions. Nevertheless, by sorting data according to the geocentric solar magnetospheric (GSM) Z coordinate (south-north direction), Lennartsson and Shelley found the O^+/H^+ density ratio to peak in a $5R_E$ wide bin centered at $Z = 0$, on average (their Figure 9b), in apparent disagreement with the greater O^+/H^+ ratio in the lobes. This may imply either that the lobe and plasma sheet ions have substantially different origins, or that the use of a fixed-scale coordinate like the GSM Z can give misleading results. It is certainly possible that a statistical peak in the O^+/H^+ ratio near $Z = 0$ is mainly the result of spatial thinning of the plasma sheet during substorms [*Hones et al.*, 1971], when the O^+/H^+ ratio is typically enhanced in both the lobes and the plasma sheet.

The difference between data and theory refers to the study by *Lennartsson and Shelley* [1986] and a recent theory of tail pressure equilibria by *Kiessling and Ziegler* [1989]. The latter, which uses statistical mechanics rather than MHD, is the first theoretical analysis of tail equilibria with two ion components present, namely H^+ and O^+ ions. Under fairly general assumptions about the relative bulk velocities of the two ion components and the electrons (affecting the cross-tail current) this theory requires that the O^+ ions form a spatially thicker sheet, in GSM Z, than do the H^+ ions (Figures 4 through 7 in that paper). As a consequence, the O^+/H^+ density ratio becomes larger than one in the tail lobes, even if it is much less than one in the central plasma sheet. This may seem to be in agreement with the result of *Sharp et al.* [1981], even though the theoretical velocity distributions are essentially isotropic, not narrow streams, but it is again in apparent disagreement with the statistical Z dependence found by *Lennartsson and Shelley* [1986]. Since the theory assumes that each ion component has identical thermal velocity distributions in the plasma sheet and the lobes, except for the overall amplitudes, it suggests that a variation of the O^+/H^+ ratio with Z can be due to local conditions rather than to the particle sources. The implication is, as stated by Kiessling and Ziegler, that the effect is produced by the different ionic mass of the two components.

This study, like the one by *Lennartsson and Shelley* [1986], treats the ion data in a statistical fashion, but it sorts them according to the calculated ion beta, instead of GSM Z, and follows them well into the lobes. This procedure, as it

Paper number 93JA03201.
0148-0227/94/93JA-03201$05.00

happens, removes the aforementioned discrepancies. The approach differs from that of *Sharp et al.* [1981] in that all detector counts are included here (corrected for background noise), not merely isolated counts exceeding three standard deviations of a Poisson distribution (at least 10 counts per unit sampling). The deficiency in individual counts is compensated for by summing them (weighted) into ion velocity moments, while keeping score of the resulting total standard deviations. The objective is to extract the maximum possible information from available data. The rationale may be described by a metaphor: if anything is hidden in a dark place, one is more likely to see it by going there with only a candle at hand than by staying under the bright porch light.

2. Database

The ion data are from the Plasma Composition Experiment on the ISEE 1 spacecraft [*Shelley et al.*, 1978] and cover for the most part the energy range between 100 eV/e and 16 keV/e. This instrument measures ions at various mass per charge (M/Q) in a cyclic fashion, usually by scanning the full range of energy per charge (E/Q) while maintaining a fixed M/Q. Each E/Q setting is typically kept fixed for at least one full spacecraft spin period (3 s). A complete energy-mass scan cycle in the magnetospheric modes of operation usually requires about 8 to 17 min and includes an M/Q setting (<1) which provides direct measurements of detector noise due to penetrating high-energy radiation (mostly MeV electrons). This detector background is subtracted from the other measurements before converting counts to velocity moments. The ion data are supplemented with magnetic field data from the ISEE 1 flux gate magnetometer [*Russell*, 1978]. A more detailed description of the instrument and the data format is given in the appendix.

The data set has been spatially limited to a "central tail" region, defined according to Figure 1 in terms of GSM coordinates. Each point in Figure 1 represents a single energy-mass scan cycle of the instrument, that is a single mass-resolved plasma sample. This region lies at GSM R between 10 and $23R_E$, the latter being the ISEE 1 apogee, and at $X < -5R_E$ and $-10R_E < Y < 10R_E$. The bias toward positive Z is a consequence of the ISEE 1 orbit. The data span a total time period from January 2, 1978, to March 1, 1980.

The GSM boundaries are somewhat arbitrary, although they encompass a region where the ISEE 1 spacecraft provides regular sampling of the tail lobes (mostly of the northern lobe). Outside of this region, at $|Y| > 10R_E$, the plasma sheet is often too thick (in the Z direction) to allow that, especially during geomagnetically quiet periods. The ISEE 1 is expected to be well inside of the magnetopause while in this region, but the data have been additionally screened for possible evidence of magnetosheath or solar wind plasmas by the data analysis program. This screening has been based on velocity moments, combining the mass-resolved H^+ and He^{++} moments as well as the "total ion" moments, assuming that the latter are well representative of H^+ ions (see appendix).

Apart from the GSM boundaries in Figure 1, the data have not been ordered explicitly by spatial coordinates here. Instead, they have been ordered by the relative strengths of the measured particle and magnetic field pressures perpendicular to the magnetic field vector, that is by the measured ion beta value in the 0.1- to 16-keV/e energy range, or strictly speaking, by an approximate estimate of the true beta. This estimate has been made with the second set of assumptions listed in the appendix (section A2), and always includes the H^+ pressure, and in most cases the partial pressures of He^{++}, He^+, and O^+ ions as well (all four species usually measured).

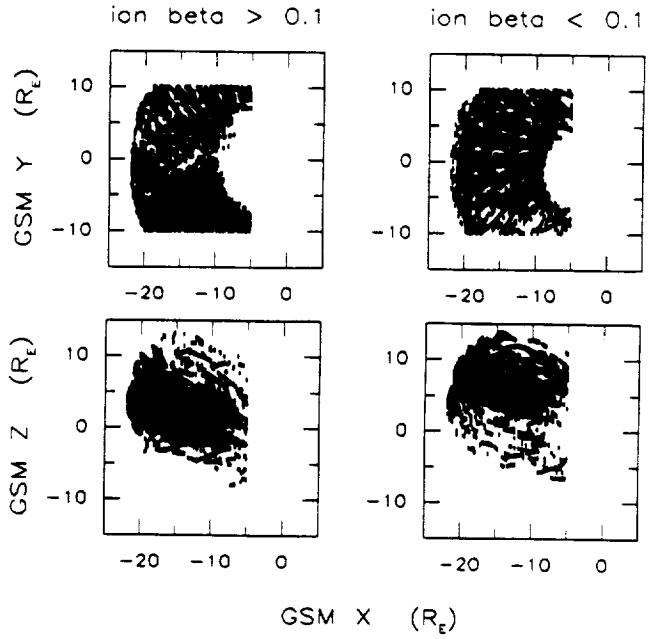

Figure 1. Spatial extent of selected tail data set in geocentric solar magnetospheric (GSM) coordinates, subdivided according to measured ion beta.

This beta value is one obtained in the frame of reference of the spacecraft, rather than the more physically correct value that would be inferred by an observer moving with the local $\mathbf{E} \times \mathbf{B}$ drift, which is not known. A rough estimate of the resulting error can be made by subtracting, from each partial ion pressure, an energy density corresponding to the trans-B component of the respective drift velocity derived with the first set of assumptions listed in the appendix (section A2). That has been tried and found to have no significant effect on the statistical picture, mainly because that component of the drift energies is relatively small in most cases.

The final size of this data set is further limited by the availability of magnetic tape records of the auroral electrojet (AE) indices, which have been used to divide the data according to geomagnetic activity (see *Kamei and Maeda* [1981] and subsequent data books). As a result, no data from 1977 have been included.

3. Statistical Results

Many aspects of the data are qualitatively similar for different ion species, so in order to save figure space, a single species, namely the H^+, will serve as an example to be referred to later. The H^+ has always been measured here, and it is almost always present in statistically significant numbers.

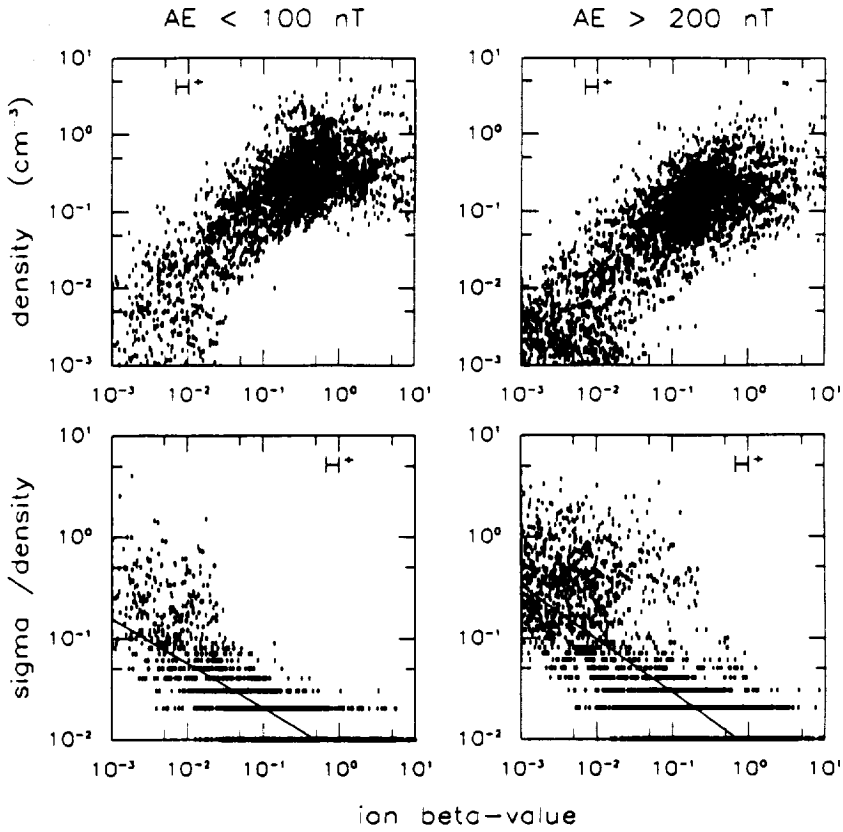

Figure 2. (Top) Density samplings of H^+ ions during (left) quiet and (right) active geomagnetic conditions (see text), and (bottom) statistical uncertainty of each sampling, ordered by corresponding total ion beta. Straight lines intersecting this and following figures are linear least squares fits referred to in the text (all fits are unweighted).

3.1. Proton Density and Energy in Central Tail

Figure 2 shows the H^+ number density (top) in the central tail (Figure 1) and the relative statistical uncertainty (one standard deviation) of this density (bottom), ordered by total ion beta, as defined above, and by geomagnetic activity. The latter has been measured each time by two consecutive hourly *AE* values, one from the preceding hour and one from the current hour (in universal time). In the left panels are only included those H^+ densities obtained when the two *AE* values were both below 100 nT, in the right panels are densities obtained when the two *AE* values were both above 200 nT. This selection does exclude a substantial portion of the data (about 34%), but the differences between quiet and active times are hardly sufficient to justify a third and intermediate group. The reason for using both the preceding and current hours for the *AE* is to allow for some inertia in the transport of ions, especially of ions from the Earth, although this precaution is somewhat academic in light of the strong autocorrelation of the *AE* index over many hours (see *Kamei and Maeda* [1981]; see also *Lennartsson and Shelley* [1986]).

The left and right panels of Figure 2 are based, respectively, on 2720 and 3804 independent density numbers, some of which fall below 10^{-3} cm^{-3}, even including some negative ones at beta $<10^{-2}$. Occasional negative "densities" are a normal statistical effect of subtracting a separately measured background count rate from the count rates in the various ion channels, when the signal-to-noise ratio falls below one. This is reflected in the bottom panels by large statistical uncertainties, or "errors," sometimes exceeding the density itself.

The errors plotted here are the ratio between the calculated standard deviation, which contains the background standard deviation twice (via a sum of variances; see *Lennartsson and Sharp* [1982]) and is positive by definition, and the absolute value of the net density. These numbers have been stored rounded to integers in the data files, representing a percentage, which accounts for the horizontal striations. Values of zero percent have been set to 0.5% when fitting the two straight lines (log-log scale) by the linear (unweighted) least squares method [*Bevington*, 1969, pp. 92–118]. These lines have no other purpose here but to highlight the inherent dependence of data quality on the local beta value. Needless to say, the corresponding correlation coefficients are significant, being $R = -0.77$ on the left and $= -0.79$ on the right [*Bevington*, 1969, pp. 119–127; *Press et al.*, 1986, pp. 484–487].

Figure 2 shows that a density of 10^{-3} cm^{-3} is typically close to the statistical limit of resolution of H^+ ions in these data. The reason is that density numbers used here, like other moments, are all based on essentially random measurements of the accessible velocity space, whether it is filled by mostly noise or mostly signal. It is possible to lower the sensitivity threshold another factor of 10, in terms of ion density, by concentrating on ions that are focused in energy and angle to within a few instrument accumulations [*Sharp*

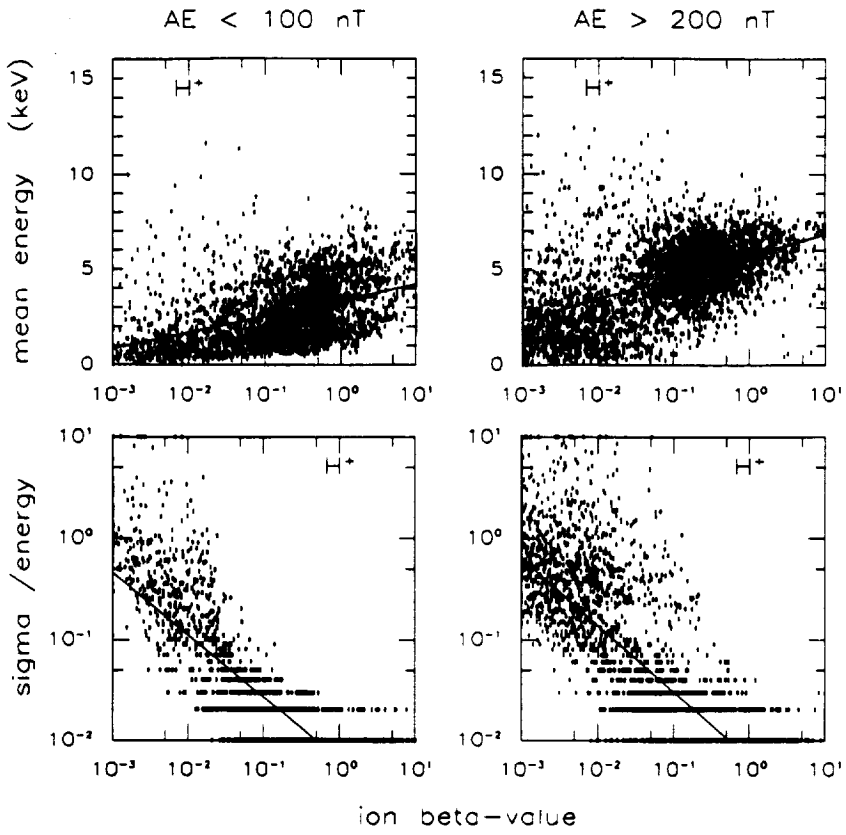

Figure 3. Corresponding (top) mean energies of H^+ ions and (bottom) their uncertainties.

et al., 1981], but that is also sure to exclude any hot and near-isotropic ion component that may be present.

To be more specific, an isotropic Maxwell-Boltzmann distribution of H^+ ions with a few keV thermal energy and a density of 10^{-3} cm^{-3} generates about one count every 2 to 4 s in this instrument, a rate roughly half as large as the typical background in the lobes, and a total of about 40 counts over the course of a full energy-angle scan of H^+ ions. That means 40 net counts after subtraction of an average background rate derived from a sum of 50 to 100 counts in the background channel (about the same total accumulation time). Hence it is practically impossible to discern such a distribution from an energy-angle spectrum of raw counts, but by subtracting an appropriate background and weighting and integrating the counts into number density it becomes possible, albeit with a standard deviation typically between 30% and 40%, because of the background standard deviation. This example illustrates the fact that the signal-to-noise ratio does not have to be greater than one in order for a calculated density to be greater than three standard deviations, but this ratio ought not to be much less than 1/2 with typical lobe background rates.

Figure 3 shows the H^+ mean energy (top) and relative uncertainty (bottom) in the same format, except that the top panels have a linear scale on the ordinate and linear regression lines as well ($R = 0.45$ on the left, $= 0.57$ on the right). Since the mean energy is a ratio between energy density and number density, it has no physical or mathematical meaning if either or both of those densities are negative, so energies have only been calculated for positive values of both densities. The resulting number of points is 2673 (left) and 3510 (right), and the regression lines in the bottom panels have $R = -0.84$ (left) and $= -0.85$ (right). It may be noted that energies, at any given beta, are typically higher at $AE > 200$ nT, while densities are lower (Figure 2).

Although the trend is clearly to have lower energies at lower beta, the very highest mean energies have also been sampled at beta <0.1. Except for a few, these extreme values are not, as one might expect, caused by large statistical errors, because most remain when these plots are redrawn including only values with a relative sigma of less than 1/3 (not shown). In some cases they appear to represent beams of H^+ ions moving toward the Earth at high speed (up to 1200 km s^{-1}; see also *DeCoster and Frank* [1979] and *Eastman et al.* [1985]), in other cases they may be the result of aliasing caused by brief enhancements in the ion flux while the instrument is sampling the higher-energy channels. The relative importance of rapid earthward flows may be judged from Figure 4, which shows the X component of the calculated bulk velocities of H^+ ions.

In any case the great majority of H^+ energies are quite low at low beta, especially at quiet times, a result that is consistent with many earlier reports of reduced proton energies adjacent to the tail lobes, as measured with regular electrostatic analyzers [e.g., *Akasofu et al.*, 1973]. Taken together, Figures 3 and 4 imply that the H^+ energies are generally dominated by random, or "thermal," motion at all beta. This will become even clearer when angular distributions are discussed in section 3.4. It should be mentioned that the regression lines in the top panels of Figure 3 remain almost identical when the plots are limited to points with sigma <1/3 (not shown). This is a good indicator that

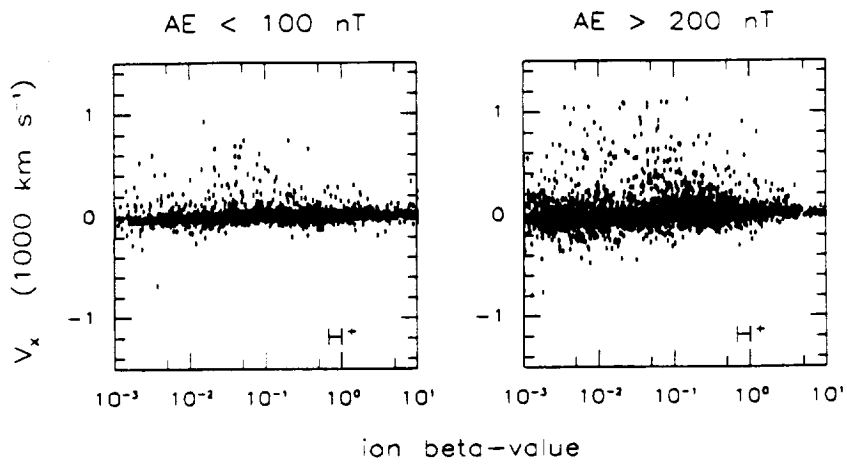

Figure 4. Corresponding drift velocity of H^+ ions along GSM (and GSE) X axis.

background counts have been properly subtracted from all samples, since the background would tend to bias the apparent mean energy toward a rather high value of about 5 keV/e.

3.2. Relative Densities of Other Ions

Figure 5 shows the ratios between the other ion densities and the H^+ density, as a function of the same beta and AE. In forming these ratios, each value of the H^+ density has first been compared with its own standard deviation, or sigma, and in the relatively rare events that it is smaller than one sigma (100% or greater error), including sign, the sigma value has been used to represent the H^+ density in each ratio. The reason for doing this is to avoid large but physically meaningless ratios.

The straight-line segments in each panel are least squares fits (log-log) to points at beta <0.1, only including positive ratios. Rather than enumerating the correlation coefficient and number of samplings for each panel, it may suffice to say that R is about −0.5 to −0.7 and is based on some 425 to 1374 samplings, which means that R is significant in each case. The feature of principal interest here is the consistent increase in the density ratios with decreasing beta. This implies that the H^+ density falls off faster than any of the other densities as one moves into a tail lobe from the plasma sheet.

There are numerous (hundreds of) negative ratios not shown in Figure 5, mostly at beta <0.1 (examples will be shown later). Negative densities are more common with He^{++}, He^+, and O^+ ions than with H^+ ions, for two reasons. One is that the heavier ions must have a larger number density in order to produce a given count rate at a given energy; the other is that the heavier ions generally have a lower count rate to begin with. The result is a lower signal-to-noise ratio and a greater sensitivity to background subtraction. This subject will be discussed in more detail below.

In order to verify the gross trends of the density ratios, Figure 6 shows a subset of the same data, one in which every ratio is based on densities, numerator as well as denominator, with a relative sigma of less than 1/3 (densities greater than 3 sigma). This subset is much smaller, especially at beta <0.01. Nevertheless, the six regression lines remain much the same in each case, and the respective correlation coefficients, ranging from a low of −0.34 (top left) to a high of −0.72 (middle left), are still significant, considering the remaining number of points. In fact, even in the least significant case, the one with the fewest points remaining (middle left; 43 points), the probability of having no actual correlation is less than 10^{-7} [*Bevington*, 1969, pp. 119–127; *Press et al.*, 1986, pp. 484–487].

It makes no difference whether the 3-sigma criterion used for Figure 6 is applied to the absolute value of each density, or only allows positive densities. At 3 sigma there are no negative ratios left, but there are still 3240 remaining positive ratios (adding all panels). Hence the problem with negative "densities" is eliminated at the 3-sigma level, in this case, although at that level a large portion of valid data is also being discarded. By comparison, there are still some 50 negative ratios left at the 2-sigma level (0.5% of all remaining values).

3.3. Intercomparison of Energies

Figure 7 is analogous to Figure 5, with mean energies substituted for densities. In Figure 7 the ratios have been formed without regard to standard deviations of either numerator or denominator. However, no negative values are involved here, since the mean energies, when calculated, are based on positive energy and number densities (see the explanation of H^+ energies above). The energies of He^{++}, He^+, and O^+ ions appear for the most part to be dominated by thermal motion, like those of the H^+ ions, but the statistics is frequently poor at low beta (see next section).

All ions, except the He^+, tend to become less energetic with decreasing beta, although the wide scatter in Figure 7 may seem to defy any trend. However, as the regression lines suggest, the He^{++} energy typically falls off at about the same rate as the H^+ energy (on a log-log scale), staying about 4 times higher than the H^+ energy, whereas the O^+ energy falls of slightly faster most of the time. The He^+ energy, for some reason, does not show this trend, so the He^+/H^+ energy ratio increases with decreasing beta.

Some of the scatter in Figure 7 is no doubt due to statistical errors, but much of it is real. As far as the He^+/H^+ and O^+/H^+ energy ratios are concerned, the large range of the scatter (two orders of magnitude) is probably real, since it remains about the same at the 3-sigma level, as do the regression lines (not shown). At that level of signifi-

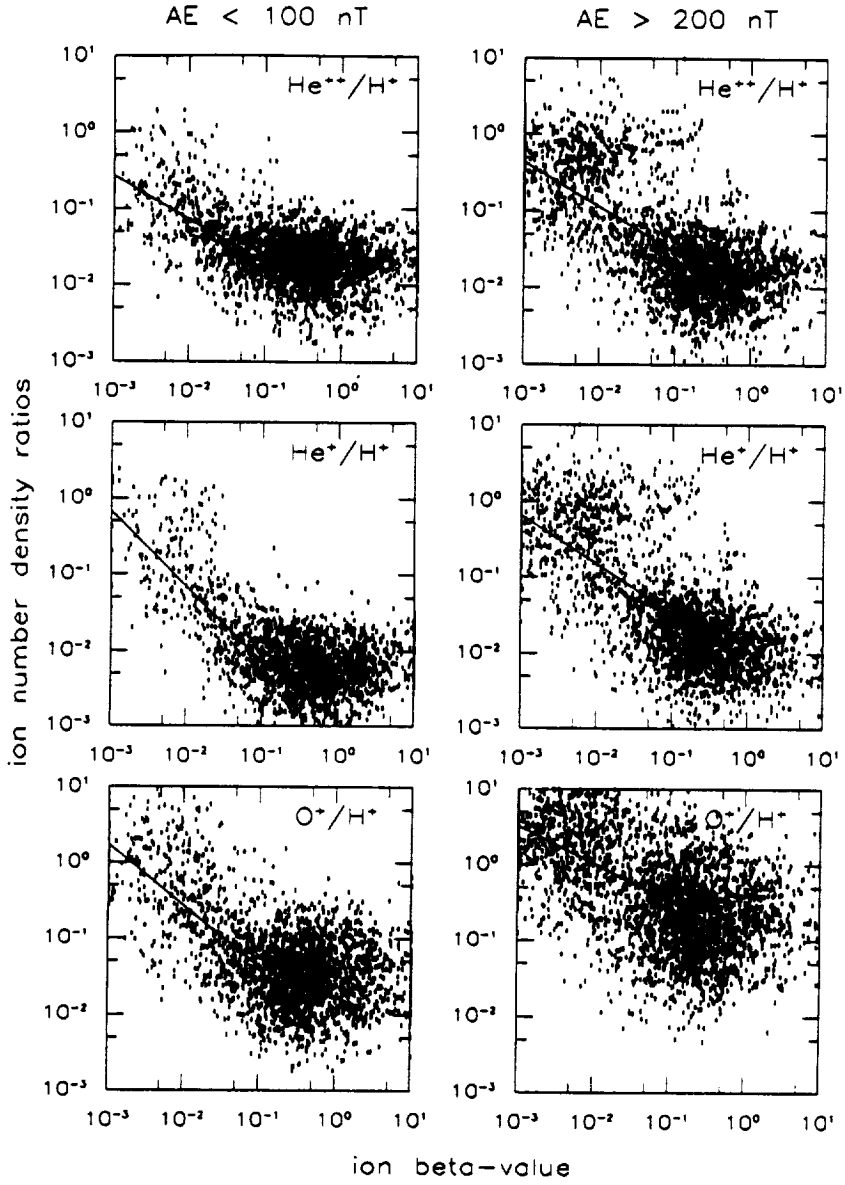

Figure 5. Densities of (top) He^{++}, (middle) He^{+}, and (bottom) O^{+}, normalized by the H^{+} density measured during same energy-mass scan cycle.

cance the He^{++}/H^{+} energy ratio is consistently greater than one and more strongly clustered near 4 (not shown).

Despite the scatter, the regression lines still have significant correlation coefficients, at least in the middle (R about -0.25; N about 2000 each) and bottom panels (R about 0.1; N about 2000 and 2700, respectively). The somewhat weaker correlation in the top panels (about -0.08) is of course consistent with a nearly flat regression line (at about 4).

3.4. Angular Distributions

Figure 8 compares the energies parallel and perpendicular to the tail magnetic field for each of H^{+}, He^{++}, and O^{+} ions under two conditions: (1) At least one of the two magnetic field directions has been sampled by the instrument field of view at all energies (extreme values of center pitch angle less than 5° or greater than 175°). (2) At least one of the two energies has been calculated with a relative sigma of less than 1/3.

The first condition gives a slight preference to ions flowing tailward along the field lines, because of the spacecraft orbit and the instrument configuration (see Figure 1 and section A1), but both field directions are commonly sampled during the same spin cycle, especially at energies below a few keV/e, where the field of view is rather wide (section A1). Of the two field directions, the tailward is favored by the O^{+} ions, especially at small beta (not shown), while the earthward is favored by He^{++} and H^{+} ions with flow speeds well in excess of 100 km s^{-1} (compare Figure 4).

The second condition prevents taking the ratio of two inaccurate numbers and thereby creating artificially large anisotropies. The main reason for not requiring a 3-sigma accuracy on both energies is to allow cases of extreme

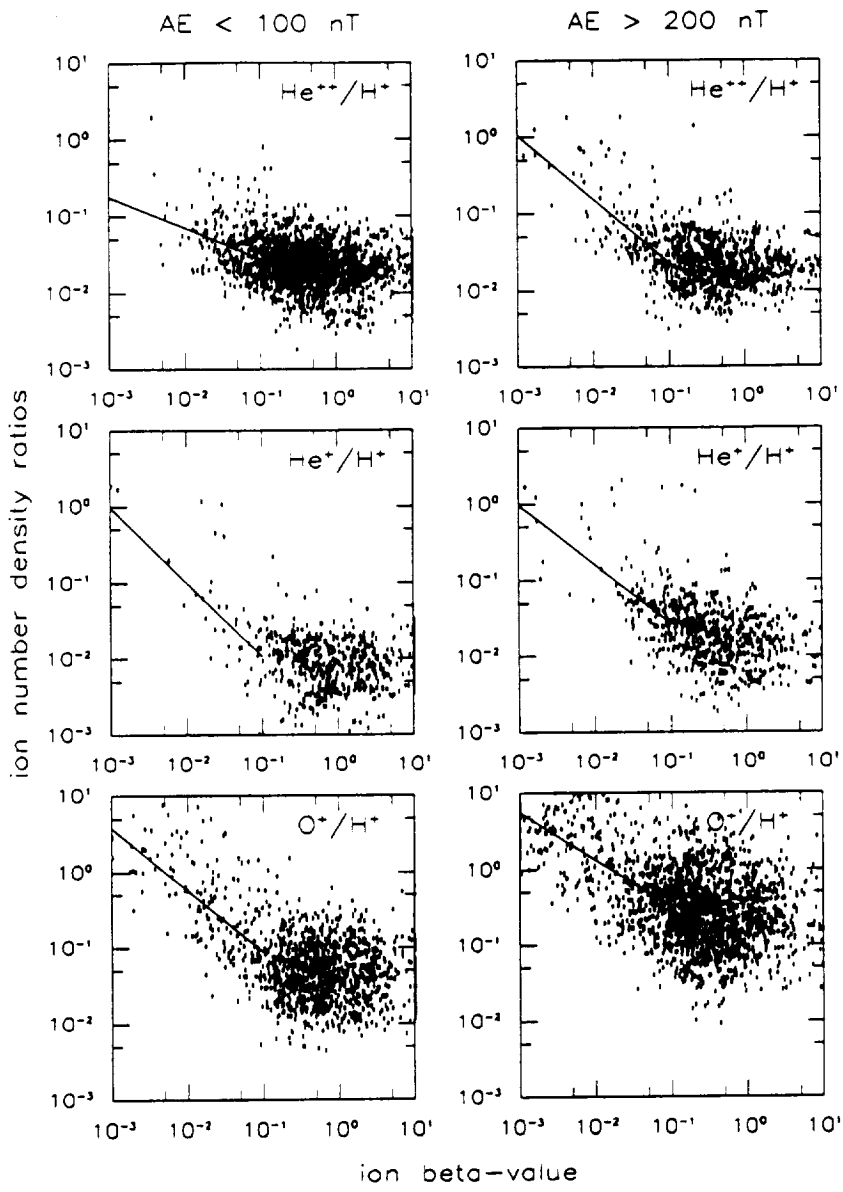

Figure 6. Same as Figure 5, but limited to measurements with less than 33% statistical uncertainty.

field-alignment, where the parallel flux contributes significant counts but the perpendicular flux may be buried in background noise. There is a barrier against very large such anisotropies, because of the 20° binning of the pitch angles during moment calculations (section A2). Even if all counts were confined to a single bin along either field direction, the center of the bin is either at 10° or 170°, so the ratio of parallel to perpendicular energy, when multiplied by two to adjust for the difference in degrees of freedom, could not exceed about 32, assuming no statistical errors in the background subtraction. However, few ratios even come close to 32 in Figure 8; the most common ratio is one, indicating a predominance of isotropic velocity distributions, at least for H^+ ions.

If the conditions on statistical accuracy are removed altogether, the main effects on Figure 8 are to increase both the number and spread of data points at small beta, especially for He^{++} and O^+ ions (about fivefold increase in number of points at beta <0.1 for O^+), as expected, but the regression lines remain very nearly the same (not shown). In other words, anisotropic ratios become more common, real or not, but they show no greater preference for either large or small values than already indicated in Figure 8. It may also be mentioned that He^+ ions, which are not part of Figure 8, have ratios similar to the O^+ ions, although they have fewer ratios with small sigmas.

A proper comparison of parallel and perpendicular energies should compensate for $\mathbf{E} \times \mathbf{B}$ drift. Since the latter is unknown here, the next best move is to determine the cross-B component of the measured ion drift velocity in the spacecraft spin plane (approximately the GSE X-Y plane), and subtract the corresponding drift energy from the perpendicular energy, so as to approximate pure gyrational (thermal) energy. In practice, this makes little difference, because the cross-B drift speed is generally small (mostly less than 50 km s^{-1}) compared to thermal velocities in these data.

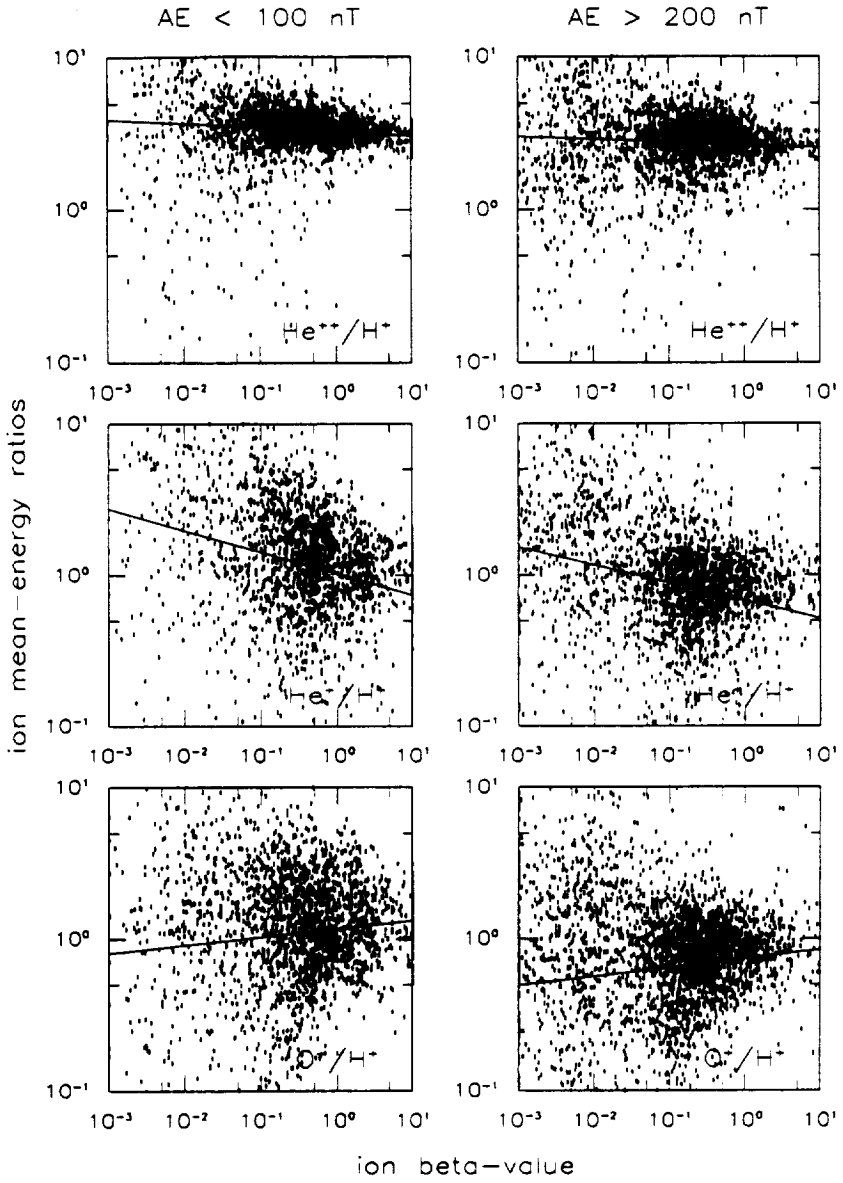

Figure 7. Mean energies of (top) He^{++}, (middle) He^{+}, and O^{+} (bottom), normalized by the H^{+} mean energy.

However, the ratios shown in Figure 8 have in fact all been "corrected" this way.

3.5. Extending the Energy Range Downward to 10 eV/*e*

The lowest-energy channel, from 10 eV/*e* to about 100 eV/*e*, not counting the variable RPA settings, has been sampled in about 90% of these data and is represented by a partial number density for each ion species, a quantity that may or may not be an accurate measure, depending on such unknowns as spacecraft potential and **E** × **B** drift direction and speed. This partial density can be added to the normal number density, and by weighting it with a suitable energy (40 eV/*e*) it can also be used to derive a modified value for the total mean energy.

Adding this low-end density has somewhat different effects at different beta, and the effects also vary with ion species. At beta >0.1, that is including the plasma sheet proper, the effects are consistently small, especially for H^{+} and He^{++} ions, whose density and energy are rarely changed by more than a few percent. The corresponding changes for He^{+} and O^{+} ions are somewhat larger, often reaching some 10 to 20%. At smaller beta, usually meaning smaller densities as well, the effects are much more variable, sometimes doubling or tripling the density, especially that of O^{+} ions. However, if Figures 2 through 8 are redrawn, including this energy channel whenever it has been sampled, the new figures (not shown) are difficult to distinguish from the old ones. There is some increase in the range of scatter, but very little change in the gross trends.

4. Discussion

The most intriguing result of this study is the variation of ion density ratios with beta in Figure 5, that is the increase at

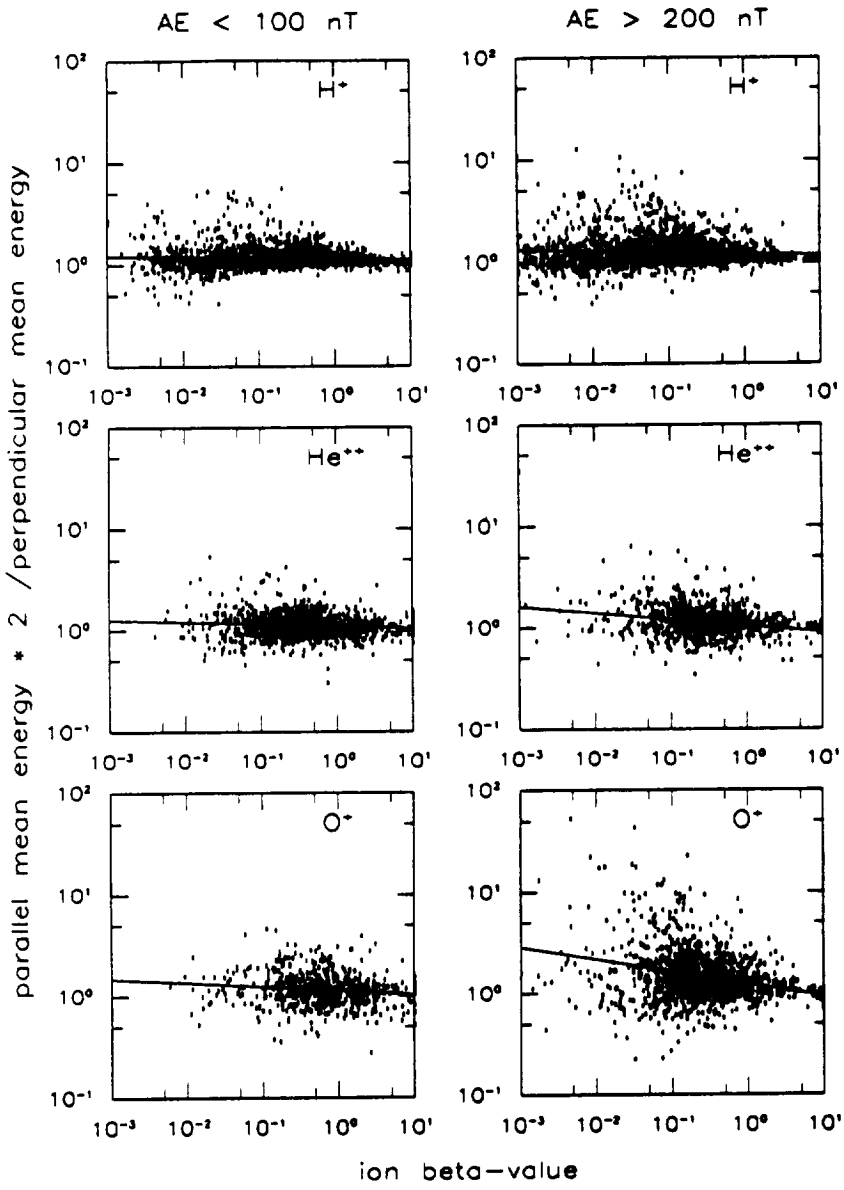

Figure 8. Parallel-to-perpendicular energy ratios for (top) H^+, (middle) He^{++}, and (bottom) O^+, when energies obtained with less than 33% statistical uncertainty (see text for details).

low beta. On one hand, it is in qualitative agreement with the theoretical result of *Kiessling and Ziegler* [1989] regarding the O^+/H^+ ratio, but on the other hand there are instrumental and statistical effects that will conspire to produce a similar result, as shown by the absolute values of negative ratios in Figure 9 (top panels). These effects are due to low count rates, low signal-to-noise ratio, and occasional time aliasing associated with the separate sampling of different ions and of ions and background. The data have been examined very extensively for evidence of these effects, both by imposing various selection criteria in the statistical analysis and by studying many sample events in detail. They are no doubt significant, as Figure 9 proves, but they do not appear to be the sole or even dominant reason.

Figure 10 illustrates some of the ambiguities inherent in low count rates and a low signal-to-noise ratio. Figure 10 actually represents one of the "better" events, in a formal sense, in that the signal-to-noise ratio is still greater than one, if only marginally, at the times when the He^{++}/H^+ ratio approaches unity. Even so, the low count rates make it fruitless to try to compare the ions in the raw data; it is necessary to sum counts into moments before any kind of pattern can be recognized. In this case the densities of H^+ and He^{++} ions become roughly comparable twice, when the H^+ density is at a local minimum (top panel).

This could still be a time aliasing effect in the background subtraction, since the background measured during the corresponding instrument cycles may have been lower than the actual background during the He^{++} samplings. However, by also comparing the mean energies of the two species in Figure 10, both on an E/Q (middle panel) and E/M basis (bottom panel), it appears that the data are at least consistent with a continuous signal for both H^+ and He^{++} ions. It is clear that the two sets of energies in this case are more

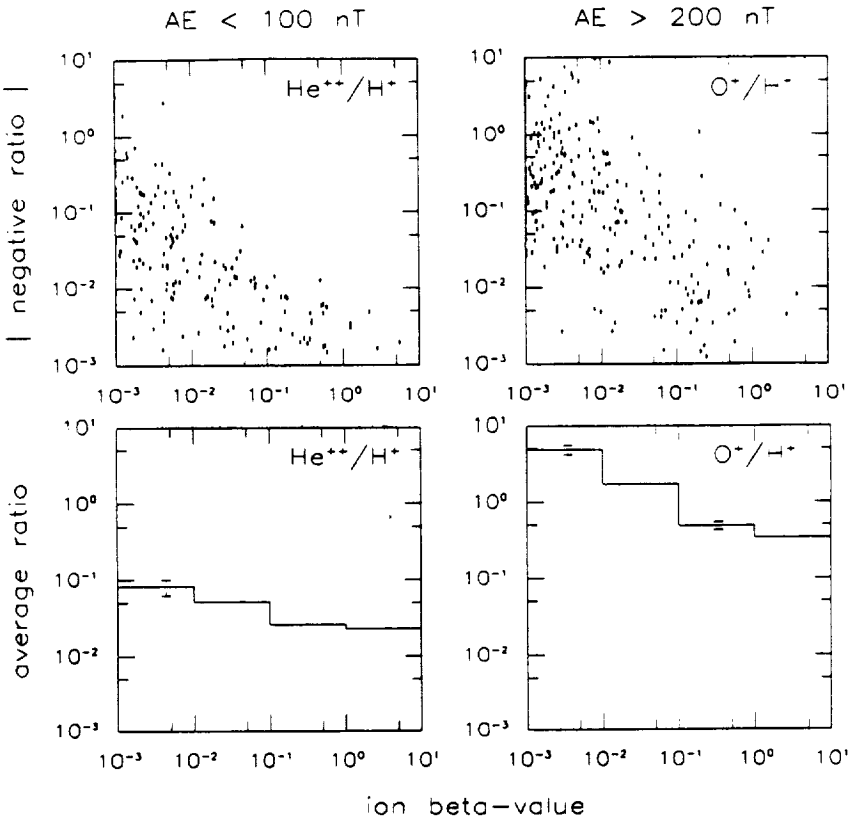

Figure 9. (Top) Examples of negative numbers (modulus) corresponding to the various panels of Figure 5. (Bottom) Corresponding averages (unweighted) when positive and negative numbers are both included (error bars indicate standard deviation of average when larger than line width).

nearly equal on an E/M basis. This would not be expected if background were dominant. In that case the energies would be widely scattered but have a tendency to show equal energy per charge on average, since the total range is measured in E/Q and only positive values are being calculated (the two species sometimes have equal mean E/Q even when their signals are far above background).

In some cases the He^{++}/H^+ ratio is significantly reduced when the energy range of the data is extended to include the 10- to 100-eV/e channel, but in general the inclusion of this channel only serves to increase the scatter, while the trends remain much the same, as already mentioned in section 3.5. It is worth noting that the H^+ ions in the 100-eV to 16-keV range usually have a mean energy of at least 500 eV even at low beta (Figure 3), and if these ions are part of a Maxwell-Boltzmann type distribution, their companions at energies below 100 eV have less than 20% of the total density. In those cases where a significantly larger H^+ density is present below 100 eV, that partial density is probably due to H^+ ions with a different history than the main population [cf. *Parks et al.*, 1992].

There are three principal reasons why the statistical trends in Figure 5 are probably real, at least qualitatively, even if many of the individual values are not. The first is that the trends in Figure 5 still survive in Figure 6, after all densities (numerator and denominator) with an absolute magnitude smaller than or equal to three sigmas have been discarded. The top and middle panels of Figure 6 have few points left at small beta, but the ones that do remain are consistent with the same kind of elevated ratios and cannot be easily ascribed to poor counting statistics. At this level of significance the background subtraction should be less critical, and that is confirmed by the elimination of negative ratios altogether, as mentioned above. In order for that to be an artifact, the formulas for density calculations would have to give lower weights to count rates from the background channel than they did to count rates from the ion channels, but those formulas do in fact give identical weight to both, except for the sign.

The second reason is that the same basic trends remain when the H^+ density is replaced by the "total" density from the energy-analysis section of the instrument (not shown). This density is calculated each time a mass-resolved density is produced (section A2), providing a continuous time reference that helps to eliminate time aliasing as a significant factor. There is only a minor reduction in the ratios using this replacement, consistent with the multiple-ion contribution to the total count rate (proportional to the square root of Q/M at a given energy).

The third reason is that those trends also emerge when the data are binned in beta and averaged within each bin, including all ratios, positive and negative. Two examples are shown in the bottom panels of Figure 9, the left one corresponding to the top left panel of Figure 5, the right one to the bottom right panel of Figure 5. These two examples essentially bracket the slopes of the average ratios corresponding to the other four panels of Figure 5 and are a strong indication that there is an underlying bias toward increased

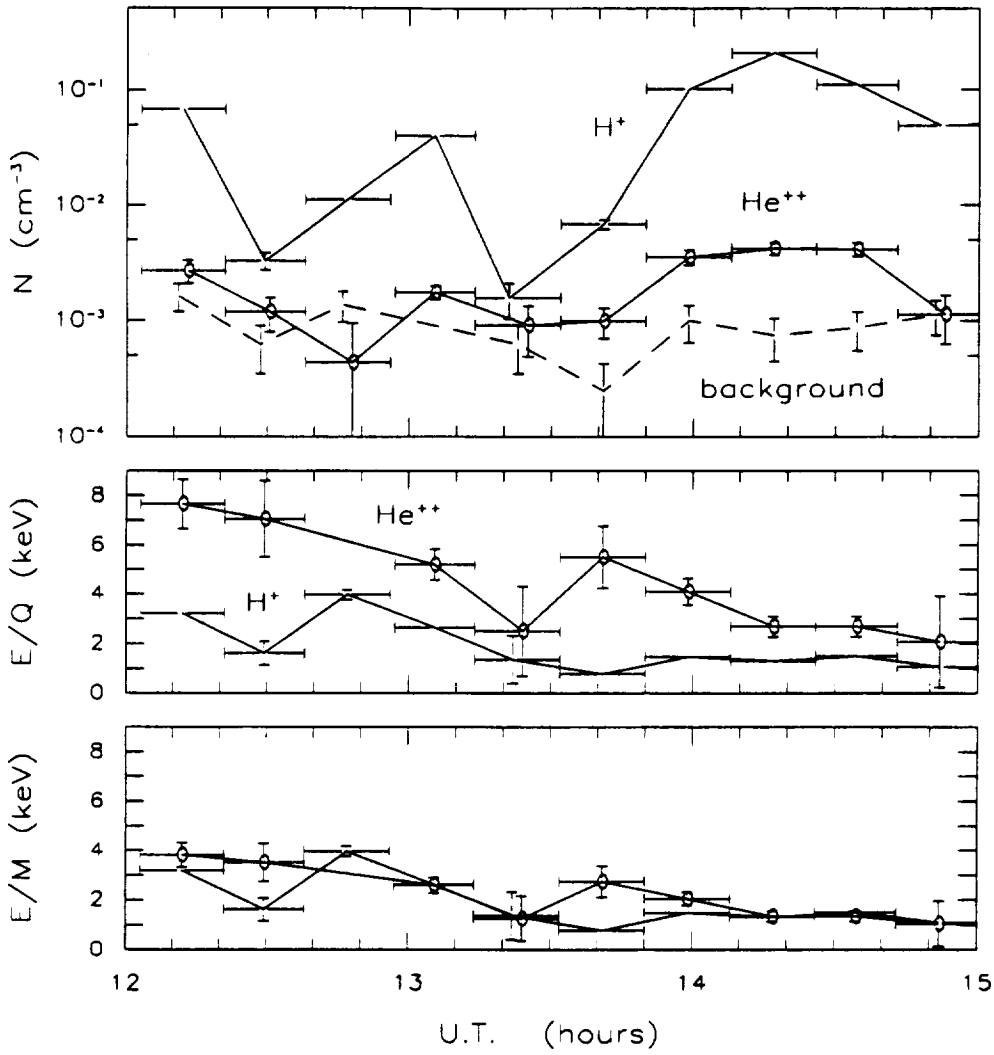

Figure 10. A 3-hour segment of data taken near local midnight on March 13, 1979, at 10 to 14R_E. Top panel shows densities of H^+ (line without symbols) and He^{++} (open circles), with background already subtracted, as well as the "density" of the background alone (dashed line) using weights corresponding to He^{++} ions. Lower panels show mean energies normalized by (middle) ionic charge or (bottom) mass. Horizontal bars indicate energy-mass scan cycle, vertical bars show standard deviation carried over from counting statistics.

positive ratios at low beta. This bias cannot be instrumental, because the detector response to penetrating radiation is independent of the M/Q setting of the optical parts and, as already stated, the formulas for density calculations would produce negative numbers as often as positive ones if count rates in the background channel and the ion channels were from the same statistical distribution.

Granted that there is a geophysical explanation for Figures 5 and 6, what specific physical quantity separates the different ions? One candidate might be the mean or median gyroradius of each species. At a geocentric distance $R > 10R_E$, and at beta <0.1 the tail magnetic field, as measured by the ISEE 1 magnetometer, typically ranges between 20 and 60 nT (depending mostly on distance from Earth). This means that a 3-keV H^+ ion, for example, has a gyroradius of 130 to 400 km at 90° pitch angle, and therefore a transverse range of 260 to 800 km during each gyration. This is small compared to the cross section of the tail, but not necessarily small compared to the transition region between the plasma sheet and tail lobes [e.g., *Parks et al.*, 1992, and references therein].

To make this point more tangible, assume the following: (1) Each density $n(i)$ of species i falls off with increasing distance dz from the plasma sheet proper with the functional dependence exp $(-dz/H)$, starting with $dz = 0$ at a point where beta = 0.1 (magnetic field already near its lobe value). (2) The "scale height" $H = H(i)$ is proportional to the mean gyroradius $g(i)$, and the proportionality constant is the same for all species. (3) The mean energy of each species is independent of dz, that is $H(i)$ is approximately constant. (4) Beta is dominated by the H^+ ions, which have the mean radius $g(H^+)$. Under these assumptions the coordinate dz can be approximated by

$$dz \approx H(H^+) \times \log [\text{beta}(0)/\text{beta}(dz)]/ \log (2.718)$$

and the ratio $r(i) = n(i)/n(H^+)$ is related to beta by

$$\log [r(i)] \approx A(i) - C(i) \times \log (\text{beta}) \quad (1)$$

where A and C are constants and

$$C(i) = [g(i) - g(H^+)]/g(i). \quad (2)$$

Considering that the gyroradius at a given pitch angle is proportional to the square root of the product of mass and energy and inversely proportional to charge, it would appear from the left panels of Figure 7 ($AE < 100$ nT), that the He^{++} ions should have a mean gyroradius twice that of H^+ ions (4 times the energy), assuming roughly isotropic velocity distributions (Figure 8), and the O^+ ions one that is about 4 times that of H^+ ions (about the same energy as the H^+). This means that the values of $C(i)$ for He^{++}/H^+ and O^+/H^+ in (2) ought to be about 1/2 and 3/4, respectively. Those numbers are in fact very close to the slopes of the respective regression lines in the left panels of Figure 5 (−0.56 and −0.80), a result that is surprising in view of the extreme simplicity of the assumptions.

Removing (3) and taking into account that the mean energies $E(i)$ of H^+, He^{++}, and O^+ ions decrease with decreasing beta, that is with increasing dz, means adding a third term $C(i) \times \log [E(H^+, dz)/E (H^+, 0)]$ on the right side of (1), but A and C are still constants as long as $E(i)/E (H^+)$ is constant. Inserting typical numbers for $E (H^+)$ from Figure 3 yields only small absolute values for this third term, at least an order of magnitude smaller than the second right-hand term in (1), so this equation is still a fair approximation, within the remaining assumptions, for the He^{++}/H^+ and O^+/H^+ ratios at $AE < 100$ nT.

On the other hand, (1) predicts that the He^+/H^+ ratio should have a slope intermediate between those of the He^{++}/H^+ and O^+/H^+ ratios, even after proper consideration of energies (A and C are not constant for He^+), while the left panels of Figure 5 (and Figure 6) show the steepest slope for the He^+/H^+ ratio. Furthermore, as beta receives greater contributions from ions other than the H^+ ions, especially from O^+ ions at active times, the slope of the log $[r(i)]$ versus log(beta) ought to increase, and that is not borne out in the right panels of Figure 5, so this simple "model" probably has severe limitations. All it really does is make it plausible that Figures 5 and 6 have a geophysical explanation. It should also be pointed out that the far more elaborate model of *Kiessling and Ziegler* [1989] does not have gyroradii as separate input parameters, although it does make the implicit assumption that the O^+ ions have four times larger gyroradii than the H^+ ions by assuming that both species have the same temperature (independent of beta).

5. Conclusions

To begin with, the large O^+/H^+ ratios in Figures 5 and 6 provide further evidence that ions of terrestrial origin constitute a large fraction of the tenuous energetic plasma in the tail lobes. This is keeping with the reasoning of *Sharp et al.* [1981], who based theirs on the large oxygen content of magnetic field-aligned ion streams. If one defines the lobes by beta <0.1 in these figures, it appears that during disturbed conditions ($AE > 200$ nT) the O^+ concentration typically exceeds that of H^+ ions, and is quite compatible with the finding by Sharp et al. that O^+ ions comprise about 2/3 to 3/4 of the tail lobe ion streams for $Kp > 3+$ (their Table 1). Since Figures 5 and 6 are based on all ion flux entering the instrument, not merely the peak flux, the large O^+ concentration measured here can be considered a generalization of the result of Sharp et al.

Where do H^+ ions fit in this picture? What is their principal origin? As far as their energies are concerned, they are much better correlated with the He^{++} ions than they are with either the O^+ or He^+ ions, according to Figure 7, which suggests that a majority of the H^+ ions in the Earth's tail are of solar rather than terrestrial origin, most of the time. This impression is strengthened by the observation that the H^+ and He^{++} ions tend to have about the same energy per nucleon in the top panels of Figure 7 (see specific example in Figure 10), a relationship that is characteristic of H^+ and He^{++} ions in the solar wind.

It should be mentioned that the slight negative slope of the He^{++}/H^+ regression lines in Figure 7 is probably an instrumental effect, caused by a combination of higher ion energies at higher beta (Figure 3) and the upper energy cutoff at 16 keV/e. Since the latter is measured in energy per charge, it leads to a more rapid loss of He^{++} than H^+ ions from the measured energy range if these ions are energized in proportion to either ionic mass or initial energy (see more extensive discussion of this subject by *Lennartsson and Shelley* [1986]). The same effect is probably responsible for the slight downward shift of the regression line at $AE > 200$ nT, since the H^+ and He^{++} energies are higher during active times (Figure 3).

Assuming that the H^+ ions are indeed mostly of solar origin, and ignoring for a moment the He^{++} ions, it follows from the bottom panels of Figures 5 and 6 that the solar ions usually outnumber the terrestrial ions in the plasma sheet, at beta >0.1. How do the solar ions reach the near-Earth plasma sheet? Do all of these ions arrive from the distant tail by the combined means of earthward jetting along the magnetic field lines and earthward convection in a predominantly dawn-dusk oriented electric field [e.g., *Speiser*, 1965], or do they enter in large part by cross-tail convection from the dawn and dusk flanks, as argued in *Lennartsson* [1992]? The answer to that question depends on the actual geometry and temporal behavior of the tail electric field, neither of which is well known at present. However, there are some features of these data that seem to favor the second means of transportation, that is the cross-tail convection.

As Figure 4 shows, it is easy to find rapid (hundreds of km s^{-1}) earthward flows of H^+ ions, especially during disturbed conditions ($AE > 200$ nT). However, these flows are not the normal state of motion of the H^+ ions, not even at low beta; the normal state is to have slow (tens of km s^{-1}) bulk motion, including both earthward and tailward components. If the H^+ ions were mostly arriving from the distant tail, say from $100R_E$ downtail [*Zwickl et al.*, 1984], moving along magnetic field lines while at the same time convecting into the plasma sheet, that is convecting toward higher beta, they would tend to disperse according to field-aligned speed, leaving the faster ions at the lower beta. There is really no evidence of that in Figure 4; faster and slower flows occur at the same beta, at least at beta <0.1, and the slower flows are dominant everywhere. This situation would seem to imply that the bulk of the H^+ ions must be able to reach the near-Earth plasma sheet from somewhere besides the distant tail, and one possible mode of access would be by inward

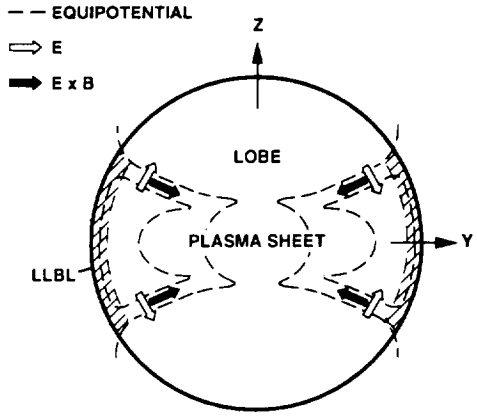

Figure 11. Hypothetical electric equipotentials (dashed lines) allowing inward tail convection from dawn and dusk flanks. These may originate in the low-latitude boundary layer (LLBL), as indicated by closed contours [*Lennartsson*, 1992], or in the solar wind, as indicated by open contours (assuming dawn-dusk directed E field in solar wind).

convection from the tail flanks, in an electric field that is locally north-south directed in a proper sense, for example as outlined in Figure 11.

It should be noted that the predominantly small V_X values at low beta in Figure 4 cannot be ascribed to poor counting statistics, since they cannot be consistently smaller than their absolute errors. Neither can they be ascribed to infrequent sampling of the earthward magnetic field-aligned direction, because the pitch angle range of the data is generally the widest at the lowest beta, and even when the data are limited to those with the most complete pitch angle coverage, as done in Figure 8, there is no significant field-aligned anisotropy in the H^+ population as a whole (top panels). So even though rapid earthward flows are common, a nearly isotropic velocity distribution is more common yet among H^+ ions at all beta. It is also worth mentioning that the particle counter in the energy-analysis section of the instrument does not detect a significantly more frequent occurrence of rapid earthward flows than does the "mass detector," even though its angular response is more favorable (in the northern lobe), counting ions moving in the spin plane or slightly downward (not shown).

Returning to the He^{++} ions, which may all be of solar origin, it should be mentioned that they have V_X values similar to those of the H^+ ions (not shown), including numerous negative ones (see examples in the work by *Lennartsson* [1992]), although the scatter is enhanced by frequently poor counting statistics. Of greater interest, however, is the difference between the He^{++} and H^+ ions in terms of their density gradients, as implied by Figures 5 and 6 (top panels). It is hard to imagine how this could arise from velocity dispersion among ions streaming earthward from the distant tail, since there is no indication that He^{++} ions are moving any faster than H^+ ions in general (about same E/M in Figure 7). Furthermore, this spatial relationship between the He^{++} and H^+ ions is basically similar to the relationship between the O^+ and H^+ ions, even though the O^+ ions are flowing almost exclusively tailward at low beta (not shown) and have generally small velocities as well (fairly low energies in Figure 7 despite the large ionic mass).

As suggested by the simple exercise in the preceding section, the varying density gradients may be physically related to the different gyroradii of different ions. If that is true, it would seem to require that the gyrocenter motion of all ions is largely perpendicular to the density gradients, that is parallel to the boundary between the plasma sheet and the lobes. That state of motion could be set up in accordance with Figure 11, for example.

Since the mass-dependent gradients in Figures 5 and 6 are qualitatively similar to the theoretical result of *Kiessling and Ziegler* [1989] for H^+ and O^+ ions, whether or not the ion gyroradii are truly the ordering parameters, it is reasonable to assume that there may also be some fundamental similarities between actual and modeled particle drifts. It is therefore interesting to note that their model, which has only two spatial coordinates, GSM X and Z, assumes purely one-dimensional bulk motion along the Y axis, that is along surfaces of constant magnetic field and constant beta. Despite the two-dimensional character of their model, that state of motion is conceptually similar to having ions convect according to Figure 11.

The obvious test to make with the existing data is to examine how the calculated bulk velocities in the GSE Y direction vary across the tail. A preliminary study along those lines has been made, using the ion beta as a measure of latitude, but the results are not yet conclusive. The calculated V_Y values are typically in the range of tens of km s^{-1}, and are to some extent consistent with Figure 11 (not shown), but it appears that beta is inadequate as a measure of location across the shear boundary in the velocity field, and further study is required. In order to extract true bulk velocities it is also necessary to consider the effects of a gradient in the spatial distribution of ion gyrational motion (due to the density gradients).

Finally, it is natural to view Figures 5 and 6 against the now well-documented "deficiency" in the magnetospheric content of He^{++} ions when compared to the solar wind [e.g., *Young et al.*, 1982; *Gloeckler and Hamilton*, 1987]. The central plasma sheet was found to have a higher He^{++}/H^+ ratio than the inner magnetosphere by *Lennartsson and Shelley* [1986], reaching average values of about 3% during quiet conditions, but still lower than the typical solar wind ratio of about 4% during the same phase of the solar cycle (rising phase; see for example *Feldman et al.* [1978]). According to Figures 5 and 6, the He^{++}/H^+ ratio is instead enhanced over solar wind values in the tail lobes. Does this mean that solar wind He^{++} ions are partially stripped away from the accompanying H^+ ions during entry into the geotail and subsequently left behind in the lobes? This scenario cannot be excluded at this point, but if Figure 11 properly depicts the plasma convection, then the He^{++} ions would eventually rejoin the H^+ ions when the convection turns into the central plasma sheet. Another possible explanation for the reduced He^{++}/H^+ ratio in the central plasma sheet (and inner magnetosphere) is of course the admixture of terrestrial H^+ ions. Being that the H^+ and He^{++} ions often have about equal velocity distribution in the tail (Figure 7), this admixture may start at an early stage of solar plasma entry, for example in the cusp regions, as perhaps suggested by the numerical modeling of *Delcourt et al.* [1989].

Appendix

A1. Instrumentation

The ISEE 1 spacecraft (along with the ISEE 2) was launched on October 22, 1977, into an orbit with apogee at almost $23R_E$ (geocentric), perigee at about 300 km altitude, an inclination of 29°, and an orbital period of 57 hours. It was placed in a spinning mode with the axis nearly perpendicular to the solar ecliptic plane and with a period of approximately 3 s.

The Lockheed ion composition experiment on the ISEE 1 is one of a family of instruments using the same type of ion optics and covering nearly the same range of energies (0 eV/e to about 17 keV/e) which have also been flown on GEOS 1 and 2, DE 1, and AMPTE/CCE [*Shelley et al.*, 1978]. The ISEE 1 instrument consists of two nearly identical mass spectrometers with the respective fields of view centered 5° above and 5° below the spin plane, that is about 5° above and below the solar ecliptic plane. Data used in this study are from one of these, the one looking below the spin plane (seeing ions moving upward). Each field of view is about 10° wide along the spin plane, and some 10° to 50° wide transverse to this plane, being the widest at the low energy end (due to preacceleration) and gradually decreasing toward 10° with increasing energy. Information on the instantaneous pitch angles (at center of field of view) is provided by the ISEE 1 flux gate magnetometer [*Russell*, 1978].

Each spectrometer consists of an electrostatic analyzer to select energy per charge, followed by a combined electrostatic and magnetic analyzer to select mass per charge. Both analyzer sections have particle detectors, so at each energy setting the experiment provides both the total ion flux and the partial flux at a selected mass per charge. On ISEE 1 each combination of energy and mass is maintained for at least 1/16 s in high telemetry bit rate and 1/4 s in low (normal) bit rate. Different combinations are stepped through in a cyclic fashion according to patterns controlled by a random access memory which is programmable from the ground. The various ISEE 1 patterns, or "modes," used inside the magnetosphere require anywhere from 2 to 20 min to complete. The mass selections usually include one that blocks all ions from reaching the second detector, allowing intermittent measurements during each cycle of the noise associated with penetrating radiation. These measurements are later used to correct the count rates of mass analyzed ions. The total count rate in the first detector is not corrected this way, but this detector is much less susceptible to penetrating radiation because of its small size (spiraltron).

The maximum energy range of the ISEE 1 instrument is 0 eV/e (or spacecraft potential) to 17.9 keV/e, divided into 32 contiguous channels, although only a subset of these may be used in a given mode. The lowest channel, from 0 eV/e to about 100 eV/e, is normally limited to energies above 10 eV/e by a retarding potential analyzer (RPA) in the entrance. That same RPA is used to provide "cold plasma" data from 0 to 100 eV/e (retarding within the lowest channel) during parts of some scan cycles. Because of measurement uncertainties associated with spacecraft charging and plasma convection, the lowest-energy channel is treated separately when calculating velocity moments. Data from the highest-energy channel (above 16 keV/e) are excluded altogether here, because of a slight variation over time of the mass response of the ISEE 1 instrument in that channel. The numerical procedures used for weighting and summing counts from the various energy channels are such that the velocity moments correspond to an energy range of either 100 eV/e to 16 keV/e (in all figures) or 10 to 100 eV/e (discussed separately), the latter assuming no spacecraft charging.

The data used here have been obtained in several different energy-mass scan modes, but only in modes spanning at least the 0.1- to 16-keV/e energy range, whether that range is covered in a contiguous fashion (normally true) or not (see below), and only in modes which provide H^+ data from the mass analyzer, as opposed to modes which rely on "total ion" counts for approximate H^+ measurements. Any sampling that has not been corrected for background noise, because of gaps in the telemetry, for example, has been discarded.

A2. Data Format

This study makes use of an archival data set recently completed for NASA's Explorer Project and placed in the NSSDC under index number 77-102A-12I. The format of these data is designed to be a compact representation with roughly the same time resolution as that provided by the instrument energy-mass scan cycle. Although these data include various spectral information, this study is mainly based on files which contain velocity moments. Only a brief outline of the format can be provided here; a detailed explanation (user guide) may be obtained from the NSSDC. The time coverage of these data spans the so called "prime period" of ISEE operations, from the time of launch of ISEE 1 and 2 through the end of February 1980.

The main type of file used here contains separate velocity moments for the four principal ion species, H^+, He^{++}, He^+, and O^+, or in some cases a subset of these ions, depending on the instrument operating mode. The moments have been calculated once each energy-mass scan cycle, using two different methods to be explained below. In cases where the energy scans have left some channels unsampled, sometimes every other channel, an interpolation procedure has been employed, essentially assuming a linear variation of the differential flux. Each moment has a statistical uncertainty (standard deviation) assigned to it, calculated with standard formulas for error propagation [e.g., *Bevington*, 1969, pp. 56–64] assuming Poisson counting statistics and including the uncertainty in background subtraction [*Lennartsson and Sharp*, 1982].

A second type of file has velocity moments for "total ions," based on the total ion count rate in the electrostatic analyzer and assuming that this rate is due entirely to H^+ ions. These moments have been calculated once per energy scan, providing a time resolution of a couple of minutes or better, and usually have nearly continuous time coverage. The reason for using "total" moments here is to help interpret the mass-resolved moments (see text).

To calculate full three-dimensional velocity moments from the raw ISEE 1 data, the ion fluxes measured within the near-ecliptic field of view have been extrapolated to other angles using either of two sets of approximating assumptions:

1. The principal ion flow is parallel to the solar ecliptic plane and the ion fluxes have rotational symmetry around the flow vector, regardless of the magnetic field orientation. The direction of the flow vector within this plane is deter-

mined by the measured flow within the instrument field of view. The single angular variable in this case is divided among twelve 30° spin angle bins, roughly approximating the inherent angular resolution of the ISEE 1 instrument in normal low-bit-rate operation.

2. Fluxes are gyrotropic (independent of gyration angle) over the sampled range of pitch angles, and isotropic outside of this range, maintaining the values measured at the smallest and largest pitch angles, respectively. The pitch angles are divided among nine 20° bins. This assumption is only applied to number densities, mean energies, parallel and perpendicular to the magnetic field, and energy densities. It ignores any net bulk flow perpendicular to the magnetic field.

The moments reported here are those obtained with 1, except when they refer specifically to components parallel and perpendicular to the magnetic field, thus necessitating the use of 2. The two sets of assumptions usually provide about the same densities and total mean energies, within statistical uncertainties, but the numbers obtained with 1 are believed to be at least marginally more accurate in most cases. Although the drift direction in 1 is determined from average fluxes in 30° wide bins, the weighting involved in the integrations usually provides an accuracy much better than 30°.

The moment data have been supplemented with a third type of file, containing a form of energy-angle spectra for the same four ion species (and for O^{++} ions). These spectra consist of spin-averaged count rates in each energy channel (typically all 32 channels), averaged over a single energy-mass scan cycle, combined with information about the maximum count rate at each energy during that cycle. This information includes the time and spin angle of the maximum, the maximum rate, and the angular range of counts greater than 1/3 of the maximum rate. These have been used to verify that the moments still have reasonable values when count rates are narrowly focused in angle or energy and are otherwise low, as often happens in the tail lobes [*Sharp et al.*, 1981].

Acknowledgments. The author wishes to thank H. L. Collin for helpful discussions and for his assistance in preparing computer plotting routines and computer records of geophysical indices. The author is also indebted to C. T. Russell for the use of spacecraft magnetometer data and to the National Oceanic and Atmospheric Administration for the use of magnetic tape records of the geophysical indices. This work was supported by NASA under contracts NAS5-31209 and NAS5-33047 and by Lockheed Independent Research.

The Editor thanks H. K. Hills and H. J. Ziegler for their assistance in evaluating this paper.

References

Akasofu, S.-I., E. W. Hones, Jr., S. J. Bame, J. R. Asbridge, and A. T. Y. Lui, Magnetotail and boundary layer plasmas at a geocentric distance of ~$18R_E$: VELA 5 and 6 observations, *J. Geophys. Res.*, *78*, 7257, 1973.

Bevington, P. R., *Data Reduction and Error Analysis for the Physical Sciences*, McGraw-Hill, New York, 1969.

DeCoster, R. J., and L. A. Frank, Observations pertaining to the dynamics of the plasma sheet, *J. Geophys. Res.*, *84*, 5099, 1979.

Delcourt, D. C., C. R. Chappell, T. E. Moore, and J. H. Waite, Jr., A three-dimensional numerical model of ionospheric plasma in the magnetosphere, *J. Geophys. Res.*, *94*, 11,893, 1989.

Eastman, T. E., L. A. Frank, and C. Y. Huang, The boundary layers as the primary transport regions of the earth's magnetotail, *J. Geophys. Res.*, *90*, 9541, 1985.

Feldman, W. C., J. R. Asbridge, S. J. Bame, and J. T. Gosling, Long-term variations of selected solar wind properties: Imp 6, 7, and 8 results, *J. Geophys. Res.*, *83*, 2177, 1978.

Gloeckler, G., and D. C. Hamilton, AMPTE ion composition results, *Phys. Scr.*, *T18*, 73, 1987.

Hardy, D. A., H. K. Hills, and J. W. Freeman, Occurrence of lobe plasma at lunar distance, *J. Geophys. Res.*, *84*, 72, 1979.

Hones, E. W., Jr., J. R. Asbridge, and S. J. Bame, Time variations of the magnetotail plasma sheet at $18R_E$ determined from concurrent observations by a pair of Vela satellites, *J. Geophys. Res.*, *76*, 4402, 1971.

Hones, E. W., Jr., T. A. Fritz, J. Birn, J. Cooney, and S. J. Bame, Detailed observations of the plasma sheet during a substorm on April 24, 1979, *J. Geophys. Res.*, *91*, 6845, 1986.

Kamei, T., and H. Maeda, Auroral electrojet indices (*AE*) for January-June 1978, Data Book 3, World Data Cent. C2 for Geomagn., Kyoto, Jpn., April 1981.

Kiessling, M., and H. J. Ziegler, A theory of self-consistent two-dimensional tail equilibria for quasi-neutral $e^- H^+ O^+$ mixtures, *J. Geophys. Res.*, *94*, 261, 1989.

Lennartsson, W., A scenario for solar wind penetration of Earth's magnetic tail based on ion composition data from the ISEE 1 spacecraft, *J. Geophys. Res.*, *97*, 19,221, 1992.

Lennartsson, W., and R. D. Sharp, A comparison of the 0.1–17 keV/*e* ion composition in the near equatorial magnetosphere between quiet and disturbed conditions, *J. Geophys. Res.*, *87*, 6109, 1982.

Lennartsson, W., and E. G. Shelley, Survey of 0.1- to 16-keV/*e* plasma sheet ion composition, *J. Geophys. Res.*, *91*, 3061, 1986.

Parks, G. K., et al., Low-energy particle layer outside of the plasma sheet boundary, *J. Geophys. Res.*, *97*, 2943, 1992.

Press, W. H., B. P. Flannery, S. A. Teukolsky, and W. T. Vetterling, *Numerical Recipes*, Cambridge University Press, New York, 1986.

Russell, C. T., The ISEE 1 and 2 fluxgate magnetometers, *IEEE Trans. Geosci. Electron.*, *GE-16*, 239, 1978.

Sharp, R. D., D. L. Carr, W. K. Peterson, and E. G. Shelley, Ion streams in the magnetotail, *J. Geophys. Res.*, *86*, 4639, 1981.

Shelley, E. G., R. D., Sharp, R. G. Johnson, J. Geiss, P. Eberhardt, H. Balsiger, G. Haerendel, and H. Rosenbauer, Plasma composition experiment on ISEE-A, *IEEE Trans. Geosci. Electron.*, *GE-16*, 266, 1978.

Speiser, T. W., Particle trajectories in model current sheets, 1, Analytical solutions, *J. Geophys. Res.*, *70*, 4219, 1965.

Young, D. T., H. Balsiger, and J. Geiss, Correlations of magnetospheric ion composition with geomagnetic and solar activity, *J. Geophys. Res.*, *87*, 9077, 1982.

Zwickl, R. D., D. N. Baker, S. J. Bame, W. C. Feldman, J. T. Gosling, E. W. Hones, Jr., D. J. McComas, B. T. Tsurutani, and J. A. Slavin, Evolution of the Earth's distant magnetotail: ISEE 3 electron plasma results, *J. Geophys. Res.*, *89*, 11,007, 1984.

O. W. Lennartsson, Lockheed Missiles and Space Company, Incorporated, Research and Development, Palo Alto, CA 94304-1191. (e-mail.SPAN.lockhd::Lenn)

(Received July 30, 1993; revised October 8, 1993; accepted November 8, 1993.)

JOURNAL OF GEOPHYSICAL RESEARCH, VOL. 98, NO. A11, PAGES 19,443–19,454, NOVEMBER 1, 1993

Experimental Investigation of Possible Geomagnetic Feedback From Energetic (0.1 to 16 keV) Terrestrial O^+ Ions in the Magnetotail Current Sheet

O. W. LENNARTSSON, D. M. KLUMPAR, E. G. SHELLEY, AND J. M. QUINN

Division of Research and Development, Lockheed Missiles and Space Company, Incorporated, Palo Alto, California

Data from energetic ion mass spectrometers on the ISEE 1 and AMPTE/CCE spacecraft are combined with geomagnetic and solar indices to investigate, in a statistical fashion, whether energized O^+ ions of terrestrial origin constitute a source of feedback which triggers or amplifies geomagnetic activity, as has been suggested in the literature, by contributing a destabilizing mass increase in the magnetotail current sheet. The ISEE 1 data (0.1–16 keV/e) provide in situ observations of the O^+ concentration in the central plasma sheet, inside of 23 R_E, during the rising and maximum phases of solar cycle 21, as well as inner magnetosphere data from same period. The CCE data (0.1–17 keV/e), taken during the subsequent solar minimum, all within 9 R_E, provide a reference for long-term variations in the magnetosphere O^+ content. Statistical correlations between the ion data and the indices, and between different indices, all point in the same direction: there is probably no feedback specific to the O^+ ions, in spite of the fact that they often contribute most of the ion mass density in the tail current sheet.

1. INTRODUCTION

Singly charged oxygen is a variable but usually substantial component of the magnetospheric plasmas at most energies [*Shelley et al.*, 1972; *Ghielmetti et al.*, 1978; *Balsiger et al.*, 1980; *Sharp et al.*, 1981; *Lundin et al.*, 1982; *Lennartsson and Shelley*, 1986; *Möbius et al.*, 1987; *Gloeckler and Hamilton*, 1987; *Chappell et al.*, 1987]. It is perhaps, besides H^+ and He^{++} ions, the most important ion component from a scientific point of view, for at least two reasons. One is its principal source, Earth's atmosphere [*Young et al.*, 1982; *Kremser et al.*, 1988], which makes it a unique measure of electrical solar-terrestrial interactions. This is the one aspect that has received the closest attention in the literature so far. Another reason, however, is the large mass or mass per charge of the O^+ ions compared to that of the H^+ ions. A mere 10% admixture of O^+ ions in an otherwise pure H^+ population will more than double the mass density of the plasma, even though the number density and charge density remain almost the same. And a 50-50 mixture of O^+ and H^+ ions, often reached in the inner magnetosphere [*Lennartsson and Sharp*, 1982] and sometimes in the central plasma sheet as far out as 20 R_E [*Peterson et al.*, 1981], will have almost an order of magnitude greater mass density than the corresponding number of only H^+ ions. This property of the O^+ component may have significant consequences for the plasma dynamics; it certainly has for hydromagnetic wave propagation [e.g., *Singer et al.*, 1979].

Although the energetic (keV) O^+ ions observed in the near-equatorial magnetosphere are commonly perceived to be a product of geomagnetic storm or substorm activity, a good case has been made for feedback effects as well [e.g., *Baker et al.*, 1982, 1985; *Delcourt et al.*, 1989; *Daglis et al.*, 1990, 1991; *Moore and Delcourt*, 1992; *Swift*, 1992]. *Baker et al.* [1982] argued that the addition of such O^+ ions in the tail current sheet, after the onset of a substorm, will have a destabilizing effect on this sheet, especially at $-15\ R_E <$ GSM $X < -10\ R_E$, the reason being that the large mass per charge of the O^+ ions may cause the sheet ion population to become increasingly demagnitized and therefore more susceptible to ion tearing mode instabilities. This course of reasoning allows for the initial increase in the tail O^+ population, after a period of geomagnetic quiescence, to be induced entirely by external forces, but it suggests that the increased concentration of O^+ ions will promote consequent substorm onsets, thereby prolonging and strengthening many active periods.

One observational fact that may seem to fit with that kind of scenario is the tendency of very strong substorms, those with a peak AE index of 1000 nT or greater, to occur in clusters during extended periods (often a day or longer) of elevated AE (see, for example, *Kamei and Maeda* [1981] and *Baker et al.* [1985]). On the other hand, more long-term records of geomagnetic and solar activity, covering several years, may not seem to fit the same trend, because the energetic O^+ population has been found to vary substantially in density over the course of a solar cycle without causing a parallel long-term variation of geomagnetic activity [*Young et al.*, 1982; *Yau et al.*, 1985; *Lennartsson*, 1989]. None of the long-term studies of O^+ ions has been specifically directed towards the feedback aspect, however, so there is still room for doubt either way.

This study attempts to clarify, to the extent possible with statistical methods, whether there is a geomagnetic feedback specific to the O^+ ions, by comparing extensive sets of near-equatorial ion composition data with common geomagnetic and solar activity indices. In order to utilize the long-term observations now available from similar experiments, data obtained during the rising and maximum phases of solar cycle 21 by a mass spectrometer on the International Sun-Earth Explorer (ISEE 1) spacecraft are intercompared with data obtained near the end of the same cycle, at the minimum phase, by the same kind of spectrometer on the Charge Composition Explorer (CCE) spacecraft of the Ac-

Paper number 93JA01991.
0148-0227/93/93JA-01991$05.00

tive Magnetosphere Particle Tracer Explorer (AMPTE) mission.

The focus of this study is on the consequences, if any, of increasing the average mass per ion in the central plasma sheet by adding O^+ ions, or replacing H^+ ions with O^+ ions. It is recognized that the O^+ ions, along with other ions of terrestrial origin, energetic or not, must have some role in magnetosphere dynamics simply by contributing a positive plasma component but that aspect is more complex and does not necessarily distinguish the O^+ as a species. It is the exceptional capability of the O^+ to enhance the plasma mass density that is of principal interest here.

2. Instrumentation

The ISEE 1 spacecraft (along with the ISEE 2) was launched on October 22, 1977, into an orbit with apogee at almost 23 R_E (geocentric), perigee at ~300 km altitude, an inclination of 29°, and an orbital period of 57 hours. It was placed in a spinning mode with the axis nearly perpendicular to the solar ecliptic plane and with a period of approximately 3 s. The AMPTE CCE, one in a stack of three separate spacecraft, was launched on August 16, 1984, and directed into a very nearly equatorial orbit with apogee at almost 9 R_E, perigee at ~1000 km altitude, an inclination of less than 5°, and an orbital period of 15.6 hours. The AMPTE CCE is also in a spinning mode, but its spin axis is parallel to Earth's equatorial plane, pointing some 10° to 30° from the Sun direction, and its spin period is 6 s.

The Lockheed ion composition experiments flown on ISEE 1 and AMPTE/CCE are two of a family of instruments using the same type of ion optics and covering nearly the same range of energies (0 eV/e to ~17 keV/e) which have also been flown on GEOS 1 and 2 and on DE 1 [*Shelley et al.*, 1978, 1985]. The ISEE 1 instrument consists of two nearly identical mass spectrometers with the respective fields of view centered 5° above and 5° below the spin plane, that is about 5° above and below the solar ecliptic plane. Data used in this study are from one of these, the one looking below the spin plane. The CCE instrument has a single mass spectrometer with the field of view centered in the spin plane, which in that case is roughly perpendicular to the solar ecliptic plane, oriented somewhat like the GSE *Y-Z* plane. Each field of view is ~10° wide along the spin plane, and some 10° to 50° wide transverse to this plane, being the widest at the low-energy end (due to preacceleration) and gradually decreasing toward 10° with increasing energy. Information on the instantaneous pitch angles (at center of field of view) is provided by the ISEE 1 fluxgate magnetometer [*Russell*, 1978] and the AMPTE CCE Magnetic Field Experiment [*Potemra et al.*, 1985].

Each spectrometer consists of an electrostatic analyzer to select energy per charge, followed by a combined electrostatic and magnetic analyzer to select mass per charge. Both analyzer sections have particle detectors, so at each energy setting the experiments provide both the total ion flux and the partial flux at a selected mass per charge. On ISEE 1 each combination of energy and mass is maintained for at least 1/16 s in high telemetry bit rate and 1/4 s in low (normal) bit rate, on CCE the corresponding time is 1/32 s. Different combinations are stepped through in a cyclic fashion according to various patterns controlled by a random access memory which is programmable from the ground. The ISEE 1 patterns, or "modes," used inside the magnetosphere usually require from 2 to 17 min to complete. Most commonly used CCE patterns require ~2 min per cycle. The mass selections include one that blocks all ions from reaching the second detector, allowing intermittent measurements of the noise associated with penetrating radiation. These measurements are later used to correct the count rates of mass analyzed ions.

The maximum energy range is 0 eV/*e* (or spacecraft potential) to 17.9 keV/*e*, divided into 32 contiguous channels, although only a subset of these may be used in a given mode (typically only 15 channels on CCE). The lowest channel, from 0 eV/*e* to ~100 eV/*e*, is normally limited to energies above 10 eV/*e* on ISEE 1 and above 30 eV/*e* on CCE by an RPA (retarding potential analyzer) in the entrance. That same RPA is used to provide "cold plasma" data from 0 to 100 eV/*e* (retarding within the lowest channel) during part of some measurement cycles. Because of measurement uncertainties associated with spacecraft charging and plasma convection, the lowest energy channel is treated separately when calculating velocity moments. Data from this channel are not included in the statistical material here but are discussed briefly in a separate section. In the case of ISEE 1, data from the highest-energy channel (above 16 keV/*e*) are also excluded from moment calculations, because of a slight variation over time of the mass response in that channel. Whenever the energy scans have left some intermediate energy channels unsampled, an interpolation procedure has been employed, assuming a linear variation of the differential flux. Given these considerations, and given the numerical procedures used for weighting and summing counts from the various energy channels, the velocity moments displayed in the following figures correspond to an energy range of ~100 eV/*e* to 16 keV/*e* for ISEE 1 and 100 eV/*e* to 17 keV/*e* for AMPTE/CCE.

3. Data Formats

This study is the first extensive application of two archival data sets recently completed for NASA's Explorer Project. The formats of these data are designed to be a compact representation, with roughly the same time resolution as that provided by the instrument energy-mass scan cycle. Although these data sets include various spectral information, only the files containing velocity moments have been used here.

The ISEE 1 data files contain separate velocity moments for the four principal ion species, H^+, He^{++}, He^+, and O^+, calculated once each energy-mass scan cycle, using two different methods to be explained below. Each moment has a statistical uncertainty (standard deviation) assigned to it, calculated with standard formulas for error propagation assuming Poisson counting statistics and including the uncertainty in background subtraction. In addition, there are velocity moments for "total ions," based on the total ion count rate in the electrostatic analyzer and assuming that this rate is due entirely to H^+ ions. These moments are calculated once per energy scan, providing a time resolution of a couple of minutes or better, and usually have nearly continuous time coverage. The reason for including "total" moments here is to help separate mass-resolved moments taken in different plasma regimes (see next section).

To calculate full three-dimensional velocity moments from

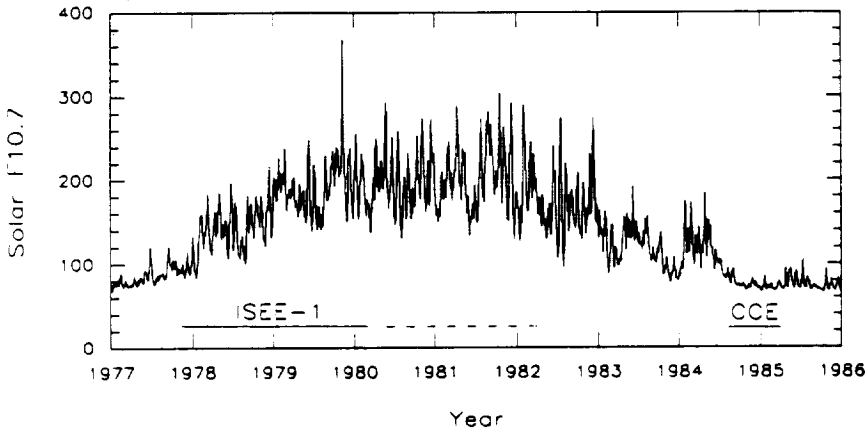

Fig. 1. Time ranges of available ion composition data in relation to solar activity. Only the solid line (archived) portion of the ISEE 1 data is used here (years labeled at beginning).

the raw ISEE 1 data, the ion fluxes measured within the near-ecliptic field of view have been extrapolated to other angles using either of two sets of approximating assumptions:

1. The principal ion flow is parallel to the solar ecliptic plane and the ion fluxes have rotational symmetry around the flow vector, regardless of the magnetic field orientation. The direction of the flow vector within this plane is determined by the measured flow within the instrument field of view. The single angular variable in this case is divided among 12 30° spin-angle bins, roughly approximating the inherent angular resolution of the ISEE 1 instrument in normal low-bit-rate operation.

2. Fluxes are gyrotropic (independent of gyration angle) over the sampled range of pitch angles, and isotropic outside of this range, maintaining the values measured at the smallest and largest pitch angles, respectively. The pitch angles are divided among nine 20° bins. This assumption is only applied to number densities, mean energies, parallel and perpendicular to the magnetic field, and energy densities. It ignores any net bulk flow perpendicular to the magnetic field.

The two sets of assumptions typically yield about the same number densities and total energy densities, within statistical uncertainties, except for cases of substantial ecliptic ion drift across the magnetic field (substantial when compared to thermal velocities), when 1 appears to provide more accurate values, especially for number densities. This has been verified by comparing the ion densities with electron densities derived from ISEE 1 and 2 wave experiments on several occasions. Although the drift direction in 1 is determined from average fluxes in 30° wide bins, the weighting involved in the integrations usually provides an accuracy much better than 30°. For simplicity, the ISEE 1 number densities illustrated here are those derived from 1 when referring to the magnetotail (plasma sheet) and from 2 when referring to the inner magnetosphere (for comparison with CCE densities).

The AMPTE/CCE moment files use a common integration time of 6.4 minutes for both the mass resolved data and the total ion data. The CCE velocity moments have all been calculated according to approximation 2 above, including a standard deviation for each moment, except that the counts were initially separated between the right and left side of the magnetic field direction, in order to allow a cross-B velocity to be calculated (along with a parallel velocity). Because of the attitude and orbit of the spacecraft, the CCE instrument normally samples fluxes along the magnetic field direction. In addition to the H^+, He^{++}, He^+, and O^+ ions these files also include O^{++} ions. It is clear from these data that the O^{++} ions, as was assumed during the preparation of the ISEE 1 files, are generally much less abundant than the O^+ ions at these energies, typically by 1 to 2 orders of magnitude (see also *Young et al.* [1982]). The same appears to hold at higher energies as well, according to data from the CHEM experiment on AMPTE/CCE [*Kremser et al.*, 1988].

4. Data Selection

The time coverage of the ISEE 1 and AMPTE/CCE data sets through solar cycle 21 is illustrated in Figure 1, along with the daily index of 10.7-cm wavelength solar radio flux. This index is commonly used as a proxy for the solar extreme ultraviolet (EUV) radiation [*Hinteregger*, 1981] and is therefore an indirect measure of the solar radiant effects on the terrestrial O^+ source [e.g., *Young et al.*, 1982, and references therein]. Figure 1 shows the reason for intercomparing the two data sets; the ISEE 1 set was acquired during strongly varying solar activity, including the peak, the CCE set during weak and extremely steady solar activity. The significance of this will be clarified later.

Of all the ISEE 1 data available, only three subsets have been used here, one obtained in the central plasma sheet, the other two in the inner magnetosphere, in the same spatial region as the CCE data. The spatial distribution of the plasma sheet samplings is illustrated in Figure 2 in GSM coordinates, with each point representing one instrument energy-mass cycle. The samplings are all from geocentric distances beyond 10 R_E and have been further limited to -10 $R_E <$ GSM $Y <$ 10 R_E and GSM $X < -5$ R_E. The main reason for choosing this particular region is that the plasma sheet O^+ density has been found to have a rather broad maximum within 10 R_E of either side of local midnight during periods of hourly $AE > 200$ nT (see Figure 7*d* of *Lennartsson and Shelley* [1986]).

The central plasma sheet has been defined by the following conditions:

1. The sum of the H^+, He^{++}, He^+, and O^+ densities is at least 0.1 cm^{-3}.

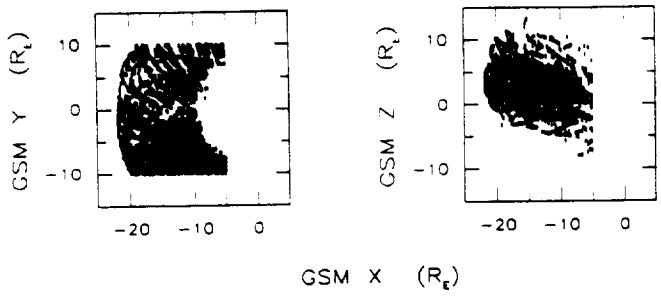

Fig. 2. Spatial extent of selected plasma sheet data set (ISEE 1) in Geocentric Solar Magnetospheric (GSM) coordinates.

2. The plasma beta value produced by these same ions is at least 0.1.

3. The multiple densities derived from the total ion count rates during the course of each energy-mass scan cycle, assuming only H^+ ions (see previous section), are all at least 0.05 cm^{-3}.

These conditions differ slightly from those used by *Lennartsson and Shelley* [1986] but lead to essentially the same selection, given the spatial constraints. The present data set is further constrained by the requirement that concurrent *AE* indices be available, resulting in the exclusion of samplings from 1977 (see *Kamei and Maeda* [1981], and subsequent data books). The resulting number of samples is 4056 (~1000 hours).

For this study the CCE samplings have first been binned and averaged into a time-space matrix of 1 hour UT by 1 hour MLT by one dipole L unit, in order to make the set more compact. The spatial distribution of the elements (average coordinates) is illustrated in Figure 3 in SM coordinates (same as GSM, except for a rotation around the Y axis to make the Z axis equal to the northward dipole axis). The samplings have been limited to $L > 6$ in order to ensure that the ion composition is controlled by the particle sources rather than by charge exchange decay [*Lennartsson and Sharp*, 1982]. In addition, the samplings have been confined to the inside of the magnetopause, by elimination of data that might be interpreted as magnetosheath or solar wind (based in part on total moments). The reason for dividing the data by year is that *AE* indices, at this writing, are not available on magnetic tape for 1985. The set is made up of 7998 individual 6.4-min samplings from 1984, and 8211 such samplings from 1985, binned and averaged into 1732 and 1728 matrix elements, respectively.

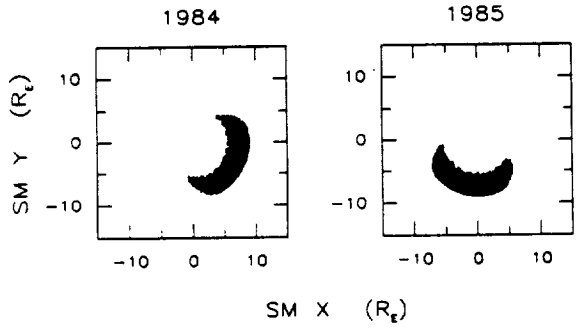

Fig. 3. Spatial extent of selected CCE data sets in Solar Magnetic (SM) coordinates. These extend in geomagnetic latitude from −16° to +12°. Equivalent regions are used for ISEE 1 data as well (see text).

The two spatial regions thus defined by the CCE data have in turn been used to select two "inner magnetosphere" sets of ISEE 1 data as well (similarly excluding magnetosheath and solar wind). The resulting number of samples in these ISEE 1 sets is 581 (corresponding to 1984 CCE set) and 693 (1985 CCE set).

5. Statistical Results

Whether auroral substorms, as defined by enhancements in the *AE* index, for instance, are triggered by an increasing concentration of O^+ ions in the tail current sheet [e.g., *Baker et al.*, 1982], or always start independently of the O^+, may seem to be a simple question of timing. The answer is not readily found by studying individual events, however, because the O^+ data from within the plasma sheet are rather spotty during active periods, due to plasma sheet motion and thinning, and the substorm activity is often recurring too rapidly to allow a unique association between enhancements in the *AE* and in the O^+ density. The only firm conclusion that can be drawn from previous event studies is that there are numerous cases where the ISEE 1 is in the central plasma sheet at a substorm expansion onset and does not observe a large concentration of O^+ (>10%) until after onset (R. D. Sharp, unpublished manuscript, 1982; see also *Baker et al.* [1985]). Hence we have had reasons to believe that substorms can occur before the O^+ density is enhanced in the tail, but we still do not know whether they occur more easily if the O^+ density is already high, or if they are stronger in that case.

5.1. *Relative Timing*

As a first step in addressing this question, the entire set of ISEE 1 plasma sheet data, as defined above (see Figure 2), was scoured for evidence that the O^+/H^+ density ratio might sometimes undergo a significant increase shortly before such an increase takes place in the *AE* index. Several different approaches were tried, using different definitions of "significant increase" and "shortly before." The result was essentially negative; there was no clear evidence that any increment in the *AE* could be uniquely associated with a preceding, or even simultaneous, increase in the O^+/H^+ ratio, and this was due in part to the difficulties already mentioned. One approach, for example, was to use hourly *AE* indices and pose the following problem:

Find each sampling with an O^+/H^+ ratio greater than 30%, which is preceded by at least a 3-hour period of samplings with O^+/H^+ consistently less than 20%, allowing no more than 60 min for data gaps during that period, and check whether the concurrent or succeeding hourly *AE* is greater, by any amount, than the preceding 3-hour average *AE*. The result: No case of a succeeding increase in the hourly *AE*, but one case of a concurrent increase. In that one case the 1-min *AE* indices were examined next, and the *AE* proved to increase ahead of the increase in the O^+/H^+ ratio.

5.2. *Correlation Between AE and Average Ion Mass in Plasma Sheet*

Figure 4 shows a purely statistical approach, where each plasma sheet sampling is represented by its linearly averaged

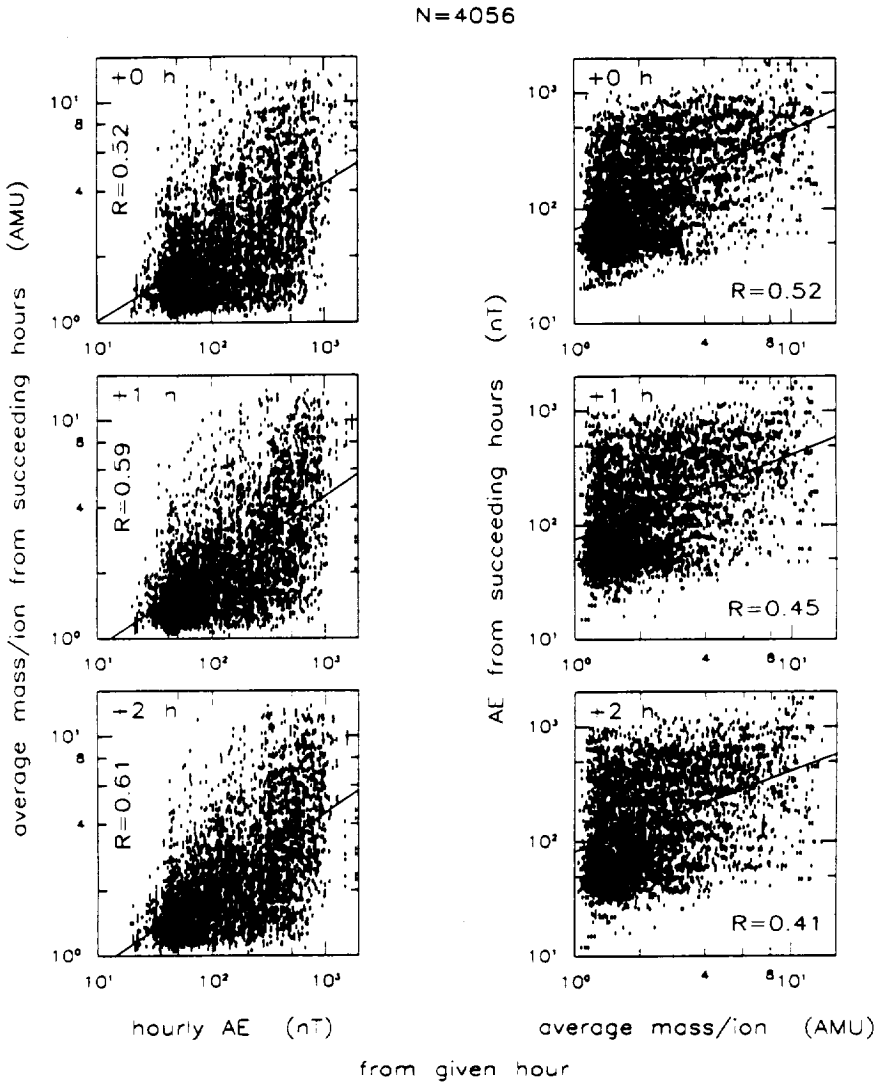

Fig. 4. Scatterplots of average ion mass in plasma sheet versus hourly *AE* (left) and vice versa (right). The top panels compare *AE* readings and mass samplings from same hour, the lower panels compare *AE* or mass with mass and *AE* from the first (middle) and second (bottom) succeeding hour. The regression lines in this and following figures have a correlation coefficient as indicated by parameter *R*. The parameter *N* indicates the number of data points in each panel.

ion mass, weighted by the respective densities of H^+, He^{++}, He^+, and O^+ ions (thus having a range of 1.0 to 16.0 amu), and is associated with hourly *AE* indices from the same (top panels) or adjacent hours. Because the He^{++} ions are always in minority here (almost always less than 10% of total number density), the average mass is also approximately the average mass per charge, which may be the physically more significant quantity (or mass divided by the square of the charge). This mass, whether associated with ion or charge, is not expected to be significantly defective by not including O^{++} ions (see end of section 3).

In the left panels of Figure 4 the average mass is treated as a function of the hourly *AE* index, allowing up to 2 hours delay from each *AE* reading to the plasma sheet sampling. The slanted straight line in each panel is the linear least squares fit of log (mass) versus log (*AE*). The reason for using a linear fit here is that when the *AE* is binned, rather than scattered, the logarithm of the average mass in each *AE* bin is approximately a linear function of the logarithm of *AE* (not shown). The correlation coefficient, denoted by the letter R, is significant in each case, given the large number of points (4056). The generally greater mass/ion during active times is due to a combination of increasing O^+ density and decreasing H^+ and He^{++} densities [see *Lennartsson and Shelley*, 1986]. The He^+ ions contribute a negligible density in the central plasma sheet at most times. It can be seen that the correlation is somewhat better with a 2-hour delay than with a shorter delay, or no delay. The correlation with a 2-hour delay is in fact at its maximum; it declines again with longer delays, reaching a value of $R = 0.45$ with a 5-hour delay, for instance (not illustrated).

In the right panels of Figure 4 the *AE* index is similarly treated as a function of the average mass, using the same set of plasma sheet samplings. In this case the correlation coefficient declines monotonically with increasing delay, reaching $R = 0.45$ already with a 1-hour delay (and $R = 0.31$ with a 5-hour delay). Clearly, the *AE* is less well correlated with preceding values of the average ion mass

TABLE 1. Autocorrelation of Log (Hourly AE) in 1978–1979 (N = 17520)

Lag Time, hours	Correlation Coefficient
1	0.87
2	0.70
3	0.61
4	0.55
5	0.51
6	0.46

than vice versa. Note also that the regression line in the top right panel is different from the corresponding line in the top left panel, even though the two correlation coefficients are the same (by definition).

Figure 4 displays all plasma sheet samplings corresponding to Figure 2, including both dawn and dusk halves. It may be true that conditions in the dusk half are usually the most relevant to substorm onset, as argued by *Baker et al.* [1982], but these ion composition data show no significant asymmetry between dusk and dawn and do not justify limiting the statistical material to the dusk side only. By including the dawn half it is possible to admit more samplings from early 1978 and early 1980 and thus cover a wider range of solar surface activity (see Figure 1). This is a desirable objective in the next section. It may suffice to mention that if the scatterplots of Figure 4 are limited to the dusk half, where there are 1366 samplings, the least squares fits are virtually identical to those in Figure 4, and the correlation coefficients differ by at most 0.02.

It is quite possible that the nonzero correlation of the AE with the preceding values of the average ion mass in the right panels of Figure 4, with 1- and 2-hour delays, is purely accidental, because the AE has a very high degree of autocorrelation over long periods of time. This is illustrated by Table 1, which lists the correlation coefficients for hourly AE values taken from one to six hours apart during 1978 and 1979 (17520 hours). As can be seen, the AE at any one time is still better correlated with the AE from as much as 6 hours earlier than it is with the average ion mass during the immediately preceding hour.

5.3. *Solar Cycle Effects*

Figure 5 relates the average ion mass in the central plasma sheet to solar surface activity, as measured by the $F_{10.7}$, as well as geomagnetic activity. The ion mass samplings in the left panel are from geomagnetically "quiet" times, defined by requiring that the hourly AE index be consistently less than 100 nT over a 3-hour period, where the middle hour contains the mass sampling. The right panel has samplings from "disturbed" times, similarly defined by hourly AE indices being consistently greater than 200 nT over that same 3-hour period. By considering AE indices taken both before and after the mass sampling it is ensured that no bias is placed on the causal relationship between the AE and the ion mass, although the strong autocorrelation of the AE index makes the precise timing less important (see Table 1). In any case the average ion mass is found to increase with increasing solar activity, regardless of substorm activity level, and this is mainly a consequence of an increasing O^+ density (see also *Young et al.* [1982] and *Lennartsson* [1989]). The regression lines are again based on log (mass), because a logarithmic y scale and a linear x scale provide a roughly linear dependence when data points are binned in x and averaged in y (not shown).

Although the correlation coefficient is only about 0.3 in both panels of Figure 5, the large number of data points makes it significant. It can be seen, by using standard statistical tests [*Bevington*, 1969, pp. 119–127; *Press et al.*, 1986, pp. 484–487], that the probability of having no actual correlation between the ion mass and the solar activity is negligible (less than 10^{-8}). Essentially, the same statistical results are reached even if the samplings are limited to the dusk half of the plasma sheet, thereby reducing the number of data points as well as the range of $F_{10.7}$. In that case, N = 339 and R = 0.25 in the left panel (AE < 100 nT) and N = 348 and R = 0.36 in the right panel (AE > 200 nT), and the respective regression lines remain identical within one standard deviation of either the slope or the vertical location.

By contrast, the substorm activity, as measured by the AE or Kp indices, does not increase with increasing solar surface activity during this time period, neither in terms of frequency of substorm onsets nor in terms of peak ampli-

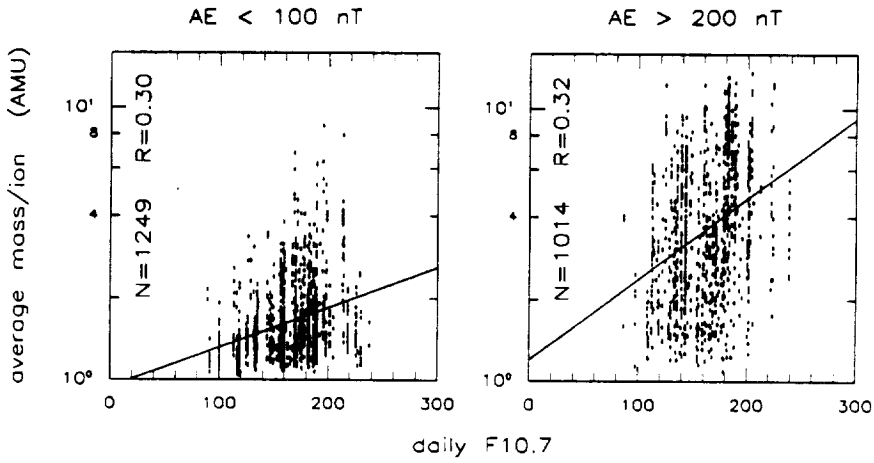

Fig. 5. Comparison of ion mass in plasma sheet with the Ottawa daily $F_{10.7}$ index (solar radio flux) during geomagnetically (left) quiet and (right) disturbed conditions (see text for selection of AE). The ion samplings have been ordered by Ottawa local time here, rather than by the usual universal time.

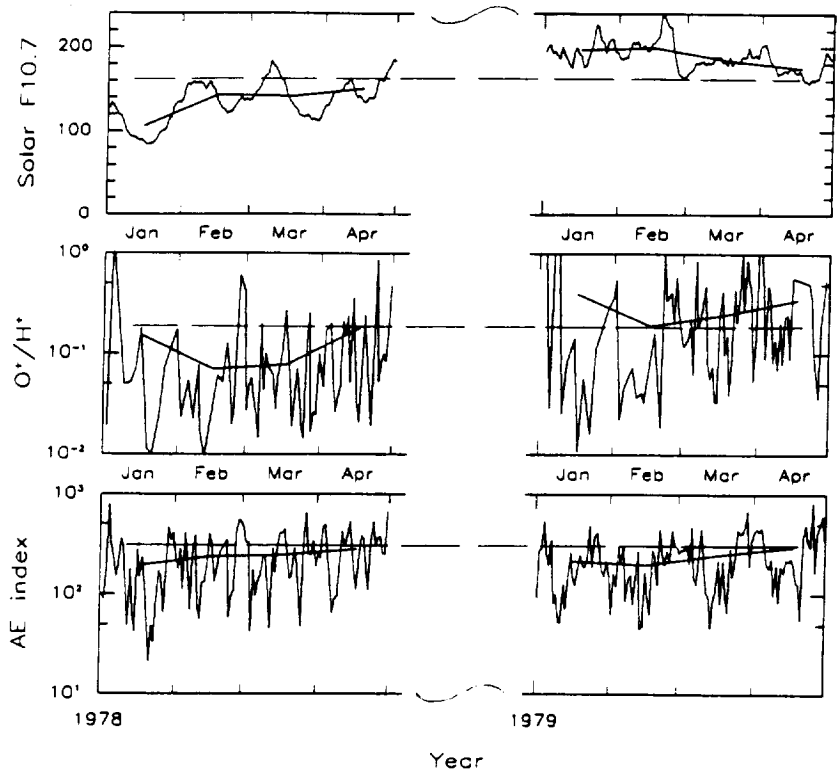

Fig. 6. (Top) Daily (jagged line) and monthly $F_{10.7}$; (middle) daily and monthly averaged plasma sheet O^+/H^+ density ratio; (bottom) daily and monthly averaged AE index. The dashed horizontal lines are for visual reference.

tude. This is partly illustrated for the AE index by Figure 6, which covers two 4-month intervals with similar ISEE 1 samplings of the plasma sheet (as defined in Figure 2), one in 1978, the other in 1979. The daily solar $F_{10.7}$ (top panel), and presumably also the concurrent EUV flux, is almost consistently higher in the later interval, resulting in a generally greater O^+/H^+ density ratio in the central plasma sheet, also represented by "daily" numbers here (middle panel), obtained by averaging all available samplings each day. These trends are still more distinct in terms of monthly averages, shown here by points centered on each month and connected by straight lines. However, the AE index (bottom panel) shows no signs of increasing from 1978 to 1979, neither as a daily nor as a monthly average (see also Figure 3 in the work by *Young et al.* [1982]). As far as the frequency of substorm onsets is concerned, a visual inspection of 1-min AE records (see *Kamei and Maeda* [1981] and subsequent data books) reveals no obvious increase from 1978 to 1979 (not illustrated here).

It may be argued that Figure 6 does show some change from 1978 to 1979 in the daily averaged AE index, since in 1979, but not in 1978, the AE appears to be modulated at a rate resembling the solar rotation period, which ranges from 25 to 36 days, depending on latitude and physical feature [*Hansen et al.*, 1969, and references therein]. This is probably not caused by a solar-induced periodicity in the O^+ density, however, since the $F_{10.7}$ index is much less periodic in 1979 than in 1978. The fact that the O^+/H^+ ratio in Figure 6 does not show a clear solar rotation modulation, not even in 1978, can probably be ascribed to the rapidly varying sampling conditions, including the spacecraft motion along the orbit (at least 7 R_E per day) and the orbital drift relative to the tail (~12 R_E per month at apogee).

Returning to Figure 1, it is clear that the $F_{10.7}$ index continues to have strong oscillations for the next couple of years, including those caused by solar rotation, but it does not begin to change in a more long-term fashion again until 1983, when it starts declining, and it is not until the second half of 1984 that it reaches a low and steady level, coincident with the AMPTE/CCE data interval. At this time the $F_{10.7}$ is very close to its minimum daily (65.8 on October 8, 1985) and monthly values (69.4 in September 1986, which is the canonical end of solar cycle 21). Accordingly, the CCE data set should have substantially lower O^+ concentrations than the ISEE 1 set, even if the ISEE 1 set is averaged over most of the rising phase (to improve statistics). The CCE data contain no samplings from the plasma sheet region shown in Figure 2, but it is known from the ISEE 1 data that O^+ ions in the inner magnetosphere ($R < 10\ R_E$) have virtually the same response to the $F_{10.7}$ index as do the plasma sheet O^+ ions [*Lennartsson*, 1989]. Hence, if the CCE data do show much lower O^+/H^+ ratios than do the ISEE 1 data, given the same inner magnetosphere sampling region for both sets, then it is fair to assume that the plasma sheet O^+/H^+ ratios are also substantially reduced at solar minimum (reversing the time sequence in Figure 6).

Figure 7 shows one kind of comparison between ISEE 1 and CCE data within the bounds of available AE indices. In this case each ion sampling has been associated with the average of 6 successive hourly AE indices, the last of which is concurrent. There is no special reason for choosing a 6-hour period per se, but the statistical correlation is somewhat better when an average of several hourly AE values is used rather than some single preceding value. Using preceding rather than succeeding AE values here seems intuitively

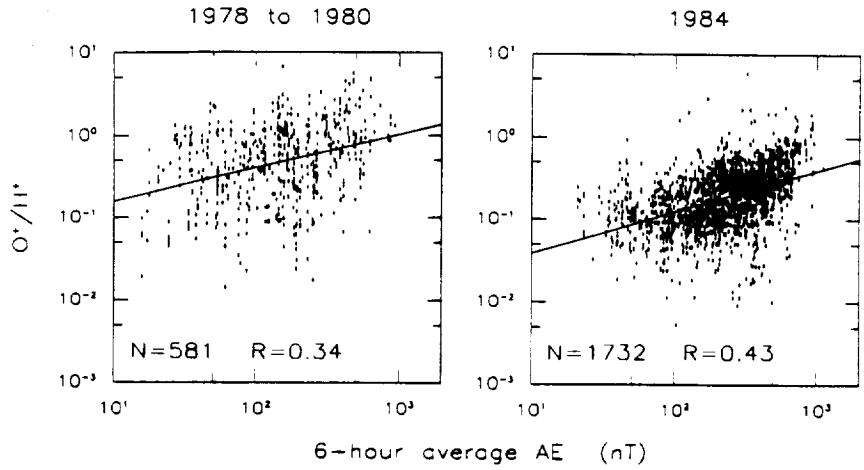

Fig. 7. Comparison of O^+/H^+ density ratio in the equatorial magnetosphere (dawn to noon; see left panel of Figure 3) with the preceding 6-hour average *AE* index during (left) rising-to-maximum and (right) minimum solar activity. The grand average *AE* during the two data sampling intervals was (left) 203 ± 7 nT and (right) 280 ± 5 nT.

right [cf. *Strangeway and Johnson*, 1984], regardless of the role of O^+ ions in the plasma sheet, and that choice is also justified by improved correlation.

Figure 7 confirms that the O^+/H^+ ratio has declined quite substantially in late 1984, near solar minimum, as compared to typical values during the rising phase of 1978 to early 1980. Even though the two instruments have different pitch angle coverage in this region of space (sections 2 and 3), the difference in the O^+/H^+ ratio between the left (ISEE 1) and right (CCE) panels is quite consistent with a time reversal of the results obtained between 1978 and 1980 at geosynchronous altitude ($L \approx 6.6$) by the GEOS 2 instrument (measuring nearly perpendicular to the magnetic field). If a median $F_{10.7}$ of 175 is assigned to the ISEE 1 data [*Lennartsson*, 1989] and an $F_{10.7}$ of 70 to the CCE data (Figure 1), the logarithmic regression formula in Table 3*b* of *Young et al.* [1982] predicts a reduction in the ratio by a factor of ~3.5 in 1984 for geomagnetically quiet conditions. Comparing the two regression lines in Figure 7 at low *AE* yields a somewhat larger reduction by a factor of 4.1, but the difference is probably within the margins of error, considering that the ISEE 1 data in Figure 7 span such a wide range of $F_{10.7}$. In any case there is a clear downward displacement of the regression line in 1984, and there is relatively less scatter about this line, resulting in a higher correlation coefficient. The improved correlation with the *AE* index is consistent with the strongly reduced fluctuations in the daily $F_{10.7}$ index (Figure 1), provided the O^+/H^+ ratio, as implied by Figure 5, depends not only on long-term but also on day-to-day variations in the solar irradiation.

In spite of this substantial long-term reduction in the O^+/H^+ ratio, there is no corresponding reduction in substorm activity. Instead, there is a modest but statistically significant increase over the same time period, as measured by for instance daily averages of the *AE* index (see *Kamei and Maeda* [1981], and subsequent data books). This trend is reflected in Figure 7 by the different grand average *AE* values during the two intervals of ion sampling (203 nT in the ISEE 1 interval, 280 nT in the CCE interval, the two mean values differing by more than ten times the standard deviation of either mean).

These opposing effects are even more clearly demonstrated by means of the *Kp* index, which allows all of the CCE data to be used (and more than twice as much of the ISEE 1 data; see end of section 4). In Figure 8 each ion sampling has been associated with the linear average of the concurrent and the two immediately preceding *Kp* indices, assigning the numerical values +1/3 and −1/3 to the graduating plus and minus symbols on the *Kp* index. The resulting 9-hour average *Kp* has been binned, as shown, and the density ratios have been averaged within each bin. The grand average *Kp* during the two sets of ion samplings is indicated in the respective panel, in conventional notation, and further described in the caption. When expressed in decimal numbers, the two mean values differ by 50 times the standard deviation of either mean.

To place these results in a broader perspective, the hourly and daily averaged *AE* for all of 1978 through 1984 have been plotted versus the daily $F_{10.7}$ in Figure 9 (except for 1 day of missing $F_{10.7}$ index in 1983). Although small in magnitude, the resulting correlation coefficients are statistically significant, considering the large number of points [*Bevington*, 1969, pp. 119–127; *Press et al.*, 1986, pp. 484–487]. The fact that the two regression lines have almost exactly the same slope (same within two decimal places), even though the two sets of data points differ in size by a factor of 24, makes it almost certain that the correlation is real and not merely due to numerical rounding errors. The negative sign of the correlation is consistent, in a superficial sense, with the long-term anticorrelation just found between the O^+/H^+ ratio and the *AE* (Figure 7) and *Kp* (Figure 8), since the O^+ density is positively correlated with the $F_{10.7}$ (Figure 5; see also *Young et al.* [1982] and *Lennartsson* [1989]). This does not by itself imply a physical relationship between the *AE* and the $F_{10.7}$, however, because Figure 9 spans the better part of a solar cycle, and the important physical parameter may be solar cycle phase, or simply time. Indeed, if the *AE* is sorted by the $F_{10.7}$ on a year-by-year basis, the correlation does not even show a persistent sign. This is illustrated by Table 2.

5.4. *Effects of Including Lowest Energy Channel*

The possible role of ions with energies below 100 eV/e is primarily an issue with data obtained in situ, that is the ISEE

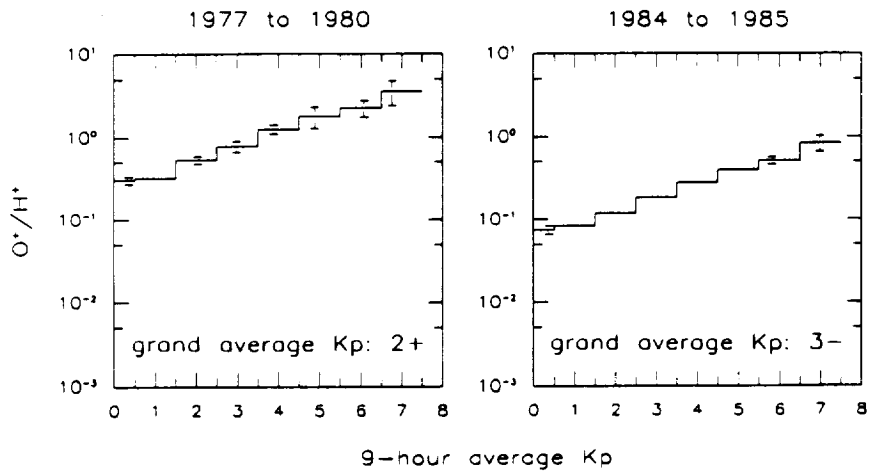

Fig. 8. Averages of same ratio as a function of the preceding 9-hour average Kp index, covering similar phases of the solar cycle, but including a larger spatial region (left and right panels of Figure 3 combined). The error bars indicate the standard deviation (plus and minus) of the average ratio in each Kp-bin, and is drawn at the average Kp within the bin (when greater than the line width). The grand average Kp in each panel represents an actual decimal number of (left) 2.26 ± 0.01 and (right; see text) 2.76 ± 0.01.

1 plasma sheet data (Figure 2). The nominal range of 10–100 eV/e, not including variable RPA settings, has been measured in ~90% of the 4056 plasma sheet samplings, and these measurements almost always cover all 12 spin angle sectors at least once.

Count rates in this single energy channel have been converted to partial ion number densities assuming rotational symmetry of the ion flux around the same flow vector used for the main velocity moments (assumption 1 in section 3). This average flow vector, one for each ion species, has been based on count rates in all the other energy channels (except the highest one) and does not always approximate the true flow direction of the 10- to 100-eV/e ions. This can be a significant problem when the flux of low-energy ions is strongly focused in spin angle, in which case an error in the axis of symmetry leads to exaggerated densities.

Adding these partial densities, when measured, to the main densities has almost no effect on the statistical picture, however. In most samplings from the central plasma sheet the O^+ and He^+ densities are increased by less than 15% and the H^+ and He^{++} densities by less than 5%. Table 3 shows the average increases. Part of the reason for these modest numbers may be that the low-energy cutoff is actually higher than 10 eV/e in much of the plasma sheet data, perhaps more typically between 10 and 20 eV/e, because of positive spacecraft charging associated with photo electron emission (see Figure 1 of *Mozer et al.* [1983]).

When Figures 4 and 5 are reproduced with the lowest-energy channel included (not shown), the new scatter patterns are virtually identical to the old ones. There is a barely perceptible flattening of the regression lines, corresponding quantitatively to a change in the third decimal place of the respective slopes. This flattening is accompanied by a slight reduction in the correlation coefficients as well, and this is again limited to the third decimal place in all cases but the left panel of Figure 5, where R is reduced to 0.28. Although very small, the reductions in the slopes and correlation coefficients of each regression line both indicate disordering. Hence, as far as the ion composition is concerned, adding the 10- to 100-eV/e partial densities in the central plasma

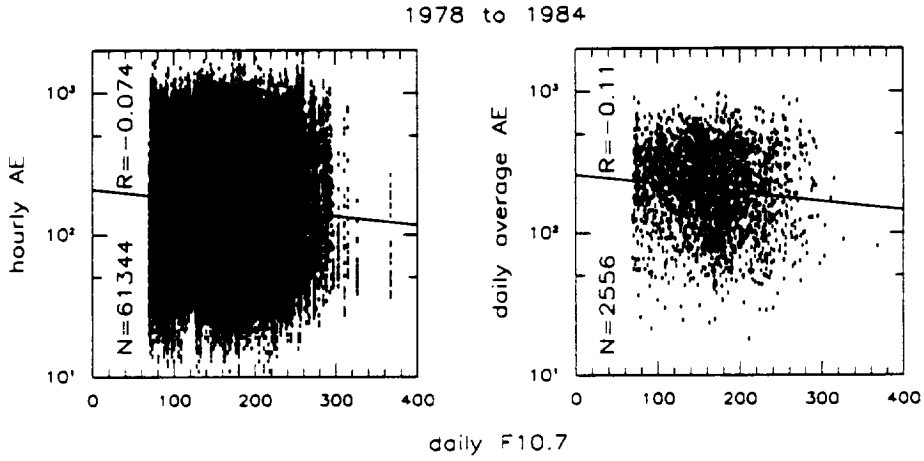

Fig. 9. Comparison of hourly (Ottawa LT; left) and daily (UT; right) AE indices with the daily solar $F_{10.7}$ index during a 7-year period (year-by-year comparison is made in Table 2).

TABLE 2. Correlation of Log (Hourly AE) With Daily $F_{10.7}$

	Year						
	1978	1979	1980	1981	1982	1983	1984
Number values	8760	8760	8784	8760	8760	8736	8784
Correlation coefficient	0.002	−0.118	0.041	0.074	0.074	0.026	0.065

sheet makes no significant physical difference, but it appears to slightly increase the measurement errors, which is the main reason for keeping the low-energy cutoff at 100 eV/e in this study.

6. Concluding Remarks

The preceding section makes no mention of the mean energy of the O^+ ions, and there is actually no new information from this study that warrants a discussion beyond what was presented by *Lennartsson and Shelley* [1986] and *Lennartsson* [1989]. The only potentially critical issue here is whether the O^+ energy in the central plasma sheet decreases with increasing O^+ density, so as to offset the expected increase in the ion inertial effects. It was found previously that the O^+ mean energy in the 0.1- to 16-keV range is indeed slightly anti-correlated with both geomagnetic [*Lennartsson and Shelley*, 1986] and solar activity [*Lennartsson*, 1989], that is anticorrelated with density, but the effect appears far too small to be of any significance here. Specifically, the O^+ mean energy in the central plasma sheet is typically ~4 to 5 keV during low geomagnetic and solar activity and ~3 to 4 keV during moderate to strong activity.

Returning to the far greater variations in the O^+ density, and in the O^+/H^+ density ratio, the challenge is now to interpret their various statistical relations with geomagnetic and solar activity. If one makes the very reasonable assumption that Figures 7 and 8 show a long-term trend that applies also to the central plasma sheet, it is clear that the frequency of occurrence of very large O^+/H^+ ratios in the tail current sheet can be substantially reduced over time with no hindrance to substorms. On the contrary, substorm activity increases. Is this increased activity actually caused by the relative decrease in O^+ content? Considering Figure 5, such a scenario is consonant with the negative correlation between the AE and the $F_{10.7}$ in Figure 9. However, Table 2 shows that this negative correlation, when ordered by calendar year, is not an ordinary feature, but is limited to one (1979) of seven years. This makes it much more likely that the long-term variation of the AE is controlled by a solar process which depends on the solar cycle phase but is not well measured by the $F_{10.7}$, nor by the EUV flux.

Figure 10 may provide additional clues. It appears from Figure 10 that the year 1979 is unique in the sense that the AE activity then approaches its absolute minimum in the 7 years considered, a minimum reached in early 1980. Since this occurs while the $F_{10.7}$ is approaching its absolute maximum (Figure 1), it probably accounts for the net negative correlation in Figure 9 (even without the singular $F_{10.7}$ peak in early November 1979). It certainly accounts for the long-term increase in the AE and the Kp in Figures 7 and 8. Whether the early 1980 minimum in the monthly average AE is entirely due to solar processes, or somehow depends on solar-induced changes in the magnetosphere particle populations, it is clearly contrary to having substorm activity enhanced by increased O^+ concentration in the tail current sheet (see also Figure 6).

If there is any significant feedback from the O^+, due to its large ionic mass, it must be negative: The O^+ either inhibits the onset of substorms, acts as a damper on substorms in progress, or helps to release tail stresses at an earlier and "less harmful" stage. However, Figure 10 appears to exclude that scenario as well, since the monthly average AE starts increasing again long (2 years) before the solar $F_{10.7}$ enters its declining phase (Figure 1), which is presumably when the O^+ concentration declines in the plasma sheet (Figure 5).

Short-term correlations are less definitive, for reasons that have been outlined above, but they appear to point in the same direction. Figure 4 suggests that the O^+/H^+ ratio in the plasma sheet does depend on the previous history of the AE, at least over a 2-hour interval (maximum R with two hours delay), but it gives no hint of a similar dependence of the AE on the O^+ concentration, since the correlation in the right panels declines monotonically with time and is anyway much weaker than the autocorrelation of the AE (Table 1). Furthermore, the pattern of scattered points in Figure 4 has an almost triangular shape in the left panels, especially in the bottom panel, with one corner at small ion mass but large AE. This shape implies, ideally, that the AE can take on any large value without O^+ ions being present, and it can do that without increasing the O^+/H^+ ratio uniformly throughout the central plasma sheet, but the O^+/H^+ ratio cannot reach very large values anywhere unless the AE is already large.

TABLE 3. ISEE 1 Average Incremental Density From 10- to 100-eV/e Channel in Plasma Sheet

Ion	Increment, %
H^+	2.8
He^{++}	1.3
He^+	8.2
O^+	7.2

6.1. *Possible Role of Very Low Energy Ions*

Whether the low-energy cutoff is 10 or 100 eV/e, or some intermediate value imposed by positive spacecraft charging, does not appear to make much difference in the central plasma sheet (Table 3), but there may still be a "hidden" ion population with mean energies of a few eV, or less, associated with the terrestrial polar wind and consisting mostly of H^+ ions [e.g., *Chappell et al.*, 1987]. The question is, how large is this polar wind population of H^+ ions compared with the more energetic H^+ population measured on the ISEE 1 spacecraft? Does it have a significant effect on the average ion mass? So far there have been no direct measurements of

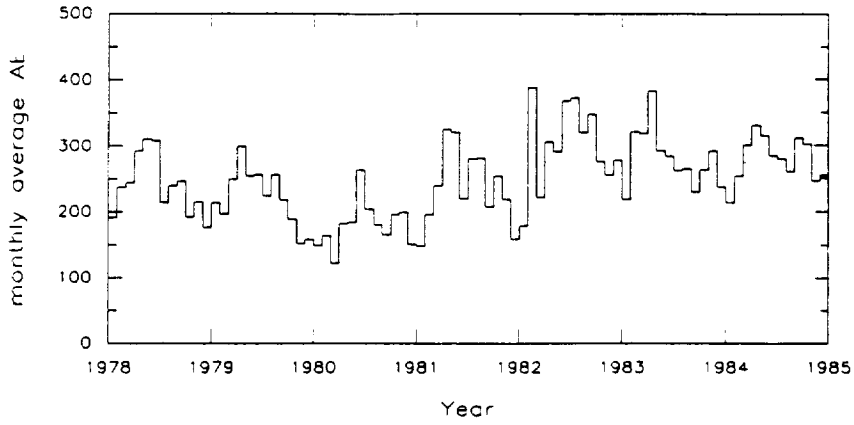

Fig. 10. Long-term variation of monthly averaged AE index (nanoteslas).

ions with only a few eV energy in the plasma sheet, beyond 10 R_E, nor have there been any large-scale attempts to infer "hidden" ions by comparing measured partial ion densities with total electron densities deduced from wave experiments, but the subject has been addressed indirectly by modeling particle trajectories, notably by *Delcourt et al.* [1989].

The numerical model of Delcourt et al. takes into account all presently known sources of terrestrial ion outflows, using the most recent measurements or estimates of source parameters, but it is restricted to radial distances less than 17 R_E, and its plasma sheet does not receive ions whose trajectories intersect the magnetopause or reach beyond 17 R_E downtail. As emphasized by the authors, the trajectory interrupts, especially downtail, set artificial and severe limits on the potential contribution to the plasma sheet density of H^+ ions with initial energies of 10 eV (cusp source) or greater (auroral zone and polar cap sources) and are the main reason why the calculated H^+ density between 10 and 17 R_E, including all energies, is only ~0.01 to 0.08 cm^{-3} (Figure 18 in their paper). However, these limits are less severe for the polar wind H^+ ions, which are all assumed to have an initial energy of only 1 eV, so this model may provide a probable upper limit on their specific contribution in Earth's plasma sheet.

According to Figure 4 in the paper by Delcourt et al., ~43% of the polar wind H^+ ions remain within the model boundaries during geomagnetically quiet conditions, whereas 41% are lost downtail, because of weak equatorward convection, and 16% are lost at the magnetopause. The 43% that remain are sufficient to dominate the H^+ density earthward of the 17 R_E boundary, but the density between 10 and 17 R_E is only about 1/10 of the energetic H^+ density measured on the ISEE 1 (Figure 18 in same paper; see also *Lennartsson and Shelley* [1986]). Fewer of the polar wind ions are lost downtail during disturbed conditions (stronger convection), only ~6%, but the ionospheric source is assumed to be weaker then, by a factor of 2/3 (their Table 2), and a somewhat greater fraction is lost at the magnetopause (23%), so the model H^+ density in the plasma sheet is still smaller, by a factor of 5 to 10, than the energetic H^+ density measured on the ISEE 1. Hence, even with all of the lost polar wind H^+ ions somehow recovered and added to its plasma sheet, this model seems to imply that the density of very low energy H^+ ions (few eV) is smaller than the known density of energetic H^+ ions in Earth's plasma sheet, possibly substantially smaller.

It is worth noting that the polar wind is expected, on theoretical grounds, to be stronger, by approximately a factor of 3, at the minimum of the solar cycle than at the maximum of same [*Chappell et al.*, 1987, and references therein], which is the opposite of the observed long-term trend of the O^+ flux. To the extent that polar wind H^+ ions do affect the ion composition in the tail current sheet, they probably amplify the difference in the O^+/H^+ ratio between solar maximum and minimum, thereby enhancing the long-term anticorrelation between average ion mass and geomagnetic activity implied by Figures 7 and 8 above.

6.2. *Corollary*

Since the energetic O^+ ions do reach the central plasma sheet, well beyond 10 R_E, and do so in sufficient numbers to have a very significant and strongly variable influence on the average mass of keV ions (Figures 4 and 5), they must have significant and variable effects on any tail instability that depends in a decisive fashion on this mass, including any such instability powerful enough to influence the geomagnetic indices. The statistical results of this study suggest therefore that the average ion mass is an unimportant parameter in the equations that govern magnetotail stability. It is clear, at least from the long-term behavior of the AE and Kp indices (Figures 6, 7, 8, and 10), that a more frequent occurrence of large average mass/ion, or mass/charge, in the tail current sheet is not sufficient cause for stronger dissipation of auroral energy. The statistical data are more compatible with reduced energy dissipation when the ion mass becomes extremely large near solar maximum. However, the lack of a consistent correlation over time between solar and geomagnetic indices seems to rule out all significant feedback (Table 2 and Figures 1 and 10). These considerations are nominally based on ion composition data from the 0.1- to 16-keV/e energy range, but probably apply to the bulk of the plasma sheet ions.

Acknowledgments. The authors wish to thank H. L. Collin for helpful discussions and for his assistance in preparing computer plotting routines and computer records of geophysical and solar indices. The authors are also indebted to C. T. Russell, T. A. Potemra, L. Zanetti, and M. H. Acuña, for the use of spacecraft

magnetometer data and to the National Oceanic and Atmospheric Administration for the use of magnetic tape records of the geophysical and solar indices. This work was supported by NASA under contracts NAS5-30565, NAS5-31209, and NAS5-33047 and by Lockheed Independent Research.

The Editor thanks J. H. Waite and H. D. Balsiger for their assistance in evaluating this paper.

REFERENCES

Baker, D. N., E. W. Hones, Jr., D. T. Young, and J. Birn, The possible role of ionospheric oxygen in the initiation and development of plasma sheet instabilities, *Geophys. Res. Lett.*, *9*, 1337, 1982.

Baker, D. N., T. A. Fritz, W. Lennartsson, B. Wilken, and H. W. Kroehl, The role of heavy ionospheric ions in the localization of substorm disturbances on 22 March 1979: CDAW-6, *J. Geophys. Res.*, *90*, 1273, 1985.

Balsiger, H., P. Eberhardt, J. Geiss, and D. T. Young, Magnetic storm injection of 0.9- to 16-keV/e solar and terrestrial ions into the high altitude magnetosphere, *J. Geophys. Res.*, *85*, 1645, 1980.

Bevington, P. R., *Data Reduction and Error Analysis for the Physical Sciences*, McGraw-Hill, New York, 1969.

Chappell, C. R., T. E. Moore, and J. H. Waite, Jr., The ionosphere as a fully adequate source of plasma for the Earth's magnetosphere, *J. Geophys. Res.*, *92*, 5896, 1987.

Daglis, I. A., E. T. Sarris, and G. Kremser, Indications for ionospheric participation in the substorm process from AMPTE/CCE observations, *Geophys. Res. Lett.*, *17*, 57, 1990.

Daglis, I. A., E. T. Sarris, and G. Kremser, Ionospheric contribution to the cross-tail current enhancement during the substorm growth phase, *J. Atmos. Terr. Phys.*, *53*, 1091, 1991.

Delcourt, D. C., C. R. Chappell, T. E. Moore, and J. H. Waite, Jr., A three-dimensional numerical model of ionospheric plasma in the magnetosphere, *J. Geophys. Res.*, *94*, 11,893, 1989.

Ghielmetti, A. G., R. G. Johnson, R. D. Sharp, and E. G. Shelley, The latitudinal, diurnal, and altitudinal distributions of upward flowing energetic ions of ionospheric origin, *Geophys. Res. Lett.*, *5*, 59, 1978.

Gloeckler, G., and D. C. Hamilton, AMPTE ion composition results, *Phys. Scr.*, *T18*, 73, 1987.

Hansen, R. T., S. F. Hansen, and H. G. Loomis, Differential rotation of the solar electron corona, *Sol. Phys.*, *10*, 135, 1969.

Hinteregger, H. E., Representations of solar EUV fluxes for aeronomical applications, *Adv. Space Res.*, *1*, 39, 1981.

Kamei, T., and H. Maeda, Auroral electrojet indices (AE) for January–June 1978, *Data Book 3*, World Data Center C2 for Geomagn., Kyoto, Japan, April 1981.

Kremser, G., W. Stüdeman, B. Wilken, G. Gloeckler, D. C. Hamilton, and F. M. Ipavich, Observations of energetic oxygen and carbon ions with charge states between 3 and 6 in the magnetosphere, *Ann. Geophys.*, *6*, 325, 1988.

Lennartsson, W., Energetic (0.1–16 keV/e) magnetospheric ion composition at different levels of solar F10.7, *J. Geophys. Res.*, *94*, 3600, 1989.

Lennartsson, W., and R. D. Sharp, A comparison of the 0.1–17 keV/e ion composition in the near equatorial magnetosphere between quiet and disturbed conditions, *J. Geophys. Res.*, *87*, 6109, 1982.

Lennartsson, W., and E. G. Shelley, Survey of 0.1- to 16-keV/e plasma sheet ion composition, *J. Geophys. Res.*, *91*, 3061, 1986.

Lundin, R., B. Hultqvist, N. Pissarenko, and A. Zakharov, The plasma mantle: Composition and other characteristics as observed by means of the Prognoz-7 satellite, *Space Sci. Rev.*, *31*, 247, 1982.

Möbius, E., M. Scholer, B. Klecker, D. Hovestadt, G. Gloeckler, and F. M. Ipavich, Acceleration of ions of ionospheric origin in the plasma sheet during substorm activity, in *Magnetotail Physics*, edited by A. T. Y. Lui, Johns Hopkins University Press, Baltimore, 231, 1987.

Moore, T. E., and D. C. Delcourt, Transport and energization of ionospheric plasma (abstract), *EOS Trans. AGU*, *73*(43), Fall Meeting suppl., 471, 1992.

Mozer, F. S., E. W. Hones, Jr., and J. Birn, Comparison of spherical double probe electric field measurements with plasma bulk flows in plasmas having densities less than 1 cm^{-3}, *Geophys. Res. Lett.*, *10*, 737, 1983.

Peterson, W. K., R. D. Sharp, E. G. Shelley, and R. G. Johnson, Energetic ion composition of the plasma sheet, *J. Geophys. Res.*, *86*, 761, 1981.

Potemra, T. A., L. J. Zanetti, and M. H. Acuña, The AMPTE CCE Magnetic Field Experiment, *IEEE Trans. Geosci. Remote Sens.*, *GE-23*, 246, 1985.

Press, W. H., B. P. Flannery, S. A. Teukolsky, and W. T. Vetterling, *Numerical Recipes*, Cambridge University Press, New York, 1986.

Russell, C. T., The ISEE 1 and 2 fluxgate magnetometers, *IEEE Trans. Geosci. Electron.*, *GE-16*, 239, 1978.

Sharp, R. D., D. L. Carr, W. K. Peterson, and E. G. Shelley, Ion streams in the magnetotail, *J. Geophys. Res.*, *86*, 4639, 1981.

Shelley, E. G., R. G. Johnson, and R. D. Sharp, Satellite observations of energetic heavy ions during a geomagnetic storm, *J. Geophys. Res.*, *77*, 6104, 1972.

Shelley, E. G., R. D. Sharp, R. G. Johnson, J. Geiss, P. Eberhardt, H. Balsiger, G. Haerendel, and H. Rosenbauer, Plasma composition experiment on ISEE-A, *IEEE Trans. Geosci. Electron.*, *GE-16*, 266, 1978.

Shelley, E. G., A. Ghielmetti, E. Hertzberg, S. J. Battel, K. Altwegg-Von Burg, and H. Balsiger, The AMPTE CCE Hot Plasma Composition Experiment (HPCE), *IEEE Trans. Geosci. Remote Sens.*, *GE-23*, 241, 1985.

Singer, H. J., C. T. Russell, M. G. Kivelson, T. A. Fritz, and W. Lennartsson, Satellite observations of the spatial extent and structure of PC 3, 4, 5 pulsations near the magnetospheric equator, *Geophys. Res. Lett.*, *6*, 889, 1979.

Strangeway, R. J., and R. G. Johnson, Energetic ion mass composition as observed at near-geosynchronous and low altitudes during the storm period of February 21 and 22, 1979, *J. Geophys. Res.*, *89*, 8919, 1984.

Swift, D. W., The role of ionospheric plasma in substorm models (abstract), *Eos Trans. AGU*, *73*(43), Fall Meeting suppl., 472, 1992.

Yau, A. W., E. G. Shelley, W. K. Peterson, and L. Lenchyshyn, Energetic auroral and polar ion outflow at DE 1 altitudes: Magnitude, composition, magnetic activity dependence, and long-term variations, *J. Geophys. Res.*, *90*, 8417, 1985.

Young, D. T., H. Balsiger, and J. Geiss, Correlations of magnetospheric ion composition with geomagnetic and solar activity, *J. Geophys. Res.*, *87*, 9077, 1982.

D. M. Klumpar, O. W. Lennartsson, J. M. Quinn, and E. G. Shelley, Lockheed Missiles and Space Company, Inc., Research and Development, Dept. 91-20, Bldg. 255, 3251 Hanover Street, Palo Alto, CA 94304.

(Received February 9, 1993;
revised June 1, 1993;
accepted July 13, 1993.)

REPORT DOCUMENTATION PAGE

Form Approved
OMB No. 0704-0188

1. AGENCY USE ONLY (Leave blank)	2. REPORT DATE	3. REPORT TYPE AND DATES COVERED
	4/20/94	Final Report, 10 Apr 91 - 9 May 94

4. TITLE AND SUBTITLE
A STUDY OF THE FORMATION AND DYNAMICS OF THE EARTH's PLASMA SHEET USING ION COMPOSITION DATA

5. FUNDING NUMBERS
C: NAS5-31209

6. AUTHOR(S)
O. W. Lennartsson, Principal Investigator

7. PERFORMING ORGANIZATION NAME(S) AND ADDRESS(ES)
Lockheed Missiles & Space Company, Inc.
Research and Development Division
0/91-20, B/255, Fac. 2
3251 Hanover Street
Palo Alto, CA 94304-1187

8. PERFORMING ORGANIZATION REPORT NUMBER
F254278

9. SPONSORING/MONITORING AGENCY NAME(S) AND ADDRESS(ES)
NASA/ Goddard Space Flight Center
Greenbelt, Maryland 20771
Technical Officer: G. D. Bullock, Code 602

10. SPONSORING/MONITORING AGENCY REPORT NUMBER

11. SUPPLEMENTARY NOTES

12a. DISTRIBUTION/AVAILABILITY STATEMENT
Unlimited/ Unclassified

12b. DISTRIBUTION CODE

13. ABSTRACT *(Maximum 200 words)*

Over two years of data from the Lockheed Plasma Composition Experiment on the ISEE 1 spacecraft, covering ion energies beween 100 eV/e and about 16 keV/e, have been analyzed in an attempt to extract new information about three geophysical issues: (1) solar wind penetration of Earth's magnetic tail, (2) relationship between plasma sheet and tail lobe ion composition, and (3) possible effects of heavy terrestrial ions on plasma sheet stability.

The results suggest: (1) The solar wind enters the magnetic tail at all times along slots between the plasma sheet and tail lobes, convected inward by the electric fringe field of the low-latitude magnetopause boundary layer. (2) The density gradient between the plasma sheet and the tail lobes is the steepest for protons, and becomes gradually smoother with increasing ionic mass, possibly associated with the different characteristic gyroradii. (3) The energetic singly charged oxygen ions of terrestrial origin do not have a significant effect on the stability of the plasma sheet, in spite of the fact that they often contribute most of the ion mass density inside of the ISEE 1 apogee near 23 earth radii downtail.

14. SUBJECT TERMS
Ion Composition, Magnetotail, Plasma Sheet, Tail Lobes, Solar Wind Entry, Energetic Ions, Ion Flows, Current Sheet

15. NUMBER OF PAGES
76

16. PRICE CODE

17. SECURITY CLASSIFICATION OF REPORT	18. SECURITY CLASSIFICATION OF THIS PAGE	19. SECURITY CLASSIFICATION OF ABSTRACT	20. LIMITATION OF ABSTRACT
Unclassified	Unclassified	Unclassified	Unlimited

GENERAL INSTRUCTIONS FOR COMPLETING SF 298

The Report Documentation Page (RDP) is used in announcing and cataloging reports. It is important that this information be consistent with the rest of the report, particularly the cover and title page. Instructions for filling in each block of the form follow. It is important to ***stay within the lines*** to meet ***optical scanning requirements***.

Block 1. Agency Use Only *(Leave blank)*.

Block 2. Report Date. Full publication date including day, month, and year, if available (e.g. 1 Jan 88). Must cite at least the year.

Block 3. Type of Report and Dates Covered. State whether report is interim, final, etc. If applicable, enter inclusive report dates (e.g. 10 Jun 87 - 30 Jun 88).

Block 4. Title and Subtitle. A title is taken from the part of the report that provides the most meaningful and complete information. When a report is prepared in more than one volume, repeat the primary title, add volume number, and include subtitle for the specific volume. On classified documents enter the title classification in parentheses.

Block 5. Funding Numbers. To include contract and grant numbers; may include program element number(s), project number(s), task number(s), and work unit number(s). Use the following labels:

C	- Contract	**PR**	- Project
G	- Grant	**TA**	- Task
PE	- Program Element	**WU**	- Work Unit Accession No.

Block 6. Author(s). Name(s) of person(s) responsible for writing the report, performing the research, or credited with the content of the report. If editor or compiler, this should follow the name(s).

Block 7. Performing Organization Name(s) and Address(es). Self-explanatory.

Block 8. Performing Organization Report Number. Enter the unique alphanumeric report number(s) assigned by the organization performing the report.

Block 9. Sponsoring/Monitoring Agency Name(s) and Address(es). Self-explanatory.

Block 10. Sponsoring/Monitoring Agency Report Number. *(If known)*

Block 11. Supplementary Notes. Enter information not included elsewhere such as: Prepared in cooperation with...; Trans. of...; To be published in.... When a report is revised, include a statement whether the new report supersedes or supplements the older report.

Block 12a. Distribution/Availability Statement. Denotes public availability or limitations. Cite any availability to the public. Enter additional limitations or special markings in all capitals (e.g. NOFORN, REL, ITAR).

- **DOD** - See DoDD 5230.24, "Distribution Statements on Technical Documents."
- **DOE** - See authorities.
- **NASA** - See Handbook NHB 2200.2.
- **NTIS** - Leave blank.

Block 12b. Distribution Code.

- **DOD** - Leave blank.
- **DOE** - Enter DOE distribution categories from the Standard Distribution for Unclassified Scientific and Technical Reports.
- **NASA** - Leave blank.
- **NTIS** - Leave blank.

Block 13. Abstract. Include a brief *(Maximum 200 words)* factual summary of the most significant information contained in the report.

Block 14. Subject Terms. Keywords or phrases identifying major subjects in the report.

Block 15. Number of Pages. Enter the total number of pages.

Block 16. Price Code. Enter appropriate price code *(NTIS only)*.

Blocks 17. - 19. Security Classifications. Self-explanatory. Enter U.S. Security Classification in accordance with U.S. Security Regulations (i.e., UNCLASSIFIED). If form contains classified information, stamp classification on the top and bottom of the page.

Block 20. Limitation of Abstract. This block must be completed to assign a limitation to the abstract. Enter either UL (unlimited) or SAR (same as report). An entry in this block is necessary if the abstract is to be limited. If blank, the abstract is assumed to be unlimited.